

# Multiphase Flows of $N$ Immiscible Incompressible Fluids: A Reduction-Consistent and Thermodynamically-Consistent Formulation and Associated Algorithm

S. Dong\*

Center for Computational and Applied Mathematics  
 Department of Mathematics  
 Purdue University  
 West Lafayette, Indiana, USA

## Abstract

We present a reduction-consistent and thermodynamically consistent formulation and an associated numerical algorithm for simulating the dynamics of an isothermal mixture consisting of  $N$  ( $N \geq 2$ ) immiscible incompressible fluids with different physical properties (densities, viscosities, and pair-wise surface tensions). By reduction consistency we refer to the property that if only a set of  $M$  ( $1 \leq M \leq N - 1$ ) fluids are present in the system then the  $N$ -phase governing equations and boundary conditions will exactly reduce to those for the corresponding  $M$ -phase system. By thermodynamic consistency we refer to the property that the formulation honors the thermodynamic principles. Our  $N$ -phase formulation is developed based on a more general method that allows for the systematic construction of reduction-consistent formulations, and the method suggests the existence of many possible forms of reduction-consistent and thermodynamically consistent  $N$ -phase formulations. Extensive numerical experiments have been presented for flow problems involving multiple fluid components and large density ratios and large viscosity ratios, and the simulation results are compared with the physical theories or the available physical solutions. The comparisons demonstrate that our method produces physically accurate results for this class of problems.

Keywords: *reduction consistency; thermodynamic consistency; surface tension; phase field; multiphase flow; N-phase flow*

## 1 Introduction

This paper concerns the formulation and simulation of isothermal multiphase flows consisting of  $N$  ( $N \geq 2$ ) immiscible incompressible fluids with possibly very different physical properties (e.g. densities, dynamic viscosities, and pair-wise surface tensions). Following our previous works [12, 15, 16] and with a slight abuse of notation, we will refer to such problems as  $N$ -phase flows, where  $N$  denotes the number of different fluid components in the system, not necessarily the number of material phases. Our primary concern is the reduction consistency and thermodynamic consistency in the formulation of such problems. By thermodynamic consistency we refer to the property that the formulation should honor the thermodynamic principles (e.g. mass conservation, momentum conservation, second law of thermodynamics, Galilean invariance). Reduction consistency is rooted in the following simple observation about  $N$ -phase systems:

- Given an  $N$ -phase system, if some fluid components are absent from the system such that only  $M$  ( $1 \leq M \leq N - 1$ ) fluids are present, then this  $N$ -phase system is equivalent to the smaller  $M$ -phase system consisting of the fluids that are present.

We insist that the mathematical formulation for the  $N$ -phase system should correspondingly satisfy the same property, namely,

---

\*Email: sdong@purdue.edu

(C0): If only  $M$  ( $1 \leq M \leq N-1$ ) fluids are present in the N-phase system (while the other fluids are absent), then the N-phase formulation should reduce to the corresponding M-phase formulation.

We refer to this property as the reduction consistency.

The overall approach taken in this work falls into the phase field (or diffuse interface) framework, and we are primarily interested in the simulation of N-phase systems with three or more fluid components (i.e.  $N \geq 3$ ). For two-phase flows we refer to several comprehensive reviews (see e.g. [2, 32, 31, 36] and the references therein) of this and related approaches. Multiphase problems involving three or more fluid components have attracted a growing interest, and a number of researchers have contributed to the advance of this field; see e.g. [28, 6, 26, 7, 27, 24, 12, 5, 15, 9, 39, 3, 37], among others. Among the past studies, a handful of phase field models (e.g. [28, 24, 12]) have been developed that take into account the conservation laws and the constitutive relations dictated by thermodynamic principles. Reduction consistency issues are investigated for a three-phase and a multi-phase Cahn-Hilliard model (without hydrodynamic interactions) [6, 8], and these studies have signified the importance in the form of the free energy density function. While the current work focuses on the hydrodynamic interactions of multiple fluids, certain consistency issues encountered here can be analogous to those facing the materials community for multi-component materials (see e.g. [34, 21, 4, 35]).

In a previous work [12] we have proposed a general phase field model for formulating an isothermal system of  $N$  ( $N \geq 2$ ) immiscible incompressible fluids. The model is derived based on and honors the mass conservation of the  $N$  individual fluid components, the momentum conservation, the second law of thermodynamics, and the Galilean invariance principle. In such a sense it is a thermodynamically consistent model. This model is formulated based on a volume-averaged mixture velocity, which can be rigorously shown to be divergence free [12]. It is fundamentally different from those of [28, 24], which are based on a mass-averaged velocity (not divergence free). This N-phase model is generalized in [15], and a class of general order parameters has been introduced to formulate the N-phase system.

While the model of [12, 15] is thermodynamically consistent, it nonetheless falls short with respect to the reduction consistency. Motivated by this inadequacy and inspired by the discussions of consistency issues in [8], we have very recently in [16] combined a modified thermodynamically consistent N-phase model and the reduction-consistency considerations, and developed a method for simulating wall-bounded N-phase flows and N-phase contact angles. We have specifically considered the following set of reduction-consistency conditions on the N-phase formulation [16]:

*If only a set of  $M$  ( $1 \leq M \leq N-1$ ) fluids are present in the N-phase system, then*

(C1): *the N-phase free energy density function should reduce to the corresponding M-phase free energy density function;*

(C2): *the set of N-phase governing equations should reduce to that for the corresponding M-phase system, together with a set of identities corresponding to the absent fluids;*

(C3): *the set of boundary conditions for the N-phase system should reduce to that for the corresponding M-phase system, together with a set of identities corresponding to the absent fluids.*

Note that the consistency conditions (C2) and (C3) are imposed for both the momentum equations and the phase field equations.

By assuming a constant mobility matrix in the formulation, we have explored in [16] the implications of the above consistency conditions on the N-phase governing equations and boundary conditions. It is found that to satisfy the reduction-consistency conditions the mobility matrix should take a particular form (specific form given in [16]) and that the “multi-well” potential free energy density function needs to satisfy a set of properties as given in [16]. The reduction-consistency problem is thus boiled down to the following:

- Given an arbitrary set of pairwise surface tension values, how does one construct the multi-well potential free energy density function to satisfy the properties given in [16]?

If one could construct such a multiwell potential energy density function, a fully reduction-consistent N-phase formulation could be obtained. This construction problem is unfortunately highly non-trivial and challenging, and it so far remains an open question. It is noted that in [8] the consistency of a Cahn-Hilliard model (no hydrodynamic interactions) is studied under a set of weaker consistency conditions. The resultant

property on the potential energy density function from [8] is weaker (it is a subset of the required properties), and does not ensure the reduction consistency of the momentum equations. Due to the lack of an appropriate potential free energy density function to ensure full reduction consistency, in [16] a particular potential free energy density form has been adopted to arrive at a specific N-phase formulation, which ensures only a partial reduction consistency of the governing equations (between  $N$  phases and two phases only). In [16] we have also developed a set of reduction-consistent N-phase contact-angle boundary conditions based on the consistency property (C3).

Recognizing the enormous challenge with the approach of [16] to fulfill the reduction consistency, we present in this paper a different approach to achieve full reduction consistency and thermodynamic consistency for the N-phase formulations. The key distinction lies in dropping the assumption that the mobility matrix be constant. This allows us to devise the mobility matrix and the free energy density function individually in an untangled fashion, which can satisfy certain appropriate reduction properties separately. Full reduction consistency for the set of N-phase governing equations can then be guaranteed based on these individual reduction properties.

More specifically, we present developments in the the following aspects in this work:

- We present a thermodynamically consistent phase field model, which is different from those of [12, 16], for the hydrodynamic interactions of the N-fluid mixture. The development process of this model mirrors that of [12], but it leads to a different model due to a different representation of the mass balances of individual fluid components and different constitutive relations to satisfy the second law of thermodynamics. This model serves as the starting point for reduction consistency considerations in this work, and it is critical to the success in achieving full reduction consistency in the N-phase formulation.
- We introduce the concepts of reduction compatibility and reduction consistency for a set of variables, functions, and equations, and look into some useful properties of reduction-consistent and reduction-compatible functions/variables.
- We provide a method (Theorem 2.1) that guarantees the reduction consistency of the set of N-phase governing equations from the aforementioned phase field model. The method consists of a set of sufficient conditions with regard to the reduction consistency and reduction compatibility of the mobility matrix and terms involving the free energy density function. The method is quite general, and suggests many ways to construct reduction-consistent and thermodynamically consistent N-phase formulations.
- We suggest a specific form for the mobility matrix and the free energy density function that satisfy the reduction properties dictated by the method. This leads to a specific reduction-consistent and thermodynamically consistent N-phase formulation.
- We present a numerical algorithm for solving the governing equations of this N-phase formulation, together with a set of reduction-consistent boundary conditions. In particular, we look into how to algorithmically deal with the variable mobility matrix involved therein.

The novelties of this paper lie in several aspects: (i) the method (Theorem 2.1) to systematically construct reduction-consistent N-phase governing equations; (ii) the specific reduction-consistent and thermodynamically consistent N-phase formulation; and (iii) the numerical algorithm for solving the set of reduction-consistent and thermodynamically consistent N-phase phase field equations with a variable mobility matrix. To the best of the author’s knowledge, the N-phase formulation presented herein is the first fully reduction-consistent and thermodynamically consistent mathematical formulation for the hydrodynamic interactions of incompressible N-phase flows.

The rest of this paper is structured as follows. In Section 2 we introduce the ideas of reduction compatibility and reduction consistency for a set of functions and equations, and present a method that allows for the systematic construction of reduction-consistent N-phase governing equations. We also present a specific reduction-consistent and thermodynamically consistent N-phase formulation based on this method. In Section 3 we present an efficient numerical algorithm for solving the N-phase phase field equations with a variable mobility matrix. This, together with the algorithm for the N-phase momentum equations summarized in Appendix E, provides an effective method for simulating incompressible N-phase flows with the

reduction-consistent and thermodynamically consistent formulation. In Section 4 we provide extensive numerical experiments to test the method developed herein, and the simulation results are compared with physical theories and exact physical solutions for problems involving multiple fluid components and large contrasts in densities and viscosities. Section 5 then concludes the paper with some closing remarks. In Appendix A we outline the development of the thermodynamically consistent phase field model for an isothermal mixture of  $N$  ( $N \geq 2$ ) immiscible incompressible fluids, on which the current work is based. We summarize the key steps in the derivation of the model based on the mass conservation, momentum conservation, and the second law of thermodynamics. In Appendix B we provide proofs for several useful properties about reduction-consistent and reduction compatible functions listed in Section 2. Appendix C and Appendix D provide proofs for the Theorems 2.1 and 2.2 given in the main body of the text. Appendix E summarizes a numerical algorithm for solving the N-phase momentum equations.

## 2 Reduction-Consistent and Thermodynamically Consistent N-phase Formulation

Consider an isothermal mixture of  $N$  ( $N \geq 2$ ) immiscible incompressible fluids contained in some flow domain. In this section we present a reduction-consistent and thermodynamically-consistent formulation for this system. The formulation is developed based on a thermodynamically consistent phase field model for the N-fluid mixture. In the Appendix A we have outlined the derivation of this N-phase model based on the mass conservation, momentum conservation, and the second law of thermodynamics. The development process for this model mirrors that for the model of [12]. However, owing to a different way to represent the mass balances and to specify the constitutive relations to ensure the second law of thermodynamics, here we arrive at a model that is different from those of [12, 16]. In this model the dynamics of the N-phase mixture is described by the equations (83a)–(83c). The model honors the mass conservation of the  $N$  individual fluid components, the momentum conservation and the second law of thermodynamics, and it is Galilean invariant. Therefore it is said to be thermodynamically consistent. We refer the reader to Appendix A for the details in the development of the model. This model serves as the starting point, and in subsequent developments we concentrate on how to fulfill reduction consistency with this model.

Given a mixture of  $N$  ( $N \geq 2$ ) immiscible incompressible fluids, let  $\tilde{\rho}_i$  ( $1 \leq i \leq N$ ) and  $\tilde{\mu}_i$  ( $1 \leq i \leq N$ ) denote the constant density and constant dynamic viscosity of pure fluid  $i$  (before mixing), respectively. Let  $\sigma_{ij}$  ( $1 \leq i \neq j \leq N$ ) denote the constant surface tension associated with the interface formed between fluid  $i$  and fluid  $j$ , satisfying the following property

$$\begin{cases} \sigma_{ij} = \sigma_{ji}, & 1 \leq i, j \leq N, \\ \sigma_{ij} > 0, & 1 \leq i < j \leq N, \\ \sigma_{ii} = 0, & 1 \leq i \leq N. \end{cases} \quad (1)$$

Let  $c_i(\mathbf{x}, t)$  ( $1 \leq i \leq N$ ) and  $\rho_i(\mathbf{x}, t)$  ( $1 \leq i \leq N$ ) denote the volume fraction and density of fluid  $i$  *within the mixture*, which are field functions of space  $\mathbf{x}$  and time  $t$ . Let  $\vec{c} = (c_1, c_2, \dots, c_N)$ , and  $\rho(\vec{c})$  and  $\mu(\vec{c})$  denote the mixture density and mixture dynamic viscosity. These and other related variables are defined in more detail in the Appendix A.

### 2.1 Reduction Compatibility and Reduction Consistency

As mentioned in the Introduction section, certain equivalence relations exist between an N-phase system and smaller M-phase systems ( $1 \leq M \leq N - 1$ ). If some fluid components are absent, then the N-phase system is physically equivalent to a smaller multiphase system consisting of the fluids that are present. We next explore these equivalence relations and introduce the concepts of reduction consistency and reduction compatibility for a set of variables/functions and equations. This provides the basis for the study of reduction consistency of N-phase governing equations.

To make the idea more concrete, let us first consider the case in which one fluid component is absent from the N-phase system. Suppose the  $k$ -th fluid ( $1 \leq k \leq N$ ) is absent from the N-phase system, i.e. the

system is characterized by

$$c_k^{(N)} \equiv 0, \quad \rho_k^{(N)} \equiv 0 \quad \text{for some } 1 \leq k \leq N, \quad (2)$$

where the superscript in  $(\cdot)^{(N)}$  accentuates the point that the variable is with respect to the N-phase system. We will use this convention about the superscript throughout this paper and, if possible, will omit this superscript for brevity where no confusion arises.

We assume that the ordering of the fluids in the resultant  $(N-1)$ -phase system follows that of the original N-phase system (excluding fluid  $k$ ). In other words, the following correspondence relations for the volume fractions  $c_i$  ( $1 \leq i \leq N$ ) hold:

$$c_i^{(N)} = \begin{cases} c_i^{(N-1)}, & 1 \leq i \leq k-1, \\ 0, & i = k, \\ c_{i-1}^{(N-1)}, & k+1 \leq i \leq N, \end{cases} \quad \text{or} \quad \begin{cases} c_i^{(N-1)} = \begin{cases} c_i^{(N)}, & 1 \leq i \leq k-1, \\ c_{i+1}^{(N)}, & k \leq i \leq N-1, \end{cases} \\ c_k^{(N)} = 0. \end{cases} \quad (3)$$

The density of fluid  $i$  *within the mixture*,  $\rho_i$  ( $1 \leq i \leq N$ ), has a correspondence relation analogous to the above between the original N-phase and the resultant  $(N-1)$ -phase systems. On the other hand, the constant density of pure fluid  $i$ ,  $\tilde{\rho}_i$  ( $1 \leq i \leq N$ ), has a similar correspondence relation but with some difference:

$$\tilde{\rho}_i^{(N)} = \begin{cases} \tilde{\rho}_i^{(N-1)}, & 1 \leq i \leq k-1, \\ \tilde{\rho}_{i-1}^{(N-1)}, & k+1 \leq i \leq N, \end{cases} \quad \text{or} \quad \tilde{\rho}_i^{(N-1)} = \begin{cases} \tilde{\rho}_i^{(N)}, & 1 \leq i \leq k-1, \\ \tilde{\rho}_{i+1}^{(N)}, & k \leq i \leq N-1. \end{cases} \quad (4)$$

The critical difference lies in that even though fluid  $k$  is absent from the system ( $c_k^{(N)} = 0, \rho_k^{(N)} = 0$ ), the density of pure fluid  $k$  remains the same non-zero constant ( $\tilde{\rho}_k^{(N)} \neq 0$ ). The constant dynamic viscosities  $\tilde{\mu}_i$  ( $1 \leq i \leq N$ ) have a correspondence relation analogous to (4).

The correspondence relations (3) and (4) characterize two different types of variables. The distinction between them lies in that in the latter type there is no constraint on the  $k$ -th variable of the original N-phase system if fluid  $k$  is absent from the system. It is important to distinguish these two types of correspondence relations and the two types of variables. Equations (3) and (4) describe how the variables  $c_i$  ( $1 \leq i \leq N$ ) and  $\tilde{\rho}_i$  ( $1 \leq i \leq N$ ) transform, respectively, if any fluid  $k$  ( $1 \leq k \leq N$ ) is absent from the N-phase system.

Let us now look into how a given set of functions of  $\vec{c} = (c_1, \dots, c_N)$  defined on the N-phase system transforms if any one fluid  $k$  ( $1 \leq k \leq N$ ) is absent from the system. Intuitively, if these functions transform in a way similar to  $c_i$ , we say that they are reduction consistent. If they transform in a way similar to  $\tilde{\rho}_i$ , we say that they are reduction compatible.

More specifically, we consider the set of variables  $v_i^{(N)}(\vec{c}^{(N)})$  ( $1 \leq i \leq N$ ) defined on the N-phase system for all  $N = 1, 2, 3, \dots$ , and investigate their transformations if any fluid is absent from the N-phase system for  $N \geq 2$ . Similarly, we also study the transformations of the sets of variables  $v_{ij}^{(N)}(\vec{c}^{(N)})$  ( $1 \leq i, j \leq N; N \geq 1$ ) and  $v^{(N)}(\vec{c}^{(N)})$  ( $N \geq 1$ ) if any fluid is absent from the system. We define the reduction compatibility and reduction consistency of these sets of variables (or functions) as follows.

**Definition 2.1.** A set of variables  $v_i^{(N)}(\vec{c}^{(N)})$  ( $1 \leq i \leq N; N = 1, 2, 3, \dots$ ) is said to be reduction-compatible if for any  $N \geq 2$ , this set transforms as follows when any fluid  $k$  ( $1 \leq k \leq N$ ) is absent from the N-phase system:

$$v_i^{(N)} = \begin{cases} v_i^{(N-1)}, & 1 \leq i \leq k-1, \\ v_{i-1}^{(N-1)}, & k+1 \leq i \leq N, \end{cases} \quad (5)$$

where  $v_i^{(N)} = v_i^{(N)}(\vec{c}^{(N)})$  and  $v_i^{(N-1)} = v_i^{(N-1)}(\vec{c}^{(N-1)})$ , and  $\vec{c}^{(N)}$  and  $\vec{c}^{(N-1)}$  are connected by the correspondence relation (3).

**Definition 2.2.** A set of variables  $v_i^{(N)}(\vec{c}^{(N)})$  ( $1 \leq i \leq N; N = 1, 2, 3, \dots$ ) is said to be reduction-consistent if (i) this set is reduction-compatible, and (ii) for any  $N \geq 2$ , this set satisfies the following additional property when any fluid  $k$  ( $1 \leq k \leq N$ ) is absent from the N-phase system:

$$v_k^{(N)} = 0. \quad (6)$$

where  $v_k^{(N)} = v_k^{(N)}(\bar{c}^{(N)})$ .

**Definition 2.3.** A set of variables  $v_{ij}^{(N)}(\bar{c}^{(N)})$  ( $1 \leq i, j \leq N$ ;  $N = 1, 2, 3, \dots$ ) is said to be reduction-compatible if for any  $N \geq 2$ , this set transforms as follows when any fluid  $k$  ( $1 \leq k \leq N$ ) is absent from the  $N$ -phase system:

$$v_{ij}^{(N)} = \begin{cases} v_{ij}^{(N-1)}, & 1 \leq i \leq k-1, 1 \leq j \leq k-1, \\ v_{ij-1}^{(N-1)}, & 1 \leq i \leq k-1, k+1 \leq j \leq N, \\ v_{i-1j}^{(N-1)}, & k+1 \leq i \leq N, 1 \leq j \leq k-1, \\ v_{i-1j-1}^{(N-1)}, & k+1 \leq i \leq N, k+1 \leq j \leq N, \end{cases} \quad (7)$$

where  $v_{ij}^{(N)} = v_{ij}^{(N)}(\bar{c}^{(N)})$  and  $v_{ij}^{(N-1)} = v_{ij}^{(N-1)}(\bar{c}^{(N-1)})$ , and  $\bar{c}^{(N)}$  and  $\bar{c}^{(N-1)}$  are connected by the correspondence relation (3).

**Definition 2.4.** A set of variables  $v_{ij}^{(N)}(\bar{c}^{(N)})$  ( $1 \leq i, j \leq N$ ;  $N = 1, 2, 3, \dots$ ) is said to be reduction-consistent if (i) this set is reduction-compatible, and (ii) for any  $N \geq 2$ , this set satisfies the following additional property when any fluid  $k$  ( $1 \leq k \leq N$ ) is absent from the  $N$ -phase system:

$$v_{ki}^{(N)} = v_{ik}^{(N)} = 0, \quad 1 \leq i \leq N \quad (8)$$

where  $v_{ik}^{(N)} = v_{ik}^{(N)}(\bar{c}^{(N)})$  and  $v_{ki}^{(N)} = v_{ki}^{(N)}(\bar{c}^{(N)})$ .

**Definition 2.5.** A set of variables  $v^{(N)}(\bar{c}^{(N)})$  ( $N = 1, 2, 3, \dots$ ) is said to be reduction consistent if for any  $N \geq 2$ , it transforms as follows when any fluid  $k$  ( $1 \leq k \leq N$ ) is absent from the  $N$ -phase system:

$$v^{(N)}(\bar{c}^{(N)}) = v^{(N-1)}(\bar{c}^{(N-1)}) \quad (9)$$

where  $\bar{c}^{(N)}$  and  $\bar{c}^{(N-1)}$  are connected by the correspondence relation (3).

**Remark 1.** For a reduction-consistent set of functions  $v_i^{(N)}$  ( $1 \leq i \leq N$ ) defined on the  $N$ -phase system, if any fluid  $k$  ( $1 \leq k \leq N$ ) is absent from the  $N$ -phase system, then the  $k$ -th function in this set will vanish while the other  $(N-1)$  functions will reduce to the corresponding functions  $v_i^{(N-1)}$  ( $1 \leq i \leq N-1$ ) for the smaller  $(N-1)$ -phase system. For a reduction-consistent function  $v^{(N)}$  defined on the  $N$ -phase system, if any fluid  $k$  ( $1 \leq k \leq N$ ) is absent from the system, then this function will reduce to the corresponding function  $v^{(N-1)}$  for the smaller  $(N-1)$ -phase system. For example, according to the definitions  $\nabla^2 c_i$  ( $1 \leq i \leq N$ ) is a reduction-consistent set of variables, and  $\rho(\bar{c}) = \sum_{i=1}^N \tilde{\rho}_i c_i$  is a reduction-consistent function.

Based on the transformation properties of variables, we can look into how a given set of equations of the  $N$ -phase system transforms if any fluid  $k$  ( $1 \leq k \leq N$ ) is absent from the system. Specifically, we define the reduction consistency of a set of equations as follows.

**Definition 2.6.** A set of equations

$$v_i^{(N)}(\bar{c}^{(N)}) = 0, \quad 1 \leq i \leq N; \quad N = 1, 2, 3, \dots$$

is said to be reduction-consistent if the set of variables  $v_i^{(N)}(\bar{c}^{(N)})$  ( $1 \leq i \leq N$ ;  $N = 1, 2, 3, \dots$ ) is reduction-consistent.

**Definition 2.7.** A set of equations

$$v^{(N)}(\bar{c}^{(N)}) = 0, \quad N = 1, 2, 3, \dots \quad (10)$$

is said to be reduction-consistent if the set of variables  $v^{(N)}(\bar{c}^{(N)})$  ( $N = 1, 2, 3, \dots$ ) is reduction-consistent.

**Remark 2.** For a reduction-consistent set of equations  $v_i^{(N)} = 0$  ( $1 \leq i \leq N$ ) defined on the  $N$ -phase system, if any fluid  $k$  ( $1 \leq k \leq N$ ) is absent, then the  $k$ -th equation in this set will reduce to an identity and the other  $(N-1)$  equations will reduce to the corresponding equations  $v_i^{(N-1)} = 0$  ( $1 \leq i \leq N-1$ ) for the smaller  $(N-1)$ -phase system. For a reduction-consistent equation  $v^{(N)} = 0$  defined on the  $N$ -phase system, if any fluid  $k$  ( $1 \leq k \leq N$ ) is absent, then this equation will reduce to the corresponding equation  $v^{(N-1)} = 0$  for the smaller  $(N-1)$ -phase system.

We next write down some useful properties about the reduction-compatible and reduction-consistent variables/functions of the N-phase system. It is straightforward to verify these properties based on the definitions. In the following we omit the superscript ( $N$ ) and assume that the variables are defined for all N-phase systems ( $N = 1, 2, 3 \dots$ ). For example, the statement below “ $v_i(\vec{c})$  ( $1 \leq i \leq N$ ) is a reduction-consistent set of functions” refers to “ $v_i^{(N)}(\vec{c}^{(N)})$  ( $1 \leq i \leq N$ ;  $N = 1, 2, 3 \dots$ ) is a reduction-consistent set of functions” to be exact, and the statement below “ $v(\vec{c})$  is a reduction-consistent function” refers to “ $v^{(N)}(\vec{c}^{(N)})$  ( $N = 1, 2, 3 \dots$ ) is a reduction-consistent set of functions”, etc.

- (J1): Reduction consistency implies reduction compatibility. The reverse is not true.
- (J2): If  $v_i(\vec{c})$  ( $1 \leq i \leq N$ ) and  $w_i(\vec{c})$  ( $1 \leq i \leq N$ ) are two reduction-consistent sets of functions, then  $av_i(\vec{c}) + bw_i(\vec{c})$  ( $1 \leq i \leq N$ ) form a reduction-consistent set of functions, where  $a$  and  $b$  are constants. The same property holds for reduction consistent sets of functions  $v_{ij}(\vec{c})$  ( $1 \leq i, j \leq N$ ) and  $w_{ij}(\vec{c})$  ( $1 \leq i, j \leq N$ ).
- (J3): If  $v_i(\vec{c})$  ( $1 \leq i \leq N$ ) and  $w_i(\vec{c})$  ( $1 \leq i \leq N$ ) are two reduction-compatible sets of functions, then  $av_i(\vec{c}) + bw_i(\vec{c})$  ( $1 \leq i \leq N$ ) form a reduction-compatible set of functions with constants  $a$  and  $b$ . The same property holds for two reduction-compatible sets of functions  $v_{ij}(\vec{c})$  ( $1 \leq i, j \leq N$ ) and  $w_{ij}(\vec{c})$  ( $1 \leq i, j \leq N$ ).
- (J4): If  $v_i(\vec{c})$  ( $1 \leq i \leq N$ ) are a reduction-consistent set of functions and  $w_i(\vec{c})$  ( $1 \leq i \leq N$ ) are a reduction-compatible set of functions, then  $v_i(\vec{c})w_i(\vec{c})$  ( $1 \leq i \leq N$ ) form a reduction-consistent set of functions.
- (J5): If  $v(\vec{c})$  and  $w(\vec{c})$  are two reduction-consistent functions, then  $av(\vec{c}) + bw(\vec{c})$  is a reduction consistent function for constants  $a$  and  $b$ , and  $v(\vec{c})w(\vec{c})$  is also a reduction-consistent function.
- (J6): If  $v_i(\vec{c})$  ( $1 \leq i \leq N$ ) are a reduction-consistent set of functions and  $w(\vec{c})$  is a reduction-consistent function, then  $v_i(\vec{c})w(\vec{c})$  ( $1 \leq i \leq N$ ) form a reduction-consistent set of functions.
- (J7): If  $v_{ij}(\vec{c})$  ( $1 \leq i, j \leq N$ ) are a reduction-consistent set of functions, and  $w_i(\vec{c})$  ( $1 \leq i \leq N$ ) are a reduction-compatible set of functions, then  $\sum_{j=1}^N v_{ij}w_j$  ( $1 \leq i \leq N$ ) and  $\sum_{i=1}^N v_{ij}w_i$  ( $1 \leq j \leq N$ ) form two reduction-consistent sets of functions.
- (J8): If  $v_{ij}(\vec{c})$  ( $1 \leq i, j \leq N$ ) are a reduction-compatible set of functions, and  $w_i(\vec{c})$  ( $1 \leq i \leq N$ ) are a reduction-consistent set of functions, then  $\sum_{j=1}^N v_{ij}w_j$  ( $1 \leq i \leq N$ ) and  $\sum_{i=1}^N v_{ij}w_i$  ( $1 \leq j \leq N$ ) form two reduction-compatible sets of functions.
- (J9): If  $v_i(\vec{c})$  ( $1 \leq i \leq N$ ) are a reduction-consistent set of functions, then  $\sum_{i=1}^N v_i(\vec{c})$  is a reduction-consistent function.
- (J10): If  $v_{ij}(\vec{c})$  ( $1 \leq i, j \leq N$ ) are a reduction-consistent set of functions, then  $\sum_{j=1}^N v_{ij}(\vec{c})$  ( $1 \leq i \leq N$ ) and  $\sum_{i=1}^N v_{ij}(\vec{c})$  ( $1 \leq j \leq N$ ) are two reduction-consistent sets of functions, and  $\sum_{i,j=1}^N v_{ij}(\vec{c})$  is a reduction-consistent function.
- (J11): If  $v_{ij}(\vec{c})$  ( $1 \leq i, j \leq N$ ) are a reduction-compatible set of functions and  $w_i(\vec{c})$  ( $1 \leq i \leq N$ ) are a reduction-consistent set of functions, then  $\sum_{i,j=1}^N v_{ij}w_iw_j$  is a reduction-consistent function.
- (J12): If  $v_{ij}(\vec{c})$  ( $1 \leq i, j \leq N$ ) are a reduction-consistent set of functions and  $w_i(\vec{c})$  ( $1 \leq i \leq N$ ) are a reduction-compatible set of functions, then  $\sum_{i,j=1}^N v_{ij}w_iw_j$  is a reduction-consistent function.
- (J13): If  $v(\vec{c})$ ,  $v_i(\vec{c})$  ( $1 \leq i \leq N$ ), and  $v_{ij}(\vec{c})$  ( $1 \leq i, j \leq N$ ) are reduction-consistent (resp. reduction-compatible) sets of functions, then  $\mathcal{P}v$ ,  $\mathcal{P}v_i$  ( $1 \leq i \leq N$ ), and  $\mathcal{P}v_{ij}$  ( $1 \leq i, j \leq N$ ) are also reduction-consistent (resp. reduction-compatible) sets of functions, where  $\mathcal{P}$  stands for one of the operators  $\frac{\partial}{\partial t}$ ,  $\nabla$ , or  $\nabla^2$ . If  $v$ ,  $v_i$  and  $v_{ij}$  are vector functions, then  $\mathcal{P}$  can also be divergence and curl operators.
- (J14): If a function  $v$  is independent of  $\vec{c}$ , then it is a reduction consistent function.
- (J15):  $c_i$  ( $1 \leq i \leq N$ ) and  $\rho_i(\vec{c})$  ( $1 \leq i \leq N$ ) are two reduction-consistent sets of variables;  $\rho(\vec{c})$  and  $\mu(\vec{c})$  (given by (84) and (86)) are each a reduction-consistent function.

(J16):  $\tilde{\rho}_i$  ( $1 \leq i \leq N$ ) and  $\tilde{\mu}_i$  ( $1 \leq i \leq N$ ) are two reduction-compatible sets of variables.  $\sigma_{ij}$  ( $1 \leq i, j \leq N$ ) are a reduction-compatible set of variables.

A proof of the properties (J7)–(J12) is provided in the Appendix B.

Let us now consider how reduction-consistent functions transform if more than one fluid components are absent from the N-phase system. If any one fluid is absent from the system, then a reduction-consistent function  $v^{(N)}$  will reduce to the function  $v^{(N-1)}$  for the corresponding  $(N-1)$ -phase system. By repeatedly applying this property, we conclude that if  $K$  ( $1 \leq K \leq N-1$ ) fluid components are absent from the N-phase system then a reduction-consistent function  $v^{(N)}$  will reduce to the function  $v^{(N-K)}$  for the corresponding  $(N-K)$ -phase system.

Similarly, given a reduction-consistent set of functions  $v_i^{(N)}$  ( $1 \leq i \leq N$ ) for the N-phase system, if any one fluid is absent, then the function in this set with the index corresponding to the absent fluid will vanish identically while the other  $(N-1)$  functions will reduce to the functions  $v_i^{(N-1)}$  ( $1 \leq i \leq N-1$ ) for the corresponding  $(N-1)$ -phase system. By repeatedly applying this property to the resultant  $(N-1)$ -phase,  $(N-2)$ -phase,  $\dots$  systems, we conclude that if  $K$  ( $1 \leq K \leq N-1$ ) fluid components are absent from the N-phase system, then those  $K$  functions in this set with indices corresponding to the absent fluids will vanish identically while the other  $(N-K)$  functions will reduce to the functions  $v_i^{(N-K)}$  ( $1 \leq i \leq N-K$ ) for the corresponding  $(N-K)$ -phase system.

It then follows from the above discussions that, given a reduction-consistent set of equations for the N-phase system, if  $K$  ( $1 \leq K \leq N-1$ ) fluid components are absent from the system, then those  $K$  equations in this set with indices corresponding to the absent fluids will each reduce to an identity, while the other  $(N-K)$  equations will reduce to the corresponding equations for the smaller  $(N-K)$ -phase system.

## 2.2 Reduction Consistency of N-Phase Governing Equations

Let us now look into the reduction consistency of the governing equations given by (83a)–(83c) for the N-phase system ( $N = 1, 2, 3, \dots$ ), that is, how these equations transform if any fluid component is absent from the system. Define

$$\mathcal{M}(\vec{c}) = \rho(\vec{c}) \left( \frac{\partial \mathbf{u}}{\partial t} + \mathbf{u} \cdot \nabla \mathbf{u} \right) + \tilde{\mathbf{J}} \cdot \nabla \mathbf{u} + \nabla p - \nabla \cdot [\mu(\vec{c}) \mathbf{D}(\mathbf{u})] + \sum_{i=1}^N \nabla \cdot \left[ \nabla c_i \otimes \frac{\partial W}{\partial (\nabla c_i)} \right], \quad (11a)$$

$$\mathcal{N}(\vec{c}) = \nabla \cdot \mathbf{u}, \quad (11b)$$

$$\mathcal{F}_i(\vec{c}) = \frac{\partial c_i}{\partial t} + \mathbf{u} \cdot \nabla c_i - \sum_{j=1}^N \nabla \cdot \left[ m_{ij}(\vec{c}) \nabla \left( \frac{\partial W}{\partial c_j} - \nabla \cdot \frac{\partial W}{\partial \nabla c_j} \right) \right], \quad 1 \leq i \leq N, \quad (11c)$$

$$\mathcal{H}_i(\vec{c}) = \frac{\partial W}{\partial c_i}, \quad 1 \leq i \leq N, \quad (11d)$$

$$\mathcal{G}_i(\vec{c}) = \frac{\partial W}{\partial (\nabla c_i)}, \quad 1 \leq i \leq N, \quad (11e)$$

$$\mathcal{J}_i(\vec{c}) = \nabla \cdot \frac{\partial W}{\partial (\nabla c_i)}, \quad 1 \leq i \leq N. \quad (11f)$$

We have the following result.

**Theorem 2.1.** *If*

- $m_{ij}(\vec{c})$  ( $1 \leq i, j \leq N$ ) are a reduction-consistent set of variables,
- $\mathcal{H}_i(\vec{c})$  ( $1 \leq i \leq N$ ) are a reduction-compatible set of variables, and
- $\mathcal{G}_i(\vec{c})$  ( $1 \leq i \leq N$ ) are a reduction-compatible set of variables,

then

- Equation (83a) is a reduction-consistent equation;
- Equation (83b) is a reduction-consistent equation;
- The  $N$  equations in (83c) are a reduction-consistent set of equations.

A proof of this theorem is provided in Appendix C.

**Remark 3.** This theorem provides a set of sufficient conditions for the reduction consistency of the  $N$ -phase governing equations. If one can choose a reduction-consistent set of functions for the coefficients  $m_{ij}(\vec{c})$ , and choose a free energy density function  $W(\vec{c}, \nabla\vec{c})$  such that  $\mathcal{H}_i(\vec{c})$  and  $\mathcal{G}_i(\vec{c})$  each forms a reduction-compatible set of variables, then the theorem guarantees that the resultant  $N$ -phase governing equations are reduction consistent. In other words, if  $K$  fluids ( $1 \leq K \leq N - 1$ ) are absent from the  $N$ -phase system, then the  $N$ -phase governing equations will exactly reduce to the  $(N - K)$ -phase governing equations that correspond to the  $(N - K)$ -phase system formed by those  $(N - K)$  fluids that are present, together with  $K$  additional identities, identically satisfied by the zero volume-fraction fields corresponding to the absent fluids.

**Remark 4.** Suppose the free energy density function takes the following form

$$W(\vec{c}, \nabla\vec{c}) = \sum_{i,j=1}^N \frac{\lambda_{ij}}{2} \nabla c_i \cdot \nabla c_j + (\text{multiwell potential term})$$

where the constants  $\lambda_{ij}$  are called the mixing energy density coefficients (symmetric), and can be related to other physical parameters such as the pairwise surface tensions by invoking the consistency condition (C1) (see e.g. [15, 16]). The multiwell potential term is assumed to be independent of  $\nabla\vec{c}$ . Then  $\mathcal{G}_i(\vec{c}) = \sum_{j=1}^N \lambda_{ij} \nabla c_j$  ( $1 \leq i \leq N$ ). Therefore, if  $\lambda_{ij}$  ( $1 \leq i, j \leq N$ ) are a reduction-compatible set,  $\mathcal{G}_i(\vec{c})$  ( $1 \leq i \leq N$ ) will be a reduction-compatible set of variables according to the property (T8) from Section 2.1. Similarly, if the free energy density function takes the form

$$W(\vec{c}, \nabla\vec{c}) = \sum_{i=1}^N \frac{\lambda_i}{2} |\nabla c_i|^2 + (\text{multiwell potential term})$$

where  $\lambda_i$  are constants, then  $\mathcal{G}_i(\vec{c}) = \lambda_i \nabla c_i$  ( $1 \leq i \leq N$ ). If  $\lambda_i$  ( $1 \leq i \leq N$ ) is a reduction-compatible set,  $\mathcal{G}_i(\vec{c})$  ( $1 \leq i \leq N$ ) will form a reduction-consistent (and thus also reduction-compatible) set of variables according to property (T4) from Section 2.1.

We next suggest a specific form for  $m_{ij}(\vec{c})$  and for  $W(\vec{c}, \nabla\vec{c})$  that satisfy the conditions for Theorem 2.1. Let  $f(c)$  denote a non-negative continuous function with the property

$$\begin{cases} f(c) = 0, & \text{if } c \leq 0; \\ f(c) > 0, & \text{if } c > 0. \end{cases} \quad (12)$$

In the current work we will use the following function for  $f(c)$ ,

$$f(c) = \begin{cases} 0, & \text{if } c < 0 \\ 2c, & \text{if } c \geq 0. \end{cases} \quad (13)$$

Let  $\tilde{m}_{ij}$  ( $1 \leq i, j \leq N$ ) denote a set of non-negative constants with the property  $\tilde{m}_{ij} = \tilde{m}_{ji}$  ( $1 \leq i, j \leq N$ ) and  $\tilde{m}_{ii} = 0$  ( $1 \leq i \leq N$ ), and that they form a reduction-compatible set of variables for  $N = 1, 2, 3, \dots$ . Some specific examples for such a set of constants are  $\tilde{m}_{ij} = \tilde{\rho}_i \tilde{\rho}_j (1 - \delta_{ij})$ ,  $\tilde{\mu}_i \tilde{\mu}_j (1 - \delta_{ij})$ , or  $\sigma_{ij}$ , where  $\delta_{ij}$  denotes the Kronecker delta. In this work we use the following  $\tilde{m}_{ij}$ ,

$$\tilde{m}_{ij} = m_0(1 - \delta_{ij}) = \begin{cases} m_0, & 1 \leq i \neq j \leq N, \\ 0, & 1 \leq i = j \leq N \end{cases} \quad (14)$$

where  $m_0 > 0$  is a positive constant. These  $\tilde{m}_{ij}$  can be shown to form a reduction-compatible set in a straightforward fashion based on the definition. We then define  $m_{ij}(\vec{c})$  as follows,

$$\begin{cases} m_{ij}(\vec{c}) = -\tilde{m}_{ij}f(c_i)f(c_j), & 1 \leq i \neq j \leq N \\ m_{ii}(\vec{c}) = -\sum_{\substack{j=1 \\ j \neq i}}^N m_{ij}(\vec{c}) = f(c_i) \sum_{\substack{j=1 \\ j \neq i}}^N \tilde{m}_{ij}f(c_j), & 1 \leq i \leq N. \end{cases} \quad (15)$$

Note that  $m_{ij}(\vec{c})$  ( $1 \leq i, j \leq N$ ) as defined above satisfy the conditions (80) and (82). So the matrix  $\mathbf{m}$  (see equation (79)) formed by these  $m_{ij}(\vec{c})$  is symmetric positive semi-definite.

For the free energy density function we consider the following form

$$W(\vec{c}, \nabla \vec{c}) = \sum_{i,j=1}^N \frac{\lambda_{ij}}{2} \nabla c_i \cdot \nabla c_j + \beta \sum_{i,j=1}^N \frac{\sigma_{ij}}{2} [g(c_i) + g(c_j) - g(c_i + c_j)] \quad (16)$$

where

$$\begin{cases} \lambda_{ij} = -\frac{3}{\sqrt{2}} \eta \sigma_{ij}, & 1 \leq i, j \leq N, \\ \beta = \frac{3}{\sqrt{2}} \frac{1}{\eta}, \\ g(c) = c^2(1-c)^2 \end{cases} \quad (17)$$

and  $\eta$  is the scale of characteristic interfacial thickness of the diffuse interfaces. We assume that the values for the pairwise surface tensions  $\sigma_{ij}$  among the  $N$  fluids are such that the  $N \times N$  symmetric matrix formed by  $\lambda_{ij}$  is positive semi-definite in order to ensure the non-negativity of the first term on the right hand side of (16). This free energy density function is equivalent to a form originally suggested in [8].

With the  $m_{ij}(\vec{c})$  and  $W(\vec{c}, \nabla \vec{c})$  defined above, we have the following result:

**Theorem 2.2.** (a) The functions  $m_{ij}(\vec{c})$  ( $1 \leq i, j \leq N$ ) as defined by (15) are a reduction-consistent set of functions. (b) The free energy density function  $W(\vec{c}, \nabla \vec{c})$  defined in (16) is a reduction-consistent function. (c) With  $W(\vec{c}, \nabla \vec{c})$  given by (16), the functions  $\mathcal{H}_i(\vec{c})$  ( $1 \leq i \leq N$ ) as defined by (11d) and the functions  $\mathcal{G}_i(\vec{c})$  ( $1 \leq i \leq N$ ) as defined by (11e) are each a reduction-compatible set of functions.

A proof of this theorem is provided in Appendix D.

We conclude based on Theorems 2.1 and 2.2 that, with  $m_{ij}(\vec{c})$  given by (15) and  $W(\vec{c}, \nabla \vec{c})$  given by (16), the N-phase governing equations (83a)–(83c) are fully reduction-consistent. With these forms for  $m_{ij}(\vec{c})$  and  $W(\vec{c}, \nabla \vec{c})$ , equations (83a) and (83c) are transformed into

$$\rho(\vec{c}) \left( \frac{\partial \mathbf{u}}{\partial t} + \mathbf{u} \cdot \nabla \mathbf{u} \right) + \tilde{\mathbf{J}} \cdot \nabla \mathbf{u} = -\nabla p + \nabla \cdot [\mu(\vec{c}) \mathbf{D}(\mathbf{u})] - \sum_{i,j=1}^N \nabla \cdot (\lambda_{ij} \nabla c_i \otimes \nabla c_j), \quad (18)$$

$$\frac{\partial c_i}{\partial t} + \mathbf{u} \cdot \nabla c_i = \sum_{j=1}^N \nabla \cdot \left[ m_{ij}(\vec{c}) \nabla \left( -\sum_{k=1}^N \lambda_{jk} \nabla^2 c_k + \mathcal{H}_j(\vec{c}) \right) \right], \quad 1 \leq i \leq N, \quad (19)$$

where  $\rho(\vec{c})$  and  $\mu(\vec{c})$  are given by (84) and (86), respectively,  $\lambda_{ij}$  ( $1 \leq i, j \leq N$ ) are given in (17), and

$$\begin{cases} \tilde{\mathbf{J}} = -\sum_{i,j=1}^N \tilde{\rho}_i m_{ij}(\vec{c}) \nabla \left[ -\sum_{k=1}^N \lambda_{jk} \nabla^2 c_k + \mathcal{H}_j(\vec{c}) \right], \\ \mathcal{H}_i(\vec{c}) = \frac{\partial W}{\partial c_i} = \beta \sum_{j=1}^N \sigma_{ij} [g'(c_i) - g'(c_i + c_j)], \quad 1 \leq i \leq N. \end{cases} \quad (20)$$

The N-phase formulation represented by (18), (83b) and (19) fully satisfies the reduction consistency conditions (C1) and (C2). This formulation is reduction-consistent and thermodynamically consistent.

**Remark 5.** The  $m_{ij}(\vec{c})$  and  $W(\vec{c}, \nabla \vec{c})$  functions suggested above are only one way to fulfill the conditions of Theorem 2.1. We would like to point out that it is possible to choose other forms for  $f(c)$ , the constants  $\tilde{m}_{ij}$ , or the free energy density function  $W(\vec{c}, \nabla \vec{c})$  to satisfy these conditions, thus leading to other reduction-consistent and thermodynamically consistent  $N$ -phase formulations. For example, the free energy density form (analogous to the one from [15])  $W(\vec{c}, \nabla \vec{c}) = \sum_{i,j=1}^N \frac{\Lambda_{ij}}{2} \nabla c_i \cdot \nabla c_j + b \sum_{i=1}^N c_i^2 (1 - c_i)^2$ , where  $\Lambda_{ij} \sim -\sigma_{ij}^2$  ( $1 \leq i, j \leq N$ ) and  $b$  is some constant, also leads to  $\mathcal{H}_i(\vec{c})$  and  $\mathcal{G}_i(\vec{c})$  functions that are reduction compatible. One can also employ for example

$$f(c) = \begin{cases} 0, & c < 0 \\ (2c)^k, & c \geq 0 \end{cases} \quad (k \geq 2 \text{ is an integer}), \quad \text{or } f(c) = \begin{cases} 0, & c < 0 \\ 1 - \cos(\pi c), & 0 \leq c \leq 1 \\ 2, & c > 1, \end{cases}$$

which leads to a reduction-consistent set of  $m_{ij}(\vec{c})$  as defined in (15).

**Remark 6.** If  $m_{ij}(\vec{c})$  ( $1 \leq i, j \leq N$ ) are assumed to be all constants and are not identically zeros, then based on Definition 2.4  $m_{ij}$  ( $1 \leq i, j \leq N$ ) cannot be a reduction-consistent set. Therefore, in this case one has to treat the term  $\sum_{j=1}^N m_{ij} \nabla [\mathcal{H}_i(\vec{c}) - \mathcal{J}_i(\vec{c})]$  in  $\mathcal{F}_i(\vec{c})$  as a whole, and try to construct  $W(\vec{c}, \nabla \vec{c})$  such that this expression results in a reduction-consistent set. This is essentially the approach taken by [8, 16], and it is extremely difficult (if not impossible) to construct such a  $W(\vec{c}, \nabla \vec{c})$  to ensure **full reduction consistency**. So far, only a partial reduction consistency (e.g. between  $N$  phases and two phases) can be achieved with this approach for an arbitrary set of given pairwise surface tension values [16, 8].

### 3 Numerical Algorithm and Implementation

We now look into how to numerically solve the reduction-consistent and thermodynamically consistent  $N$ -phase governing equations. Let  $\Omega$  denote the flow domain, and  $\partial\Omega$  denote its boundary. On  $\partial\Omega$  we assume that the velocity distribution is known,

$$\mathbf{u} = \mathbf{w}(\mathbf{x}, t), \quad \text{on } \partial\Omega \quad (21)$$

where  $\mathbf{w}$  is the boundary velocity. We consider the following boundary conditions for the volume fractions  $c_i$ ,

$$\sum_{j=1}^N m_{ij}(\vec{c}) \mathbf{n} \cdot \nabla \left[ - \sum_{k=1}^N \lambda_{jk} \nabla^2 c_k + \mathcal{H}_j(\vec{c}) \right] = 0, \quad 1 \leq i \leq N, \quad \text{on } \partial\Omega, \quad (22a)$$

$$\mathbf{n} \cdot \nabla c_i = 0, \quad 1 \leq i \leq N, \quad \text{on } \partial\Omega, \quad (22b)$$

where  $\mathbf{n}$  is the outward-pointing unit vector normal to  $\partial\Omega$ . The boundary conditions (22a) and (22b) correspond to a wall with neutral wettability (i.e. 90-degree contact angle) for all the fluid interfaces. We further assume that the distributions of the velocity  $\mathbf{u}$  and the volume fractions  $c_i$  at  $t = 0$  are known

$$\mathbf{u}(\mathbf{x}, 0) = \mathbf{u}_{in}(\mathbf{x}), \quad (23a)$$

$$c_i(\mathbf{x}, 0) = c_i^{in}(\mathbf{x}), \quad 1 \leq i \leq N \quad (23b)$$

where  $\mathbf{u}_{in}$  and  $c_i^{in}$  are the initial velocity and volume fractions.

One notes that the boundary condition (21) is a reduction-consistent equation. The  $N$  equations given in the boundary condition (22a) form a reduction-consistent set of equations, and the  $N$  equations given in (22b) also form a reduction-consistent set. Therefore, the boundary conditions (21), (22a) and (22b) satisfy the reduction consistency property (C3).

The equations (18), (83b) and (19), supplemented by the boundary conditions (21)–(22b) and initial conditions (23a)–(23b), together constitute the system to be solved in numerical simulations. Note that among the  $N$  phase field equations in (19) only  $(N - 1)$  equations are independent in light of (56) and (80). Similarly, only  $(N - 1)$  equations in the boundary condition (22a) and in (22b) are independent.

We will employ the first  $(N - 1)$  equations in (19) and in (22a)–(22b) to solve for the volume fractions  $c_i$  ( $1 \leq i \leq N - 1$ ), and then compute  $c_N$  using the relation (56).

To facilitate subsequent discussions, we re-write equation (18) in an equivalent form

$$\frac{\partial \mathbf{u}}{\partial t} + \mathbf{u} \cdot \nabla \mathbf{u} + \frac{1}{\rho} \tilde{\mathbf{J}} \cdot \nabla \mathbf{u} = -\frac{1}{\rho} \nabla P + \frac{\mu}{\rho} \nabla^2 \mathbf{u} + \frac{1}{\rho} \nabla \mu \cdot \mathbf{D}(\mathbf{u}) - \frac{1}{\rho} \sum_{i,j=1}^N \lambda_{ij} \nabla^2 c_j \nabla c_i + \frac{1}{\rho} \mathbf{f}(\mathbf{x}, t), \quad (24)$$

where  $P = p + \sum_{i,j=1}^N \frac{\lambda_{ij}}{2} \nabla c_i \cdot \nabla c_j$  is an auxiliary pressure, which hereafter will also be loosely referred to as the pressure, and we have added an external body force  $\mathbf{f}(\mathbf{x}, t)$ . We re-write the first  $(N - 1)$  equations in (19) as

$$\frac{\partial c_i}{\partial t} + \mathbf{u} \cdot \nabla c_i = \sum_{j=1}^N \nabla \cdot \left[ m_{ij}(\vec{c}) \nabla \left( -\sum_{k=1}^N \lambda_{jk} \nabla^2 c_k + \mathcal{H}_j(\vec{c}) \right) \right] + d_i(\mathbf{x}, t), \quad 1 \leq i \leq N - 1, \quad (25)$$

where we have added in each equation a source term  $d_i(\mathbf{x}, t)$  ( $1 \leq i \leq N - 1$ ), which is a prescribed function for the purpose of numerical testing only and will be set to  $d_i = 0$  in actual simulations. We re-write the boundary conditions (first  $(N - 1)$  equations) (22a)–(22b) as follows:

$$\sum_{j=1}^N m_{ij}(\vec{c}) \mathbf{n} \cdot \nabla \left[ -\sum_{k=1}^N \lambda_{jk} \nabla^2 c_k + \mathcal{H}_j(\vec{c}) \right] = d_{ai}(\mathbf{x}, t), \quad 1 \leq i \leq N - 1, \quad \text{on } \partial\Omega, \quad (26a)$$

$$\mathbf{n} \cdot \nabla c_i = d_{bi}(\mathbf{x}, t), \quad 1 \leq i \leq N - 1, \quad \text{on } \partial\Omega, \quad (26b)$$

where  $d_{ai}(\mathbf{x}, t)$  ( $1 \leq i \leq N - 1$ ) and  $d_{bi}(\mathbf{x}, t)$  ( $1 \leq i \leq N - 1$ ) are prescribed source terms on  $\partial\Omega$  for the purpose of numerical testing only, and will be set to  $d_{ai} = 0$  and  $d_{bi} = 0$  in actual simulations. In these equations  $m_{ij}(\vec{c})$  are given by (15), in which  $\tilde{m}_{ij}$  are given by (14) and  $f(c)$  is defined by (13).  $\lambda_{ij}$  are given in (17), and  $\tilde{\mathbf{J}}$  and  $\mathcal{H}_i(\vec{c})$  are given in (20).

The numerical algorithm presented below is for the equations (24), (83b) and (25), together with the boundary conditions (21), (26a) and (26b).

The momentum equations (24) and (83b) have the same structure as those encountered in previous works [12, 16]. Therefore they can be solved using the algorithm we developed in [12, 16] for the momentum equations. For the sake of completeness, we provide a summary of the scheme for the momentum equations in Appendix E. This is a semi-implicit splitting type algorithm. The computations for the pressure and velocity are de-coupled with this scheme, and it involves only constant and time-independent coefficient matrices for both the pressure and the velocity linear algebraic systems after discretization.

We present below an algorithm for numerically solving the set of phase field equations (25), together with the boundary conditions (26a) and (26b). The variable nature of the coefficients  $m_{ij}(\vec{c})$  ( $1 \leq i, j \leq N$ ) is a new feature compared with those encountered in [12, 15, 16], and must be dealt with in an appropriate way.

Let  $n \geq 0$  denote the time step index and  $\Delta t$  the time step size. We use  $(\cdot)^n$  to represent the variable  $(\cdot)$  at time step  $n$ . Let  $J$  ( $J = 1$  or  $2$ ) denote the temporal order of accuracy of the algorithm, and

$$\mathbf{R}_i(\vec{c}) = \sum_{j=1}^N m_{ij}(\vec{c}) \nabla \left[ -\sum_{k=1}^N \lambda_{jk} \nabla^2 c_k + \mathcal{H}_j(\vec{c}) \right], \quad 1 \leq i \leq N. \quad (27)$$

Given  $(\mathbf{u}^n, c_i^n)$ , we solve for  $c_i^{n+1}$  with the algorithm as follows,

$$\frac{\gamma_0 c_i^{n+1} - \hat{c}_i}{\Delta t} + \mathbf{u}^{*,n+1} \cdot \nabla c_i^{*,n+1} = \mathcal{K}_0 \nabla^2 \left[ -\nabla^2 (c_i^{n+1} - c_i^{*,n+1}) + S(c_i^{n+1} - c_i^{*,n+1}) \right] + \nabla \cdot \mathbf{R}_i(\vec{c}^{*,n+1}) + d_i^{n+1}, \quad 1 \leq i \leq N - 1, \quad (28a)$$

$$\mathcal{K}_0 \mathbf{n} \cdot \nabla \left[ -\nabla^2 (c_i^{n+1} - c_i^{*,n+1}) + S(c_i^{n+1} - c_i^{*,n+1}) \right] + \mathbf{n} \cdot \mathbf{R}_i(\vec{c}^{*,n+1}) = d_{ai}^{n+1}, \quad 1 \leq i \leq N - 1, \quad \text{on } \partial\Omega, \quad (28b)$$

$$\mathbf{n} \cdot \nabla c_i^{n+1} = d_{b_i}^{n+1}, \quad 1 \leq i \leq N-1, \quad \text{on } \partial\Omega. \quad (28c)$$

If  $\chi$  denotes a generic variable, then in the above equations  $\frac{1}{\Delta t}(\gamma_0 \chi^{n+1} - \hat{\chi})$  represents an approximation of  $\left. \frac{\partial \chi}{\partial t} \right|^{n+1}$  with the  $J$ -th order backward differentiation formula (BDF), with  $\gamma_0$  and  $\hat{\chi}$  given by

$$\hat{\chi} = \begin{cases} \chi^n, & J = 1, \\ 2\chi^n - \frac{1}{2}\chi^{n-1}, & J = 2; \end{cases} \quad \gamma_0 = \begin{cases} 1, & J = 1, \\ 3/2, & J = 2. \end{cases} \quad (29)$$

$\chi^{*,n+1}$  denotes a  $J$ -th order explicit approximation of  $\chi^{n+1}$  given by

$$\chi^{*,n+1} = \begin{cases} \chi^n, & J = 1, \\ 2\chi^n - \chi^{n-1}, & J = 2. \end{cases} \quad (30)$$

The positive constant  $\mathcal{K}_0$  is given by

$$\mathcal{K}_0 = Nm_0 \left| \sum_{i,j=1}^N \lambda_{ij} \right|. \quad (31)$$

$S$  is a chosen constant, which must satisfy a condition to be specified later.  $\bar{c}^{*,n+1}$  is defined by  $\bar{c}^{*,n+1} = (c_1^{*,n+1}, \dots, c_N^{*,n+1})$ .

The key construction in the above algorithm lies in the two extra terms in the semi-discretized phase-field equations (28a) and in the boundary conditions (28b),  $\mathcal{K}_0 \nabla^2 [\nabla^2 (c_i^{n+1} - c_i^{*,n+1})]$  and  $\mathcal{K}_0 S \nabla^2 (c_i^{n+1} - c_i^{*,n+1})$ , and the explicit treatment of the  $\nabla \cdot \mathbf{R}_i(\bar{c})$  term. Note that the two extra terms are both equivalent to zeros, to the  $J$ -th order accuracy. With these treatments the computations for different volume fractions  $c_i$  ( $1 \leq i \leq N-1$ ) are de-coupled. Moreover, for each  $c_i$  the extra terms in the algorithm allow us to transform the equation of a 4-th spatial order into two *de-coupled* 2nd-order equations, which will become clear below.

Equation (28a) can be written as

$$\begin{aligned} \frac{\gamma_0}{\mathcal{K}_0 \Delta t} c_i^{n+1} + \nabla^2 (\nabla^2 c_i^{n+1}) - S \nabla^2 c_i^{n+1} = Z_i = Q_i + \nabla^2 (\nabla^2 c_i^{*,n+1}) - S \nabla^2 c_i^{*,n+1} \\ + \frac{1}{\mathcal{K}_0} \nabla \cdot \mathbf{R}_i(\bar{c}^{*,n+1}), \quad 1 \leq i \leq N-1, \end{aligned} \quad (32)$$

where

$$Q_i = \frac{1}{\mathcal{K}_0} \left( d_i^{n+1} + \frac{\hat{c}_i}{\Delta t} - \mathbf{u}^{*,n+1} \cdot \nabla c_i^{*,n+1} \right), \quad 1 \leq i \leq N-1. \quad (33)$$

Each of the above equations has a form similar to that encountered in two-phase flows (see e.g. [19]). Therefore each of them can be transformed into two de-coupled Helmholtz-type equations using the same idea as in two-phase flows [19]. By adding/subtracting a term  $\alpha \nabla^2 c_i^{n+1}$  ( $\alpha$  denoting a constant to be determined) on the left hand side (LHS), we can transform (32) into

$$\nabla^2 [\nabla^2 c_i^{n+1} + \alpha c_i^{n+1}] - (\alpha + S) \left[ \nabla^2 c_i^{n+1} - \frac{\gamma_0}{(\alpha + S) \mathcal{K}_0 \Delta t} c_i^{n+1} \right] = Z_i, \quad 1 \leq i \leq N-1. \quad (34)$$

By requiring that  $\alpha = -\frac{\gamma_0}{(\alpha + S) \mathcal{K}_0 \Delta t}$ , we obtain

$$\alpha = \frac{1}{2} \left[ -S + \sqrt{S^2 - \frac{4\gamma_0}{\mathcal{K}_0 \Delta t}} \right], \quad \text{and the condition } S \geq \sqrt{\frac{4\gamma_0}{\mathcal{K}_0 \Delta t}}. \quad (35)$$

The chosen constant  $S$  must satisfy the above condition.

Therefore, equation (34) can be written equivalently as

$$\nabla^2 \psi_i^{n+1} - (\alpha + S) \psi_i^{n+1} = Z_i, \quad 1 \leq i \leq N-1, \quad (36a)$$

$$\nabla^2 c_i^{n+1} + \alpha c_i^{n+1} = \psi_i^{n+1}, \quad 1 \leq i \leq N-1, \quad (36b)$$

where  $\psi_i^{n+1}$  ( $1 \leq i \leq N-1$ ) are auxiliary variables and are defined by equation (36b). The two equations (36a) and (36b) are Helmholtz type equations, and they can be solved in a de-coupled fashion. Note that under the condition for  $S$  given in (35),  $\alpha < 0$  and  $\alpha + S > 0$ . In order to solve (34), one can first solve (36a) for  $\psi_i^{n+1}$  and then solve (36b) for  $c_i^{n+1}$ .

In light of equation (36b), the boundary condition (28b) can be transformed into

$$\begin{aligned} \mathbf{n} \cdot \nabla \psi_i^{n+1} - (\alpha + S) \mathbf{n} \cdot \nabla c_i^{n+1} &= \mathbf{n} \cdot \nabla \left( \nabla^2 c_i^{*,n+1} - S c_i^{*,n+1} \right) \\ &\quad + \frac{1}{\mathcal{K}_0} \mathbf{n} \cdot \mathbf{R}_i(\bar{\mathbf{c}}^{*,n+1}) - \frac{1}{\mathcal{K}_0} d_{ai}^{n+1}, \quad 1 \leq i \leq N-1. \end{aligned} \quad (37)$$

By using (28c) we can further transform the above equation into

$$\begin{aligned} \mathbf{n} \cdot \nabla \psi_i^{n+1} &= \mathbf{n} \cdot \nabla \left( \nabla^2 c_i^{*,n+1} - S c_i^{*,n+1} \right) + \frac{1}{\mathcal{K}_0} \mathbf{n} \cdot \mathbf{R}_i(\bar{\mathbf{c}}^{*,n+1}) \\ &\quad + (\alpha + S) d_{bi}^{n+1} - \frac{1}{\mathcal{K}_0} d_{ai}^{n+1}, \quad 1 \leq i \leq N-1. \end{aligned} \quad (38)$$

These are the boundary conditions for the auxiliary variables  $\psi_i^{n+1}$  ( $1 \leq i \leq N-1$ ).

We employ the spectral element method [33, 25, 40] for spatial discretizations in this work. Let us now consider how to implement the above algorithm using  $C^0$  spectral elements. We first derive the weak forms for the equations (36a) and (36b), by assuming that all variables are in the continuum space. Then we restrict the test and trial functions to the appropriate function space for spatial discretization of the weak forms.

Let  $\varphi(\mathbf{x})$  denote an arbitrary (test) function. Multiply  $\varphi$  to equation (36a) and integrate over the flow domain  $\Omega$ , and we get

$$\begin{aligned} &\int_{\Omega} \nabla \psi_i^{n+1} \cdot \nabla \varphi + (\alpha + S) \int_{\Omega} \psi_i^{n+1} \varphi \\ &= - \int_{\Omega} Q_i \varphi + \int_{\Omega} \left[ \nabla \left( \nabla^2 c_i^{*,n+1} - S c_i^{*,n+1} \right) + \frac{1}{\mathcal{K}_0} \mathbf{R}_i(\bar{\mathbf{c}}^{*,n+1}) \right] \cdot \nabla \varphi \\ &\quad + \int_{\partial\Omega} \left[ \mathbf{n} \cdot \nabla \psi_i^{n+1} - \mathbf{n} \cdot \nabla \left( \nabla^2 c_i^{*,n+1} - S c_i^{*,n+1} \right) - \frac{1}{\mathcal{K}_0} \mathbf{n} \cdot \mathbf{R}_i(\bar{\mathbf{c}}^{*,n+1}) \right] \varphi, \\ &\quad \forall \varphi, \quad 1 \leq i \leq N-1 \end{aligned} \quad (39)$$

where we have used integration by part and the divergence theorem. In light of the equations (36b) and (38), we can transform the above equation into the final weak form about  $\psi_i^{n+1}$ ,

$$\begin{aligned} &\int_{\Omega} \nabla \psi_i^{n+1} \cdot \nabla \varphi + (\alpha + S) \int_{\Omega} \psi_i^{n+1} \varphi \\ &= - \int_{\Omega} Q_i \varphi + \int_{\Omega} \left[ \nabla \left( \psi_i^{*,n+1} - (\alpha + S) c_i^{*,n+1} \right) \right. \\ &\quad \left. + \frac{1}{\mathcal{K}_0} \sum_{j=1}^N m_{ij}(\bar{\mathbf{c}}^{*,n+1}) \nabla \left( - \sum_{k=1}^N \lambda_{jk} \left( \psi_k^{*,n+1} - \alpha c_k^{*,n+1} \right) + \mathcal{H}_j(\bar{\mathbf{c}}^{*,n+1}) \right) \right] \cdot \nabla \varphi \\ &\quad + \int_{\partial\Omega} \left[ (\alpha + S) d_{bi}^{n+1} - \frac{1}{\mathcal{K}_0} d_{ai}^{n+1} \right] \varphi, \quad \forall \varphi, \quad 1 \leq i \leq N-1, \end{aligned} \quad (40)$$

where  $\psi_N^n$  is defined by  $\psi_N^n = \nabla^2 c_N^n + \alpha c_N^n$ .

Multiplying the test function  $\varphi$  to equation (36b) and integrating over the domain  $\Omega$ , we get the weak form about  $c_i^{n+1}$ ,

$$\int_{\Omega} \nabla c_i^{n+1} \cdot \nabla \varphi - \alpha \int_{\Omega} c_i^{n+1} \varphi = - \int_{\Omega} \psi_i^{n+1} \varphi + \int_{\partial\Omega} d_{bi}^{n+1} \varphi, \quad \forall \varphi, \quad 1 \leq i \leq N-1, \quad (41)$$

where we have used the divergence theorem and the boundary condition (28c).

We discretize the domain  $\Omega$  using a mesh of  $N_{el}$  non-overlapping conforming spectral elements. We use the positive integer  $K$  to denote the element order, which is a measure of the highest polynomial degree in field expansions within an element. Let  $\Omega_h$  denote the discretized domain, and  $\Omega_h^e$  ( $1 \leq e \leq N_{el}$ ) denote the element  $e$ . Define function space

$$H_\phi = \{ v \in H^1(\Omega_h) : v \text{ is a polynomial of degree characterized by } K \text{ on } \Omega_h^e, \text{ for } 1 \leq e \leq N_{el} \}. \quad (42)$$

In the following let the subscript in  $(\cdot)_h$  denote the discretized version of the variable  $(\cdot)$ . The fully discretized equations are:

For  $\psi_{hi}^{n+1}$ : find  $\psi_{hi}^{n+1} \in H_\phi$  such that

$$\begin{aligned} & \int_{\Omega_h} \nabla \psi_{hi}^{n+1} \cdot \nabla \varphi_h + (\alpha + S) \int_{\Omega_h} \psi_{hi}^{n+1} \varphi_h \\ &= - \int_{\Omega_h} Q_{hi} \varphi_h + \int_{\Omega_h} \left[ \nabla \left( \psi_{hi}^{*,n+1} - (\alpha + S) c_{hi}^{*,n+1} \right) \right. \\ & \quad \left. + \frac{1}{\mathcal{K}_0} \sum_{j=1}^N m_{hij} (\bar{c}_h^{*,n+1}) \nabla \left( - \sum_{k=1}^N \lambda_{jk} \left( \psi_{hk}^{*,n+1} - \alpha c_{hk}^{*,n+1} \right) + \mathcal{H}_{hj}(\bar{c}_h^{*,n+1}) \right) \right] \cdot \nabla \varphi_h \\ & \quad + \int_{\partial\Omega_h} \left[ (\alpha + S) d_{bhi}^{n+1} - \frac{1}{\mathcal{K}_0} d_{ahi}^{n+1} \right] \varphi_h, \quad \forall \varphi_h \in H_\phi, \quad 1 \leq i \leq N-1. \end{aligned} \quad (43)$$

For  $c_{hi}^{n+1}$ : find  $c_{hi}^{n+1} \in H_\phi$  such that

$$\int_{\Omega_h} \nabla c_{hi}^{n+1} \cdot \nabla \varphi_h - \alpha \int_{\Omega_h} c_{hi}^{n+1} \varphi_h = - \int_{\Omega_h} \psi_{hi}^{n+1} \varphi_h + \int_{\partial\Omega_h} d_{bhi}^{n+1} \varphi_h, \quad \forall \varphi_h \in H_\phi, \quad 1 \leq i \leq N-1. \quad (44)$$

Therefore, we employ the following steps to compute  $c_i$  ( $1 \leq i \leq N$ ) within each time step, which will be referred to as the **AdvancePhaseField** procedure.

**AdvancePhaseField:**

- Solve equation (43) for  $\psi_i^{n+1}$  ( $1 \leq i \leq N-1$ );
- Solve equation (44) for  $c_i^{n+1}$  ( $1 \leq i \leq N-1$ );
- Compute  $c_N^{n+1}$  and  $\psi_N^{n+1}$  by

$$c_N^{n+1} = 1 - \sum_{i=1}^{N-1} c_i^{n+1}, \quad \psi_N^{n+1} = \nabla^2 c_N^{n+1} + \alpha c_N^{n+1} = \alpha - \sum_{i=1}^{N-1} \psi_i^{n+1}. \quad (45)$$

Combining the above algorithm for the phase field equations and the algorithm outlined in Appendix E for the momentum equations, we arrive at the following overall method for solving the equations (24), (83b) and (25) together with the boundary conditions (21), (26a) and (26b). Given  $(\mathbf{u}^n, P^n, c_i^n)$ , we compute  $c_i^{n+1}$  ( $1 \leq i \leq N$ ),  $P^{n+1}$  and  $\mathbf{u}^{n+1}$  successively in a de-coupled fashion through the following steps:

- Compute  $\psi_i^{n+1}$  and  $c_i^{n+1}$  ( $1 \leq i \leq N$ ) using the **AdvancePhaseField** procedure;
- Solve equation (100) for  $P^{n+1}$ ;
- Solve equation (101) for  $\mathbf{u}^{n+1}$ .

Note that this method involves only the solution of linear algebraic systems with constant and time-independent coefficient matrices after discretization, even though the governing equations of the system involve time-dependent field variables such as  $m_{ij}(\vec{c})$ ,  $\rho(\vec{c})$  and  $\mu(\vec{c})$ .

variables	normalization constant	variables	normalization constant
$\mathbf{x}, \eta$	$L$	$t, \Delta t$	$L/U_0$
$\mathbf{u}, \tilde{\mathbf{u}}, \mathbf{w}, d_{ai}$	$U_0$	$p, P, W(\vec{c}, \nabla \vec{c}), H(\vec{c}), \mathcal{H}_i(\vec{c})$	$\varrho_d U_0^2$
$\lambda_{ij}$	$\varrho_d U_0^2 L^2$	$\rho, \rho_i, \tilde{\rho}_i, \rho_0$	$\frac{\varrho_d}{L}$
$\mu, \tilde{\mu}_i$	$\varrho_d U_0 L$	$m_{ij}(\vec{c}), \tilde{m}_{ij}, m_0, \mathcal{K}_0$	$\frac{L}{U_0 L}$
$\tilde{\mathbf{J}}, \mathbf{J}_i$	$\varrho_d U_0$	$d_i$	$U_0/L$
$\sigma_{ij}$	$\varrho_d U_0^2 L$	$d_{bi}$	$1/L$
$\mathbf{f}$	$\varrho_d U_0^2/L$	$S, \alpha, \psi_i$	$1/L^2$
$c_i, \gamma_0$	$1$	$\nu_0$	$U_0 L$
$\mathbf{g}_r$ (gravity)	$U_0^2/L$		

Table 1: Normalization of flow variables and parameters.  $L$ : a characteristic length scale;  $U_0$ : a characteristic velocity scale;  $\varrho_d$ : a characteristic density scale.

## 4 Representative Numerical Examples

In this section we present numerical simulations of several multiphase flow problems in two dimensions to demonstrate the accuracy and effectiveness of the formulation and the algorithm developed in previous sections. These problems involve multiple fluid components with large density contrasts and large viscosity contrasts, and the simulation results will be compared with theoretical results or exact physical solutions for certain cases.

A comment on the normalization of physical variables and parameters is in order. As discussed in previous works [12, 15, 16], the non-dimensionalized problem (governing equations, boundary/initial conditions) will retain the same form as the dimensional problem as long as the variables are normalized consistently. We choose a length scale  $L$ , a velocity scale  $U_0$ , and a density scale  $\varrho_d$ . The values for these scales will be specified when individual test problems are investigated. In Table 1 we list the normalization constants for the physical variables encountered in this work. According to this table, for instance, the non-dimensional pairwise surface tension is given by  $\frac{\sigma_{ij}}{\varrho_d U_0^2 L}$ . Hereafter we will assume that all physical variables have been appropriately normalized based on Table 1. All the variables in subsequent discussions are in non-dimensional forms unless otherwise specified.

### 4.1 Convergence Rates

The goal of this subsection is to numerically demonstrate the spatial and temporal convergence rates of the method developed in Section 3 using a contrived analytic solution to the system of governing equations (24), (83b) and (25).

Consider a rectangular domain,  $0 \leq x \leq 2$  and  $-1 \leq y \leq 1$ , and a four-fluid mixture contained in this domain. We assume the following analytic expressions for the flow variables of this four-phase system,

$$\left\{ \begin{array}{l} u = A_0 \sin(ax) \cos(\pi y) \sin(\omega_0 t) \\ v = -(A_0 a / \pi) \cos(ax) \sin(\pi y) \sin(\omega_0 t) \\ P = A_0 \sin(ax) \sin(\pi y) \cos(\omega_0 t) \\ c_1 = \frac{1}{6} [1 + A_1 \cos(a_1 x) \cos(b_1 y) \sin(\omega_1 t)] \\ c_2 = \frac{1}{6} [1 + A_2 \cos(a_2 x) \cos(b_2 y) \sin(\omega_2 t)] \\ c_3 = \frac{1}{6} [1 + A_3 \cos(a_3 x) \cos(b_3 y) \sin(\omega_3 t)], \\ c_4 = 1 - c_1 - c_2 - c_3 \end{array} \right. \quad (46)$$

where  $(u, v)$  are the two components of the velocity  $\mathbf{u}$ .  $A_i$  and  $\omega_i$  ( $i = 0, \dots, 3$ ),  $a$ ,  $a_i$  and  $b_i$  ( $i = 1, 2, 3$ ) are constant parameters, whose values are to be specified below. The external force  $\mathbf{f}(\mathbf{x}, t)$  in (24) and the

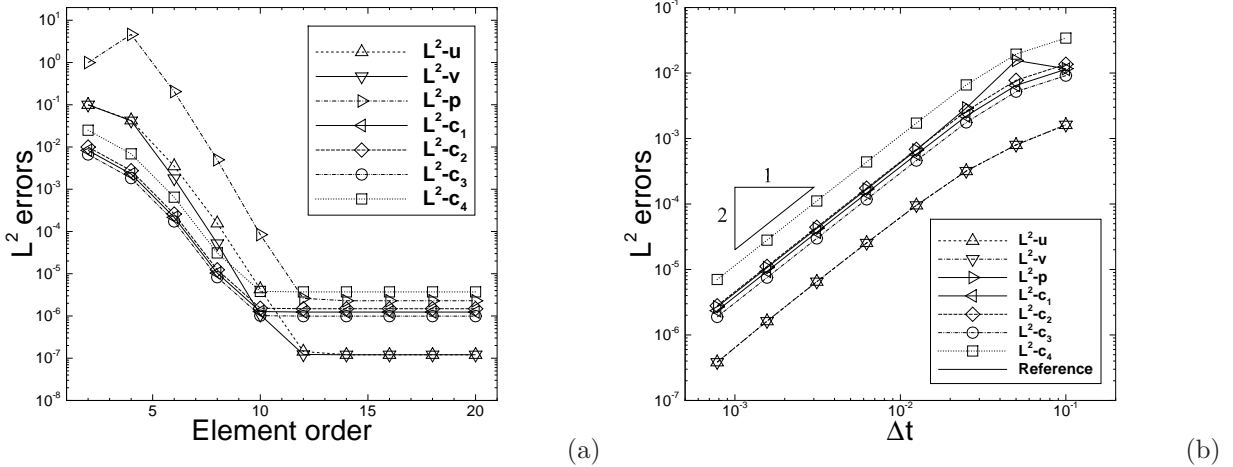


Figure 1: Spatial and temporal convergence rates (4 fluid components): (a)  $L^2$  errors of various flow variables versus element order (with fixed  $\Delta t = 0.001$  and  $t_f = 0.1$ ) showing spatial exponential convergence rate. (b)  $L^2$  errors versus time step size (with fixed Element order 16 and  $t_f = 0.2$ ) showing temporal 2nd-order convergence rate.

source term  $d_i(\mathbf{x}, t)$  ( $1 \leq i \leq N - 1$ ) in (25) are chosen such that the analytic expressions in (46) exactly satisfy the equations (24) and (25). The above expressions for  $(u, v)$  also satisfies the equation (83b).

We impose the condition (21) for  $\mathbf{u}$  and the conditions (26a) and (26b) for  $c_i$  ( $1 \leq i \leq 3$ ) on the domain boundaries, where the boundary velocity  $\mathbf{w}(\mathbf{x}, t)$  is chosen based on the analytic expressions given in (46) and the boundary source terms  $d_{ai}(\mathbf{x}, t)$  and  $d_{bi}(\mathbf{x}, t)$  are chosen such that the analytic expressions in (46) satisfy the equations (26a) and (26b) on the boundary. The initial conditions  $\mathbf{u}_{in}$  and  $c_i^{in}$  ( $1 \leq i \leq 4$ ) are chosen based on the analytic expressions in (46) by setting  $t = 0$ .

To simulate the problem we discretize the domain using two equal-sized quadrilateral elements (domain partitioned in the  $x$  direction), and the element order is varied to test the spatial convergence. The numerical algorithm from Section 3 is employed to integrate in time the governing equations for this four-phase system from  $t = 0$  to  $t = t_f$  ( $t_f$  to be specified later). Then the numerical solution and the exact solution as given by (46) at  $t = t_f$  are compared and the errors in the  $L^2$  norms for various flow variables are computed and recorded. Table 2 lists the physical and numerical parameters involved in the simulations of this problem.

The first group of tests is to examine the spatial convergence rate of the method. We fix the final time at  $t_f = 0.1$  and the time step size at  $\Delta t = 0.001$ . The element order is then varied systematically between 2 and 20. For each element order, the numerical solution at  $t = t_f$  is then obtained and compared with the exact solution. Figure 1(a) shows the  $L^2$  errors of the velocity, pressure and the four volume fractions as a function of the element order from this group of tests. The error curves approximately exhibit an exponential rate of decrease with increasing element order, before the element order reaches a certain value (10 or 12 for this case). This suggests an exponential convergence rate with respect to the element order. As the element order increases beyond about 12, the error curves essentially level off. The saturation is due to the fact that the temporal error becomes dominant as the element order becomes sufficiently large.

Figure 1(b) summarizes results for a second group of tests. In these tests we have fixed the element order at 16 and the final time at  $t_f = 0.2$ , and then varied the time step size systematically between  $\Delta t = 0.1$  and  $\Delta t = 0.00078125$ . The figure shows the  $L^2$  errors of different flow variables as a function of  $\Delta t$ . We observe a second-order convergence rate of the errors when  $\Delta t$  becomes sufficiently small.

The above results suggest that the numerical method developed herein exhibits an exponential convergence rate in space and a second-order convergence rate in time, with the reduction-consistent and thermodynamically consistent formulation for multiple fluid components.

Parameter	Value	Parameter	Value
$a, a_1, a_2, a_3$	$\pi$	$b_1, b_2, b_3$	$\pi$
$A_0$	2.0	$A_1, A_2, A_3$	1.0
$\omega_0, \omega_1$	1.0	$\omega_2$	1.2
$\omega_3$	0.8	$\eta$	0.1
$\tilde{\rho}_1$	1.0	$\tilde{\rho}_2$	3.0
$\tilde{\rho}_3$	2.0	$\tilde{\rho}_4$	4.0
$\tilde{\mu}_1$	0.01	$\tilde{\mu}_2$	0.02
$\tilde{\mu}_3$	0.03	$\tilde{\mu}_4$	0.04
$\sigma_{12}$	$6.236E-3$	$\sigma_{13}$	$7.265E-3$
$\sigma_{14}$	$3.727E-3$	$\sigma_{23}$	$8.165E-3$
$\sigma_{24}$	$5.270E-3$	$\sigma_{34}$	$6.455E-3$
$m_0$	$1.0E-3$	$t_f$	0.1 or 0.2
$\rho_0$	$\min(\tilde{\rho}_1, \dots, \tilde{\rho}_4)$	$\nu_0$	$\max\left(\frac{\tilde{\mu}_1}{\tilde{\rho}_1}, \dots, \frac{\tilde{\mu}_4}{\tilde{\rho}_4}\right)$
$J$ (temporal order)	2	Number of elements	2
$\Delta t$	(varied)	Element order	(varied)

Table 2: Simulation parameter values for the convergence-rate tests.

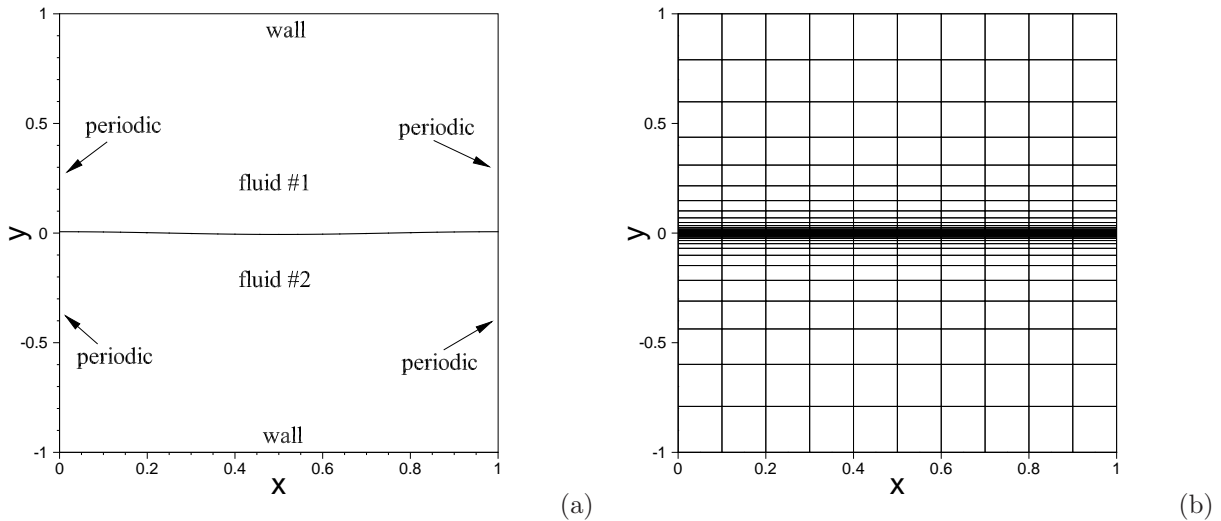


Figure 2: Capillary wave problem: (a) Computational domain and configuration. (b) Spectral element mesh of 400 quadrilateral elements.

## 4.2 Two-Phase Capillary Wave Problem

The reduction-consistent and thermodynamically consistent formulation presented in Section 2 for  $N$ -phase systems, with  $N = 2$ , leads to a two-phase formulation that is different from the usual two-phase formulations (see e.g. [38, 1, 19]), because of the  $m_{ij}(\vec{c})$  functions here. In this subsection we employ the benchmark two-phase capillary wave problem (see e.g. [19, 20]) to test the physical accuracy of the current method for  $N = 2$ . Note that both the two-phase formulation and the numerical algorithm to be tested here are different from those of [19, 20].

The problem setting is as follows. Consider two immiscible incompressible fluids contained in an infinite domain. The top half of the domain is occupied by the lighter fluid (fluid #1), and the bottom half is occupied by the heavier fluid (fluid #2). The gravity is assumed to be in the downward direction. The interface formed between the two fluids is perturbed from its horizontal equilibrium position by a small-amplitude sinusoidal wave form, and starts to oscillate at  $t = 0$ . The objective here is to study the motion of

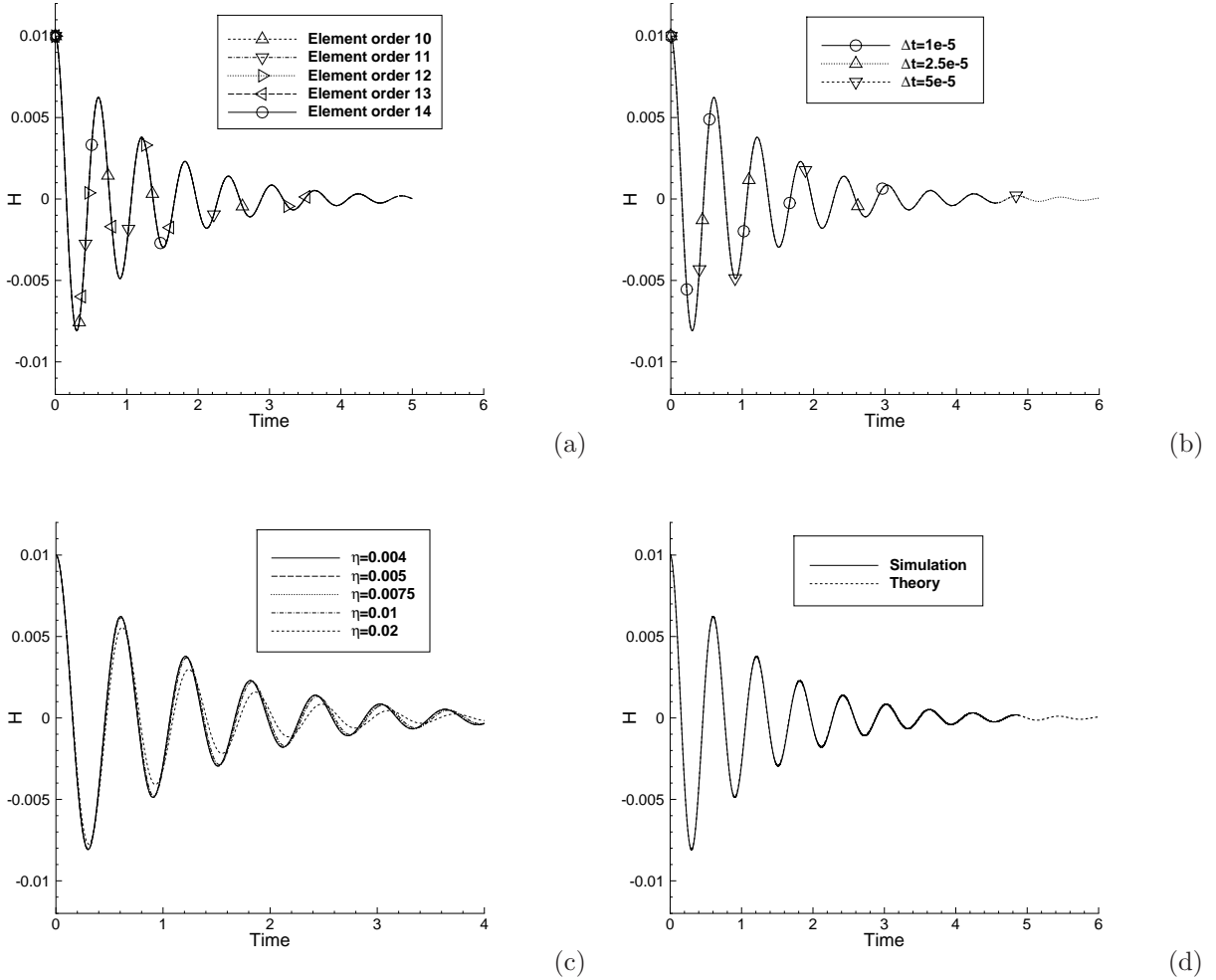


Figure 3: Two-phase capillary wave (matched density  $\tilde{\rho}_2/\tilde{\rho}_1 = 1$ ): (a) Effect of spatial resolution (element order) on the capillary amplitude history. (b) Effect of time step size  $\Delta t$  on the capillary amplitude history. (c) Effect of interfacial thickness ( $\eta$ ) on the capillary amplitude history. (d) comparison between the current simulation (solid curve) and Prosperetti's [30] exact theoretical solution (dashed curve). In (a), results are obtained with  $\eta = 0.005$ ,  $\Delta t = 2.5e - 5$  for element orders 10 to 13 and  $\Delta t = 1.0e - 5$  for element order 14. In (b),  $\eta = 0.005$ , element order is 12. In (c), element order is 12,  $\Delta t = 2.5e - 5$ . In (d), the simulation result corresponds to  $\eta = 0.004$ , element order 12, and  $\Delta t = 2.5e - 5$ . In all four plots,  $m_0 = 1.0e - 5$ .

the interface over time. In [30] an exact time-dependent standing-wave solution to this problem was reported under the condition that the two fluids must have matched kinematic viscosities (but their densities and dynamic viscosities can be different). We will simulate the problem under this condition using the method developed herein for  $N = 2$  and compare simulation results with the exact solution from [30].

The simulation setup is illustrated in Figure 2(a). We consider the computational domain  $0 \leq x \leq 1$  and  $-1 \leq y \leq 1$ . The top and bottom sides of the domain are solid walls of neutral wettability. In the horizontal direction the domain and all variables are assumed to be periodic at  $x = 0$  and  $x = 1$ . The equilibrium position of the fluid interface is assumed to coincide with the  $x$ -axis. The initial perturbed profile of the fluid interface is given by  $y = H_0 \cos(k_w x)$ , where  $H_0 = 0.01$  is the initial amplitude,  $\lambda_w = 1$  is the wave length of the perturbation profile, and  $k_w = \frac{2\pi}{\lambda_w}$  is the wave number. Note that the initial capillary amplitude  $H_0$  is small compared with the dimension of domain in the vertical direction. Therefore the effect of the walls at the domain top/bottom on the motion of the interface will be small.

Parameter	Value	Parameter	Value
$H_0$	0.01	$\lambda_w$	1.0
$\sigma_{12}$	1.0	$ \mathbf{g}_r $ (gravity)	1.0
$\tilde{\rho}_1$	1.0	$\tilde{\mu}_1$	0.01
$\frac{\tilde{\mu}_2}{\tilde{\rho}_2}$	$\frac{\tilde{\mu}_1}{\tilde{\rho}_1}$	$\tilde{\rho}_2$	(varied)
$\tilde{\mu}_2$	$\frac{\tilde{\mu}_1}{\tilde{\rho}_1} \tilde{\rho}_2$	$\eta$	(varied)
$m_0$	$1.0E - 5$	$\rho_0$	$\min(\tilde{\rho}_1, \tilde{\rho}_2)$
$\nu_0$	$\max\left(\frac{\tilde{\mu}_1}{\tilde{\rho}_1}, \frac{\tilde{\mu}_2}{\tilde{\rho}_2}\right)$	$J$ (integration order)	2
$\Delta t$	(varied)	Number of elements in mesh	400
Element order	(varied)		

Table 3: Simulation parameter values for the two-phase capillary wave problem.

We use the method presented in Section 3 to simulate this problem. The computational domain is discretized using a spectral element mesh as shown in Figure 2(b), which consists of 400 quadrilateral elements. The elements are uniform along the  $x$  direction, but are non-uniform and clustered about the region  $-0.012 \lesssim y \lesssim 0.012$  in the  $y$  direction. The element order is varied to modify the spatial resolution of the simulations, and this will be specified below. The external body force in equation (24) is set to  $\mathbf{f} = \rho \mathbf{g}_r$ , where  $\mathbf{g}_r$  is the gravitational acceleration. The source terms in equation (25) are set to  $d_i = 0$  ( $1 \leq i \leq N - 1$ ). On the top/bottom walls, the boundary condition (21) with  $\mathbf{w} = 0$  is imposed for the velocity, and the boundary conditions (26a)–(26b) with  $d_{ai} = 0$  and  $d_{bi} = 0$  ( $1 \leq i \leq N - 1$ ) are imposed for the phase field variables. The initial velocity is set to zero, and the initial volume fractions are set as follows,

$$\begin{cases} c_1 = \frac{1}{2} \left[ 1 + \tanh \frac{y - H_0 \cos(k_w x)}{\sqrt{2}\eta} \right], \\ c_2 = 1 - c_1 = \frac{1}{2} \left[ 1 - \tanh \frac{y - H_0 \cos(k_w x)}{\sqrt{2}\eta} \right]. \end{cases} \quad (47)$$

We list in Table 3 the values for the physical and simulation parameters involved in this problem.

We have varied the element order, the time step size ( $\Delta t$ ) and the interfacial thickness scale ( $\eta$ ) systematically in the simulations to ensure the convergence of the simulation results. Figure 3 summarizes some of the test results with matched densities ( $\tilde{\rho}_2/\tilde{\rho}_1 = 1$ ) for the two fluids. Figure 3(a) compares the time histories of the capillary wave amplitude obtained with element orders ranging from 10 to 14 in the simulation. The history curves corresponding to different element orders overlap with one another, suggesting independence of the results with respect to the grid resolutions. Figure 3(b) is a comparison of the capillary amplitude histories computed using several time step sizes. The results indicate the convergence with respect to  $\Delta t$ . Figure 3(c) shows the time histories of the capillary amplitude obtained with the interfacial thickness scale parameter ranging from  $\eta = 0.02$  to  $\eta = 0.004$ . Note that the simulations become much more challenging when  $\eta$  becomes small, taxing the grid resolution and the time step size. We initially observe some influence on the amplitude and the phase of the history curves as  $\eta$  decreases from 0.02 to 0.01. As  $\eta$  decreases further to  $\eta = 0.0075$  and below, on the other hand, the history curves essentially overlap with one another and little difference can be observed among them, suggesting a convergence of the results with respect to  $\eta$ . In Figure 3(d) we compare the capillary amplitude history from the current simulation (corresponding to  $\eta = 0.004$ ) and the exact theoretical solution given by [30]. The history curve from the simulation essentially overlaps with the theoretical curve, attesting to the physical accuracy of the simulation results. The above results are obtained with a mobility parameter  $m_0 = 1e - 5$ . Some other values for  $m_0$  have also been considered. The tests suggest that the computation would be unstable if  $m_0$  is too large (larger than a certain value). With decreasing  $m_0$  values, the simulation tends to require a smaller interfacial thickness  $\eta$  value for stability or accuracy, which in turn increases the computational challenge and demand.

To investigate the density ratio effect on the motion of the fluid interface, the density and dynamic viscosity of the second fluid ( $\tilde{\rho}_2$  and  $\tilde{\mu}_2$ ) have been varied systematically while the relation  $\tilde{\mu}_2/\tilde{\rho}_2 = \tilde{\mu}_1/\tilde{\rho}_1$  is maintained as required by the exact solution of [30]. In Figure 4 we show the time histories of the capillary

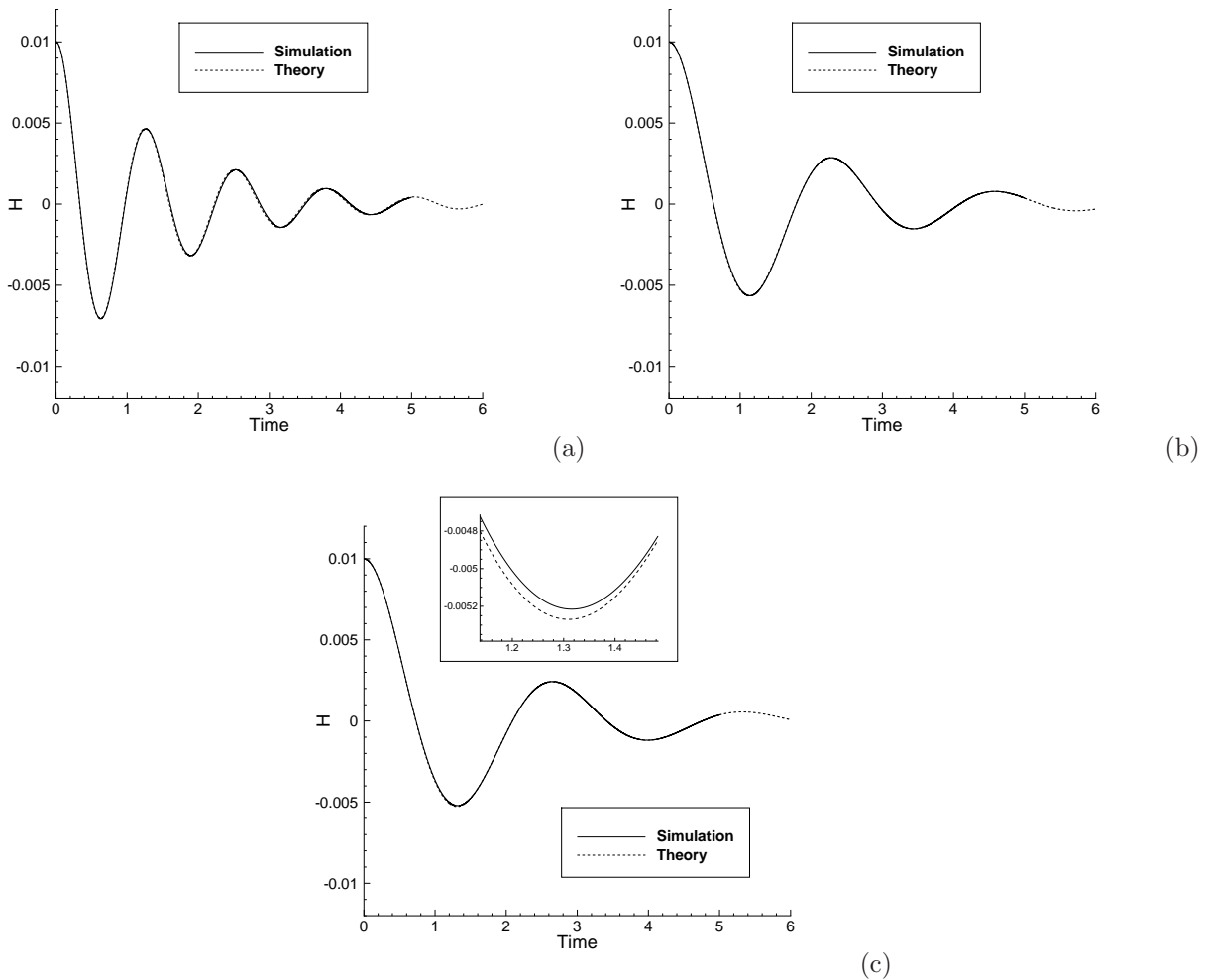


Figure 4: Two-phase capillary wave (larger density ratios): Comparison of capillary amplitude as a function of time between current simulations (solid curves) and the exact solutions [30] (dashed curves) for density ratios  $\tilde{\rho}_2/\tilde{\rho}_1 = 10$  (a), 100 (b), and 1000 (c). The inset of plot (c) shows a magnified view of a section of the curves.

amplitude corresponding to three larger density ratios  $\tilde{\rho}_2/\tilde{\rho}_1 = 10, 100$  and 1000 from our simulations, and compare them with the exact solutions from [30]. The simulation results correspond to an element order 12, time step size  $\Delta t = 5.0e - 5$ , interfacial thickness  $\eta = 0.004$ , and  $m_0 = 1.0e - 5$  in the simulations. The history curves from the simulations essentially overlap with those of the exact solutions. The inset of Figure 4(c) is a zoomed-in view of the curves for the density ratio  $\tilde{\rho}_2/\tilde{\rho}_1 = 1000$ , showing some but small difference between the simulation and the theoretical solution. These comparisons suggest that our simulation results are in good agreement with the physical solution for the whole range of density ratios considered here.

The two-phase capillary wave problem and in particular the comparisons with Prosperetti's exact solution for this problem demonstrate that the reduction-consistent formulation and the numerical method developed herein (with  $N = 2$ ) have produced physically accurate results for a wide range of density ratios (up to density ratio 1000 tested here) and at large density ratios. This provides a reference, for two fluid phases, when the method is subject to subsequent tests involving multiple fluid components.

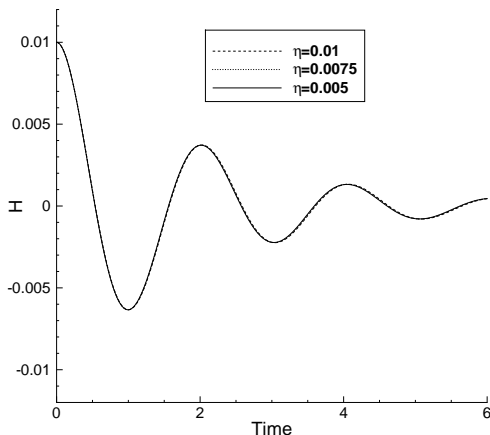


Figure 5: Effect of interfacial thickness  $\eta$  on the capillary amplitude as a function of time for the four-phase capillary wave problem with two absent fluids, where  $\tilde{\rho}_i = 1$  ( $i = 1, \dots, 4$ ).

### 4.3 Three-/Four-Phase Capillary Wave With Absent Fluid Components

In this subsection we consider a three-phase system and a four-phase system, but with some fluid components absent, so that they are physically equivalent to a system containing a smaller number of fluids. We employ a setting similar to that of Section 4.2, so these three-phase and four-phase problems are physically equivalent to the two-phase capillary wave problem. This allows us to compare the three-phase and four-phase simulation results with Prosperetti's exact physical solution [30] for two-phase problems.

More specifically, we consider the same computational domain and the same mesh as in Section 4.2, as shown in Figure 2. Consider a system of three immiscible incompressible fluids contained in this domain, but *with fluid #2 absent*. So this three-phase system is physically equivalent to a two-phase system containing fluid #1 and fluid #3. Similar to in Section 4.2, the interface between fluid #1 and fluid #3 is perturbed by a sinusoidal wave form of a small amplitude ( $H_0 = 0.01$ ) from its equilibrium position, and our goal is to study the motion of the interface over time. In the three-phase simulations, we employ periodic conditions for all flow variables in the horizontal direction. On the top/bottom walls we impose the no-slip condition, i.e. equation (21) with  $\mathbf{w} = 0$ , for the velocity and the boundary conditions (26a)–(26b) with  $d_{ai} = 0$  and  $d_{bi} = 0$  ( $i = 1, 2, 3$ ) for the volume fractions. The source terms in equation (25) are set to  $d_i = 0$  ( $1 \leq i \leq N - 1$ ). The initial velocity is zero, and the initial volume fractions are set to

$$\begin{cases} c_1 = \frac{1}{2} \left[ 1 + \tanh \frac{y - H_0 \cos(k_w x)}{\sqrt{2}\eta} \right], \\ c_2 = 0, \\ c_3 = 1 - c_1 - c_2 = \frac{1}{2} \left[ 1 - \tanh \frac{y - H_0 \cos(k_w x)}{\sqrt{2}\eta} \right]. \end{cases} \quad (48)$$

Note that the initial volume fraction of fluid #2 is  $c_2 = 0$  (absent fluid). Therefore, the solution to this three-phase problem physically consists of the exact solution given by [30] for fluid #1 and fluid #3 and  $c_2(\mathbf{x}, t) = 0$  for fluid #2.

In addition to the above three-phase problem, we also consider a four-phase system contained in this domain, in which *fluid #2 and fluid #3 are absent*. Therefore this four-phase system is physically equivalent to a two-phase system that consists of fluid #1 and fluid #4 only. We consider the motion of the interface between fluid #1 and fluid #4 after a perturbation from its equilibrium horizontal position, similar to in Section 4.2. The boundary conditions are set in an analogous way to the three-phase problem. We employ

Parameter	Value	Parameter	Value
$H_0$	0.01	$\lambda_w$	1.0
$\sigma_{ij}$ ( $1 \leq i \neq j \leq 4$ )	0.1	$ \mathbf{g}_r $ (gravity)	0.1
$\tilde{\rho}_1$	1.0	$\tilde{\mu}_1$	0.01
$\frac{\tilde{\mu}_2}{\tilde{\rho}_2}$	$\frac{\tilde{\mu}_1}{\tilde{\rho}_1}$	$\tilde{\rho}_2$	(varied)
$\frac{\tilde{\mu}_3}{\tilde{\rho}_3}$ (three-/four-phase)	$\frac{\tilde{\mu}_1}{\tilde{\rho}_1}$	$\frac{\tilde{\mu}_4}{\tilde{\rho}_4}$ (four-phase)	$\frac{\tilde{\mu}_1}{\tilde{\rho}_1}$
$\tilde{\rho}_3$ (three-/four-phase)	$\tilde{\rho}_2$	$\tilde{\rho}_4$ (four-phase)	$\tilde{\rho}_2$
$\tilde{\mu}_2$	$\frac{\tilde{\mu}_1}{\tilde{\rho}_1} \tilde{\rho}_2$	$\tilde{\mu}_3$ (three-/four-phase)	$\frac{\tilde{\mu}_1}{\tilde{\rho}_1} \tilde{\rho}_3$
$\tilde{\mu}_4$ (four-phase)	$\frac{\tilde{\mu}_1}{\tilde{\rho}_1} \tilde{\rho}_4$	$\eta$	0.005 (or varied)
$m_0$	$1.0E - 4$	$\rho_0$	$\min(\tilde{\rho}_1, \tilde{\rho}_2, \tilde{\rho}_3, \tilde{\rho}_4)$
$\nu_0$	$\max\left(\frac{\tilde{\mu}_1}{\tilde{\rho}_1}, \frac{\tilde{\mu}_2}{\tilde{\rho}_2}, \frac{\tilde{\mu}_3}{\tilde{\rho}_3}, \frac{\tilde{\mu}_4}{\tilde{\rho}_4}\right)$	$J$ (integration order)	2
$\Delta t$	$1E - 4$	Number of elements in mesh	400
Element order	10		

Table 4: Simulation parameter values for the three-phase and four-phase capillary wave problems.

a zero initial velocity and the following initial volume fraction distributions:

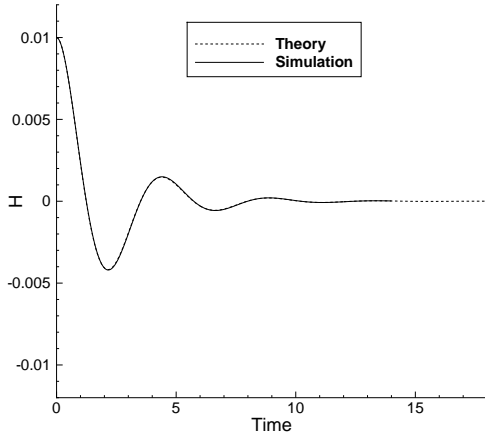
$$\begin{cases} c_1 = \frac{1}{2} \left[ 1 + \tanh \frac{y - H_0 \cos(k_w x)}{\sqrt{2}\eta} \right], \\ c_2 = 0, \\ c_3 = 0, \\ c_4 = 1 - c_1 - c_2 - c_3 = \frac{1}{2} \left[ 1 - \tanh \frac{y - H_0 \cos(k_w x)}{\sqrt{2}\eta} \right]. \end{cases} \quad (49)$$

Note that  $c_2$  and  $c_3$  are both identically zero initially, so physically they should be zero over time. In Table 4 we have listed the values of the physical and simulation parameters for the above three-phase and four-phase capillary-wave problems considered here.

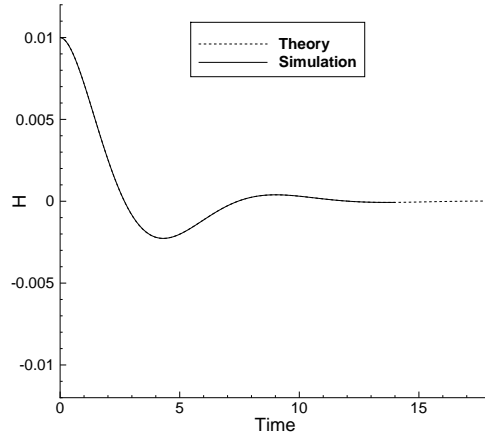
We have varied the interfacial thickness  $\eta$  to look into its effect on the simulation result. Figure 5 compares the time histories of the capillary amplitude of the interface formed between fluid #1 and fluid #4 for the four-phase capillary wave problem with  $\tilde{\rho}_i = 1$  ( $i = 1, 2, 3, 4$ ), obtained using  $\eta = 0.01, 0.0075$  and  $0.005$  in the simulations. Note that the pairwise surface tension values  $\sigma_{ij}$  and the gravity value employed here are different from those of Section 4.2, and one can observe that this has a notable effect on the period and attenuation of the capillary wave history (e.g. compare Figures 5 and 3(a)). We observe from Figure 5 that there is little difference in the simulation results corresponding to these different  $\eta$  values, suggesting the independence of the results with respect to  $\eta$ . The simulation results reported below for the three-/four-phase capillary wave problem are obtained with  $\eta = 0.005$ .

Let us next compare the simulations for the three-/four-phase capillary wave problems and Prosperetti's exact solutions [30] to study the accuracy of the simulation results. We have varied the fluid density values to look into their effect on the simulation results. Figure 6 shows a comparison of the capillary amplitude history (of the interface formed between fluids #1 and #3) between the simulation and the exact solution from [30] for the three-phase capillary wave problem, corresponding to two density ratios  $\frac{\tilde{\rho}_2}{\tilde{\rho}_1} = \frac{\tilde{\rho}_3}{\tilde{\rho}_1} = 10$  and  $\frac{\tilde{\rho}_2}{\tilde{\rho}_1} = \frac{\tilde{\rho}_3}{\tilde{\rho}_1} = 100$ . Figure 7 is a comparison of the capillary amplitude histories between the simulation of the four-phase capillary wave problem and the exact solution [30], corresponding to density ratios  $\frac{\tilde{\rho}_2}{\tilde{\rho}_1} = \frac{\tilde{\rho}_3}{\tilde{\rho}_1} = \frac{\tilde{\rho}_4}{\tilde{\rho}_1} = 1$  and  $\frac{\tilde{\rho}_2}{\tilde{\rho}_1} = \frac{\tilde{\rho}_3}{\tilde{\rho}_1} = \frac{\tilde{\rho}_4}{\tilde{\rho}_1} = 10$ . It can be observed that the history curves from the simulations almost exactly overlap with those of the physical solutions. This indicates that our simulations of the three- and four-phase capillary wave problems with absent fluid components have captured the motion of the fluid interface accurately.

In the three-phase and four-phase capillary wave problems considered here, the physical solution for the absent fluids corresponds to a zero volume-fraction field. In the simulations, however, owing to the numerical errors the computed volume-fraction fields corresponding to the absent fluids will not be exactly zero, but contain very small yet non-zero values. The results in Figure 8 demonstrate this point. Figure

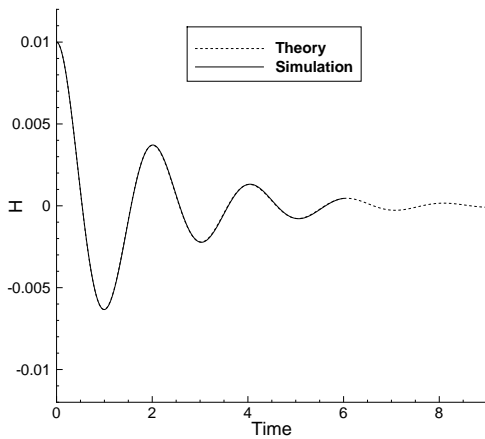


(a)

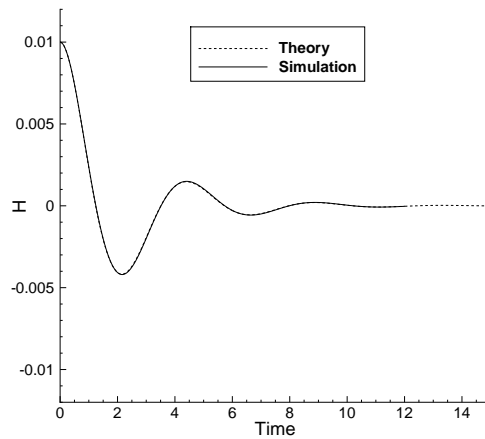


(b)

Figure 6: Three-phase capillary wave problem with one absent fluid component: Comparison of capillary amplitude versus time between simulations and the exact solutions [30], corresponding to fluid densities: (a)  $\tilde{\rho}_1 = 1, \tilde{\rho}_2 = \tilde{\rho}_3 = 10$ ; (b)  $\tilde{\rho}_1 = 1, \tilde{\rho}_2 = \tilde{\rho}_3 = 100$ . In these simulations the second fluid is absent.



(a)



(b)

Figure 7: Four-phase capillary wave problem with two absent fluid components: comparison of capillary amplitude versus time between simulations and the exact solutions [30] with fluid densities: (a)  $\tilde{\rho}_1 = \tilde{\rho}_2 = \tilde{\rho}_3 = \tilde{\rho}_4 = 1$ ; (b)  $\tilde{\rho}_1 = 1, \tilde{\rho}_2 = \tilde{\rho}_3 = \tilde{\rho}_4 = 10$ . Fluid two and fluid three are absent in the simulations.

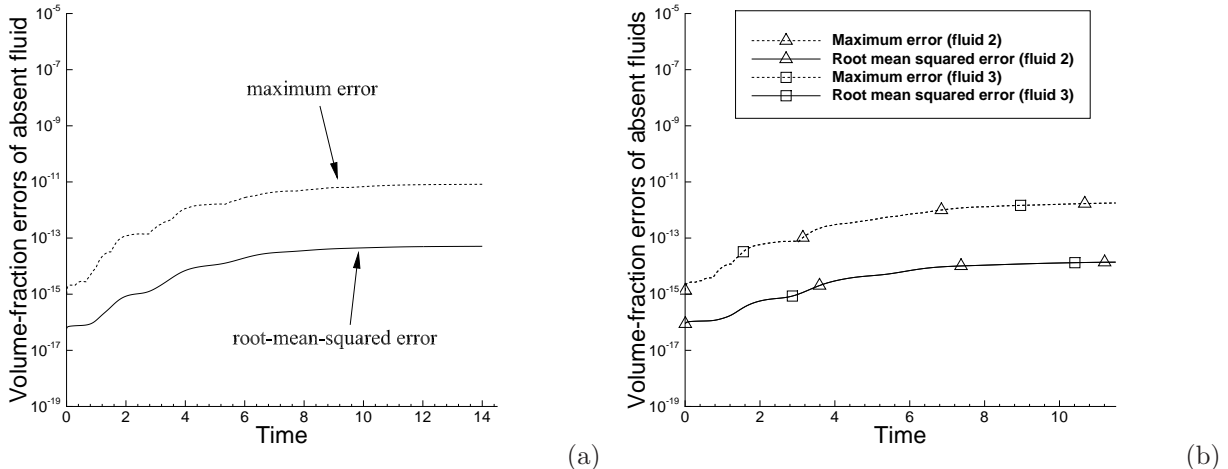


Figure 8: Time histories of volume-fraction errors of the absent fluids for the three-/four-phase capillary wave problems: (a) three-phase problem with one absent fluid, corresponding to  $\tilde{\rho}_1 = 1$ ,  $\tilde{\rho}_2 = \tilde{\rho}_3 = 10$ ; (b) four-phase problem with two absent fluids, corresponding to  $\tilde{\rho}_1 = 1$ ,  $\tilde{\rho}_2 = \tilde{\rho}_3 = \tilde{\rho}_4 = 10$ .

8(a) shows time histories of the maximum error,  $\max_{\mathbf{x} \in \Omega} |c_2(\mathbf{x}, t)|$ , and the root-mean-squared (RMS) error,  $\sqrt{\frac{1}{V_\Omega} \int_\Omega |c_2(\mathbf{x}, t)|^2 d\mathbf{x}}$  ( $V_\Omega = \int_\Omega d\mathbf{x}$  denoting the volume of domain  $\Omega$ ), of the volume fraction of fluid #2 (absent fluid) for the three-phase capillary wave problem with density ratios  $\frac{\tilde{\rho}_2}{\tilde{\rho}_1} = \frac{\tilde{\rho}_3}{\tilde{\rho}_1} = 10$ . It is observed that the errors increase initially and gradually level off over time. The maximum error approximately levels off on the order of magnitude  $10^{-11}$ , and the RMS error levels off at a level  $10^{-14}$ . Figure 8(b) shows time histories of the maximum errors and the RMS errors of the volume fractions of fluid #2 and fluid #3 (the absent fluids) for the four-phase capillary wave problem with density ratios  $\frac{\tilde{\rho}_2}{\tilde{\rho}_1} = \frac{\tilde{\rho}_3}{\tilde{\rho}_1} = \frac{\tilde{\rho}_4}{\tilde{\rho}_1} = 10$ . We observe a general behavior in the errors similar to that of the three-phase case. The curves for the maximum and RMS errors of fluid #2 basically overlap with those for fluid #3. The maximum error curves appear to level off on the order of magnitude  $10^{-11}$  and the RMS error curves appear to level off on the order of magnitude  $10^{-14}$ .

## 4.4 Floating Liquid Lens

In this subsection we employ the so-called floating liquid lens problem to test the method developed herein. The basic goal is to simulate and study the equilibrium configuration of an oil drop floating on the air-water interface. There exist theoretical results about such three-phase problems in the literature, in particular, quantitative relations about the oil-drop thickness expressed in terms of the other physical parameters have been developed for the case when the gravity is dominant by e.g. Langmuir and de Gennes [29, 10]. We will compare our simulation results with the Langmuir-de Gennes theory to evaluate the accuracy of our method. The floating liquid lens problem has also been considered in some of our previous works (see e.g. [12, 15]). It should be noted that the method to be tested here, in terms of both the formulation and the algorithm, is very different from those of [12, 15].

### 4.4.1 Floating Liquid Lens as a Three-Phase Problem

We first simulate the floating lens problem in the natural way, by treating it as a three-phase system consisting of air, water and oil. Specifically, we consider the domain sketched in Figure 9,  $-L \leq x \leq L$  and  $0 \leq y \leq \frac{4}{5}L$ , where  $L = 4\text{cm}$ . The top and bottom sides of the domain are solid walls, and in the horizontal direction the domain is periodic at  $x = \pm L$ . The walls are of neutral wettability, i.e. if any fluid interface intersects the top or bottom walls the contact angle at the wall will be  $90^\circ$ . The top half of the domain is filled with air, and the bottom half is filled with water. An oil drop, initially circular with a radius  $R_0 = \frac{1}{5}L$ , is held at

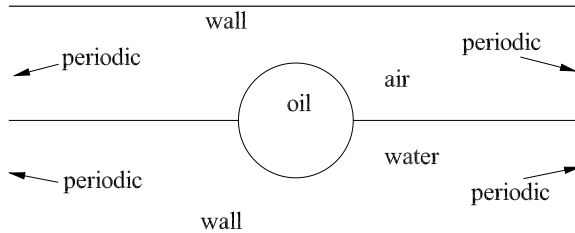


Figure 9: Floating liquid lens: problem setup and initial configuration.

Density [ $kg/m^3$ ]:	air – 1.2041	water – 998.207	oil – 577
Dynamic viscosity [ $kg/(m \cdot s)$ ]:	air – $1.78 \times 10^{-5}$	water – $1.002 \times 10^{-3}$	oil – $9.15 \times 10^{-2}$
Surface tension [ $kg/s^2$ ]:	air/water – 0.0728	air/oil – 0.055	oil/water – 0.04
Gravity [ $m/s^2$ ]:	varied from 0 to 9.8		

Table 5: Physical property values of air, water and oil.

rest on the water surface, and its center is located at  $\mathbf{x}_c = (x_c, y_c) = (0, \frac{2}{5}L)$ . The gravitational acceleration  $\mathbf{g}_r$  is assumed to be in the  $-y$  direction. At  $t = 0$  the system is released and evolves due to the interactions among the three surface tensions (air/water, air/oil, water/oil) and the gravity, reaching an equilibrium state eventually. The objective of this problem is to study the equilibrium configuration of this three-phase system.

The physical properties (including the densities, viscosities, and surface tensions) of air, water and oil employed in this problem are listed in Table 5. We choose  $L$  as the length scale, the velocity scale as  $U_0 = \sqrt{g_{r0}L}$  where  $g_{r0} = 1m/s^2$ , and the air density as the density scale  $\rho_d$ . The physical variables and parameters are then normalized according to Table 1. In the following simulations water, oil and air are assigned as the first, the second, and the third fluid, respectively.

We employ the method described in Section 3 to simulate this problem. The flow domain is discretized using a mesh of 360 equal-sized quadrilateral elements, with 30 elements along the horizontal direction and 12 elements along the vertical direction. The element orders are varied between 9 and 13, but the majority of results reported below are computed using an element order 13 within each element. The source terms in the phase field equations (25) are set to  $d_i = 0$  ( $i = 1, \dots, N-1$ ). On the top/bottom walls the no-slip condition, equation (21) with  $\mathbf{w} = 0$ , is imposed for the velocity, and the boundary conditions (26a)–(26b) with  $d_{ai} = 0$  and  $d_{bi} = 0$  are imposed for the volume fractions. In the horizontal direction all flow variables are set to be periodic at  $x = \pm L$ . The initial velocity is set to zero, and the initial volume fraction distributions are set as

$$\begin{cases} c_1 = \frac{1}{2} \left[ 1 - \tanh \left( \frac{y - y_c}{\sqrt{2}\eta} \right) \right] \frac{1}{2} \left[ 1 + \tanh \left( \frac{|\mathbf{x} - \mathbf{x}_c| - R_0}{\sqrt{2}\eta} \right) \right] \\ c_2 = \frac{1}{2} \left[ 1 - \tanh \left( \frac{|\mathbf{x} - \mathbf{x}_c| - R_0}{\sqrt{2}\eta} \right) \right] \\ c_3 = 1 - c_1 - c_2. \end{cases} \quad (50)$$

The simulation parameter values are summarized in Table 6.

We observe that a smooth field for the initial volume fractions (such as those given above) is important for the current method. Note that in the current formulation  $m_{ij}(\vec{c})$  are functions dependent on the volume fraction distributions. This places a more stringent requirement on the smoothness of the initial volume fractions. Since the initial volume fraction distributions are unknown physically and must be prescribed, any discontinuity in the prescribed initial volume-fraction distributions will affect the dynamics and may influence the time to reach the equilibrium state. For example, in [12] some Heaviside step functions are involved in the prescribed initial volume fractions for the floating liquid lens problem, inducing discontinuities in the distributions. Those initial volume-fraction distributions do not work well with the current method.

Parameters	Values
$\lambda_{ij}$	given by equation (17)
$\eta/L$	0.01 and 0.0075
$m_0 \rho_d U_0 / L$	$10^{-8}$
$U_0 \Delta t / L$	$1.0 \times 10^{-5}$
$\rho_0$	$\min(\tilde{\rho}_1, \tilde{\rho}_2, \tilde{\rho}_3)$
$\nu_0$	$5 \max\left(\frac{\tilde{\mu}_1}{\tilde{\rho}_1}, \frac{\tilde{\mu}_2}{\tilde{\rho}_2}, \frac{\tilde{\mu}_3}{\tilde{\rho}_3}\right)$
$\mathcal{K}_0$	given by equation (31)
$S$	$\sqrt{\frac{4\gamma_0}{\mathcal{K}_0 \Delta t}}$
$\alpha$	computed by equation (35)
$J$ (temporal order)	2
Number of elements	360
Element order	9 ~ 13 (mostly 13)

Table 6: Simulation parameter values for air/water/oil three-phase floating lens problem.

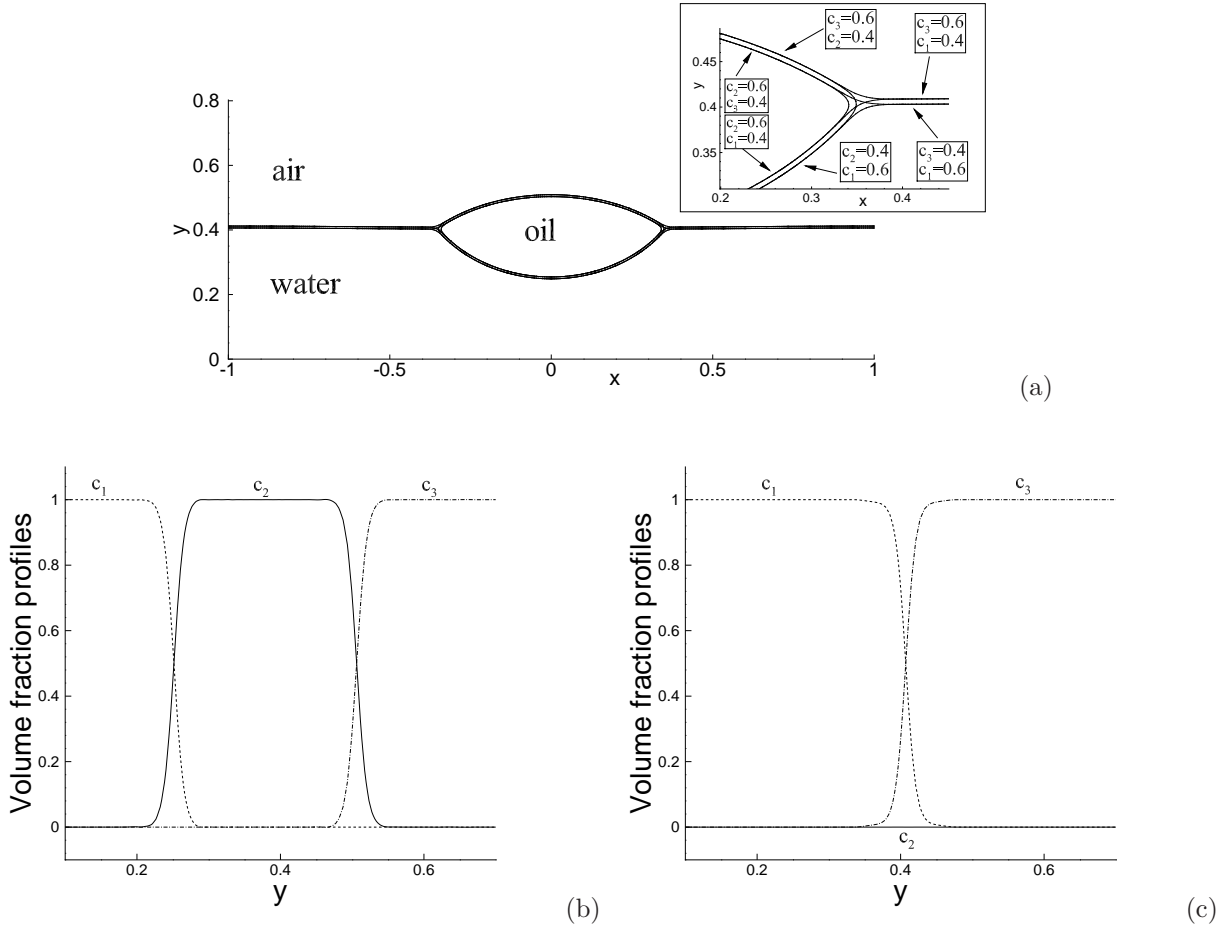


Figure 10: Floating liquid lens (gravity  $|\mathbf{g}_r| = 0.5m/s^2$ ): (a) Contour levels  $c_i = 0.4$  and  $0.6$  ( $i = 1, 2, 3$ ), and the inset shows a magnified view of the 3-phase line region. Profiles of the volume fractions  $c_i$  ( $i = 1, 2, 3$ ) along the centerline  $x = 0$  (b) and along the vertical line  $x = 0.6$  (c).

We first look into the distribution characteristics of different fluids within the domain. Figure 10(a) shows two contour levels  $c_i = 0.4$  and  $c_i = 0.6$  ( $i = 1, 2, 3$ ) of the three volume fractions for the equilibrium state of this three-phase system with a gravitational acceleration  $0.5m/s^2$ . Note that  $c_1$ ,  $c_2$  and  $c_3$  correspond to water, oil and air, respectively. The result is computed using an interfacial thickness scale  $\eta/L = 0.01$  and an element order 11. The inset of Figure 10(a) is a zoomed-in view around the three-phase line region. It can be observed that, along the air/oil interface and away from the three-phase line region, the contours  $c_3 = 0.6$  and  $c_2 = 0.4$  coincide with each other and the contours  $c_3 = 0.4$  and  $c_2 = 0.6$  coincide with each other. This is consistent with the intuition as water is not present (i.e.  $c_1 = 0$ ) on the air-oil interface away from the three-phase region. Similar distribution characteristics can be observed on the water/oil and air/water interfaces away from the three-phase line region. Figure 10(b) shows profiles of the three volume fractions along the centerline of the domain ( $x = 0$ ). One can observe that in the bulk of the water region (oil region, air region)  $c_1 = 1$  (resp.  $c_2 = 1$ ,  $c_3 = 1$ ) while the other two volume fractions are zeros. At the water/oil interface  $c_1$  decreases from the unit value to zero and  $c_2$  increases from zero to the unit value, while  $c_3 = 0$  in this region. At the air/oil interface  $c_2$  decreases from the unit value to zero and  $c_3$  increases from zero to the unit value, while  $c_1 = 0$  in this region. Figure 10(c) shows profiles of the three volume fractions along another vertical line  $x/L = 0.6$ . Since only the air and water exist in this region, one observes that  $c_2 = 0$  and that  $c_1$  transitions to  $c_3$  as the air/water interface is crossed.

Let us now look into the equilibrium configuration of this three-phase system. The physics of floating liquid lenses was explained in [29, 10]. The equilibrium shape of the oil drop is determined by the interplay of the three pairwise surface tensions and the gravity, and it is also affected by the three densities. If the surface tension effects dominate (e.g. when the oil drop is small), the equilibrium drop shape comprises two circular caps in two dimensions (or two spherical caps in three dimensions). On the other hand, if the gravity effect dominates (e.g. when the oil drop is large) the oil forms a puddle at equilibrium. To determine which effect dominates, one can compare the drop size with the three capillary lengths associated with the three fluid interfaces; see [10] for details.

We have varied the magnitude of the gravitational acceleration systematically, and simulated the equilibrium configurations of this system corresponding to these gravity values. In Figure 11 we show the equilibrium profiles of the oil drop corresponding to gravity:  $|\mathbf{g}_r| = 0, 2m/s^2$  and  $7.5m/s^2$ . The fluid interfaces are visualized by the contour levels  $c_i = 1/2$  ( $i = 1, 2, 3$ ). These results correspond to an interfacial thickness scale  $\eta/L = 0.0075$  and an element order 13 within each element in the simulations. In these plots one can observe a small star-shaped region around the three-phase line (where the three fluid regions intersect), which is due to the fact that within this region no fluid has a volume fraction larger than  $1/2$ . In Figure 11(a) (zero gravity), we have also shown two reference circles (dashed and dashed-dot curves), which overlap with the upper and lower pieces of the oil-drop profile. This indicates that with zero gravity (surface tensions dominant) the computed oil-drop profile indeed consists of two circular caps, consistent with the theory [10]. With increasing gravity the oil lens tends to spread out on the water surface (Figure 11(b)). With a gravity  $|\mathbf{g}_r| = 7.5m/s^2$  the oil forms a puddle on the water surface under the conditions considered here, with flat upper and lower surfaces (Figure 11(c)). The simulation results are qualitatively consistent with the Langmuir-de Gennes theory [29, 10].

We next show some quantitative comparisons with the Langmuir-de Gennes theory. Following [12], we define the oil-drop/-puddle thickness as the largest distance between the upper and lower boundaries of the equilibrium drop/puddle profile along the vertical direction. When the gravity is dominant, the asymptotic thickness of the oil puddle (denoted by  $e_c$ ) is given by the following expression [10]

$$e_c = \sqrt{\frac{2(\sigma_{ao} + \sigma_{ow} - \sigma_{aw})\rho_w}{\rho_o(\rho_w - \rho_o)|\mathbf{g}_r|}} \quad (51)$$

where  $\rho_w$  and  $\rho_o$  are the water and oil densities respectively,  $\sigma_{aw}$ ,  $\sigma_{ao}$  and  $\sigma_{ow}$  are the air/water, air/oil and oil/water surface tensions respectively, and  $|\mathbf{g}_r|$  is the magnitude of the gravitational acceleration. We have computed the oil-drop/-puddle thickness corresponding to different gravity magnitudes. In Figure 12 we plot the oil-drop/-puddle thickness as a function of the normalized gravity  $\frac{|\mathbf{g}_r|}{U_0^2/L} = \frac{|\mathbf{g}_r|}{g_{r0}}$  where  $g_{r0} = 1m/s^2$ . The symbols denote results from current simulations, and the dashed curve denotes the relation given by equation (51). The simulation results correspond to  $\eta/L = 0.0075$  and element order 13 in the simulations. It is observed that when the gravity becomes large ( $|\mathbf{g}_r| = 5m/s^2$  or larger) the puddle thickness values from

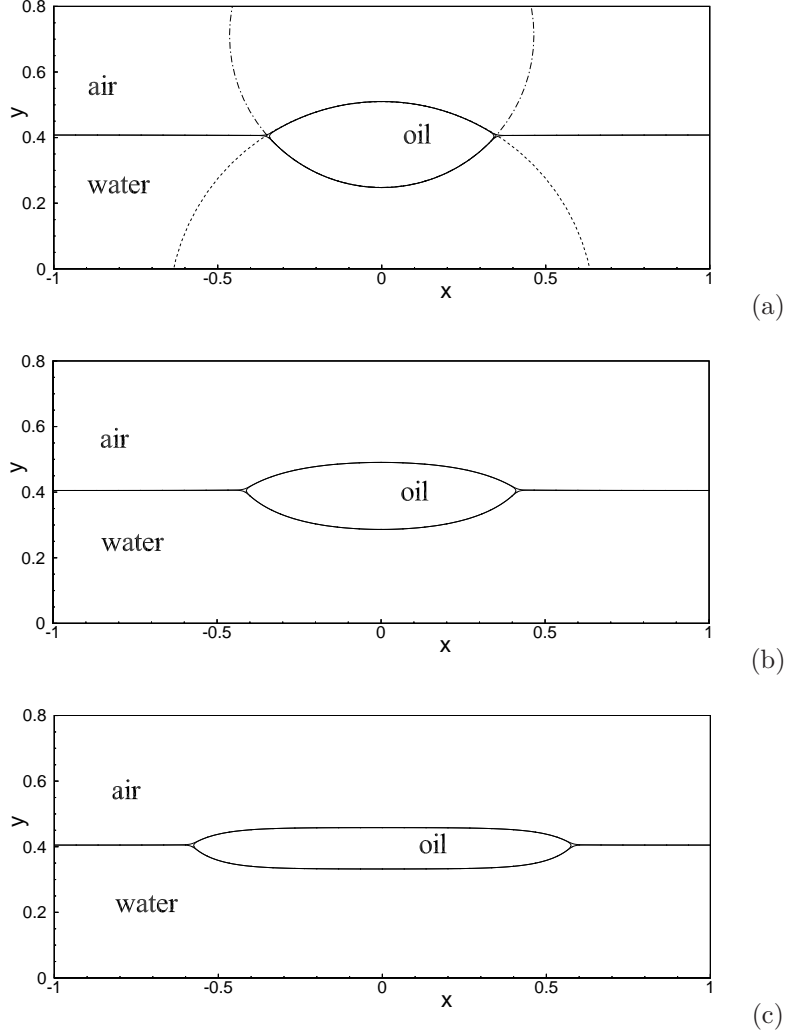


Figure 11: Floating liquid lens: equilibrium oil-drop profiles on air/water interface with (a) no gravity, (b)  $|\mathbf{g}_r| = 2m/s^2$ , and (c)  $|\mathbf{g}_r| = 7.5m/s^2$ . Fluid interfaces are visualized by contour levels  $c_i = 1/2$  ( $i = 1, 2, 3$ ). In (a) dashed and dashed-dot curves are part of two circles.

the simulations are in good agreement with the asymptotic puddle thickness values from the Langmuir-de Gennes theory [10].

#### 4.4.2 Floating Liquid Lens as a Four-Phase Problem with One Absent Fluid

The floating liquid lens problem can also be physically considered as a multiphase system consisting of more than three fluid components, in which however only the three fluids air, water and oil are present. We will next treat and simulate the floating liquid lens problem as a four-phase system, comprising air, water, oil, and another liquid referred to as  $F_A$ , in which the liquid  $F_A$  is absent however. We assume that these four fluids are mutually immiscible. Thanks to the reduction consistency of our formulation, we expect that the simulation of this four-phase problem using the method developed herein will produce the same results as the three-phase simulation.

In addition to the physical parameters given in Table 5 for the properties of air/water/oil, we assume

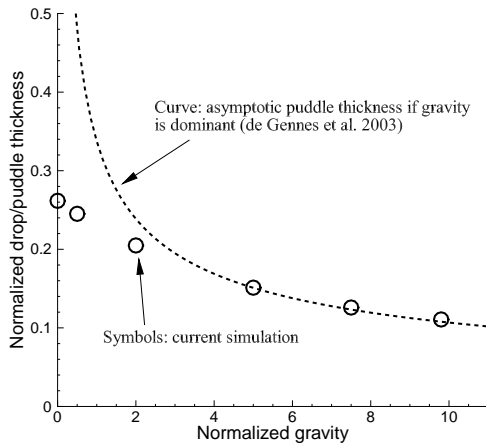


Figure 12: Comparison of oil-drop/-puddle thickness as a function of the gravity between current simulations and the de Gennes theory [10].

the following physical parameters involving  $F_A$ :

$$\begin{cases} F_A \text{ density :} & 100 \text{ kg/m}^3 \\ F_A \text{ dynamic viscosity :} & 9.0 \times 10^{-3} \text{ kg/(m} \cdot \text{s)} \\ \text{Surface tension [kg/s}^2\text{] :} & \text{air}/F_A - 0.045, \quad \text{water}/F_A - 0.05, \quad \text{oil}/F_A - 0.052. \end{cases}$$

We assign water, oil,  $F_A$ , and air as the first, the second, the third, and the fourth fluid in the simulations. We employ the same length scale, velocity scale and the density scale as in the three-phase simulations for the normalization of the problem.

The flow domain and the problem setting will be the same as those of the three-phase simulations. We use the same spectral-element mesh and the same boundary conditions for the four-phase simulations. The initial velocity is zero, and the initial volume fractions for the four-phase simulation are as follows:

$$\begin{cases} c_1 = \frac{1}{2} \left[ 1 - \tanh \left( \frac{y - y_c}{\sqrt{2}\eta} \right) \right] \frac{1}{2} \left[ 1 + \tanh \left( \frac{|\mathbf{x} - \mathbf{x}_c| - R_0}{\sqrt{2}\eta} \right) \right] \\ c_2 = \frac{1}{2} \left[ 1 - \tanh \left( \frac{|\mathbf{x} - \mathbf{x}_c| - R_0}{\sqrt{2}\eta} \right) \right] \\ c_3 = 0 \\ c_4 = 1 - c_1 - c_2 - c_3 = 1 - c_1 - c_2 \end{cases} \quad (52)$$

where  $y_c$ ,  $R_0$ ,  $\mathbf{x}_c$  are the same as those in the three-phase simulations. Note that  $c_3$  corresponds to the liquid  $F_A$ . It is set to zero (absent) initially, and so physically  $F_A$  should remain absent over time.

We consider only one case for the four-phase simulations, with a gravity  $0.5 \text{ m/s}^2$ , and employ the following simulation parameters:  $\eta/L = 0.01$ , and an element order 11 for all elements. The rest of the simulation parameters are the same as given by Table 6. We will compare the four-phase simulation results with the three-phase simulations using the same simulation parameter values.

Figure 13(a) shows the equilibrium configuration of the system (corresponding to a gravity  $0.5 \text{ m/s}^2$ ) from the four-phase simulations. The fluid interfaces are visualized by the contour lines  $c_i = \frac{1}{2}$  ( $i = 1, 2, 4$ ). Figures 13(b)–(d) show the profiles of the four volume fractions  $c_i$  ( $i = 1, 2, 3, 4$ ) along three vertical lines located at  $x = 0$ ,  $x = 0.351$  and  $x = 0.6$ . Note that the vertical line  $x = 0.351$  passes through the right star-shaped region around the three-phase line in Figure 13(a). We observe that the distributions for  $c_1$  (water),  $c_2$  (oil) and  $c_4$  (air) are very similar to those from the three-phase simulations (see e.g. Figure 10(b)–(c)). The volume fraction  $c_3$  (liquid  $F_A$ ) is practically zero, with a maximum value on the order of magnitude  $10^{-13}$  in the entire domain.

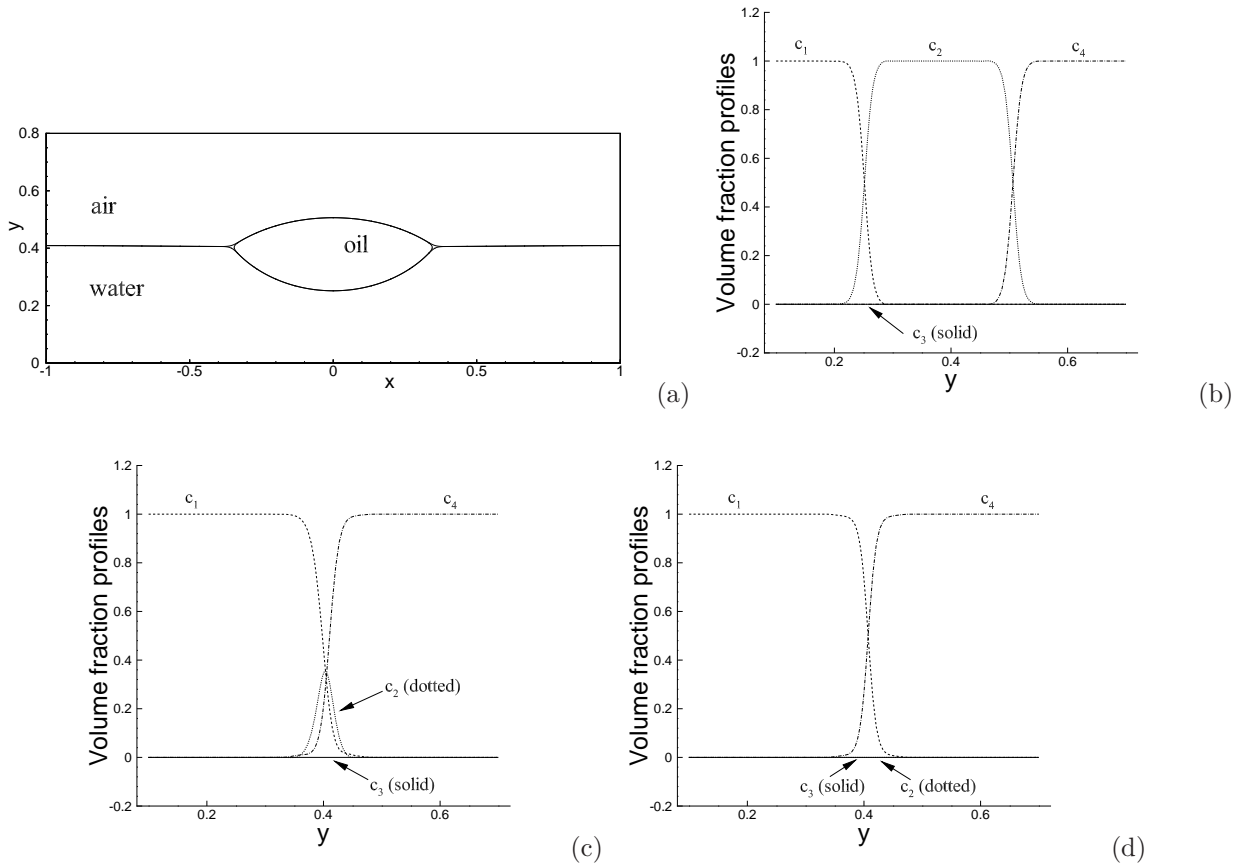


Figure 13: Floating liquid lens simulated as a four-phase problem with one absent fluid (gravity  $0.5m/s^2$ ): (a) Equilibrium configuration visualized by contour levels  $c_i = 1/2$  ( $i = 1, 2, 4$ ). (b)–(d): Profiles of volume fractions  $c_i$  ( $i = 1, 2, 3, 4$ ) along the vertical lines  $x = 0$  (b),  $x = 0.351$  (c), and  $x = 0.6$  (d).  $c_3$  corresponds to the absent fluid.

In Figure 14 we compare the volume-fraction profiles of the oil ( $c_2$ ) obtained from the four-phase simulation (with one absent fluid) and from the three-phase simulation, computed under the same simulation parameter values. The four plots correspond to the profiles along several vertical lines located at  $x = 0, 0.2, 0.351$  and  $0.6$ . The profiles from the four-phase simulation (solid curves) almost exactly overlap with those from the three-phase simulation (dashed curves), suggesting that the four-phase simulation (with one absent fluid) has produced the same results as the three-phase simulation for the floating liquid lens problem.

#### 4.5 Dynamics of a Four-Phase Problem

In this subsection we study a dynamic problem involving four fluid components as another test for the method developed in this work. The problem setting is illustrated by Figure 15(a). We consider a rectangular domain  $-L/2 \leq x \leq L/2$  and  $0 \leq y \leq 1.6L$ , where  $L = 2cm$ , and four immiscible incompressible fluids contained in this domain: air, water, liquid “F1”, and liquid “F2”. F1 and F2 are both heavier than air and lighter than water. The domain is bounded by two solid walls of neutral wettability on the top and bottom sides, and is periodic in the horizontal direction. The gravitational acceleration  $\mathbf{g}_r$  is in the  $-y$  direction. The top half of the domain is initially filled with air, and the bottom half is filled with water. A drop of the liquid F1, initially circular with a diameter  $0.3L$ , is suspended in the air and held at rest. A drop of the liquid F2, initially circular with a diameter of  $0.3L$  also, is trapped in the water and held at rest. The centers of the

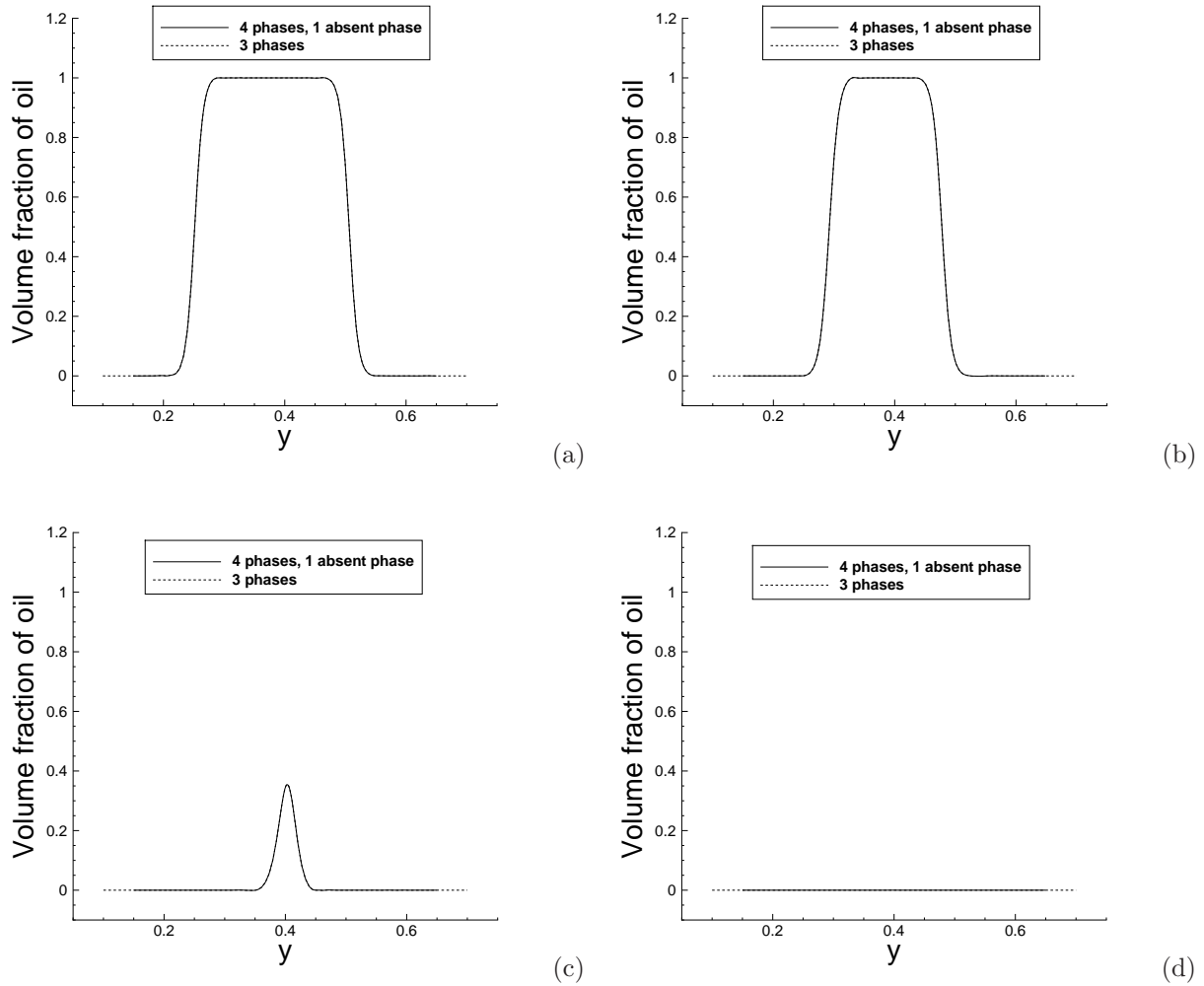


Figure 14: Comparison of volume-fraction profiles of the oil (gravity  $0.5m/s^2$ ) simulated as a three-phase problem and as a four-phase problem with one absent fluid, along vertical lines located at (a)  $x = 0$ , (b)  $x = 0.2$ , (c)  $x = 0.351$ , (d)  $x = 0.6$ .

Density [ $kg/m^3$ ]:	air - 1.2041	water - 998.207	F1 - 870	F2 - 50
Dynamic viscosity [ $kg/(m \cdot s)$ ]:	air - $1.78E - 5$	water - $1.002E - 3$	F1 - 0.0915	F2 - 0.01
Surface tension [ $kg/s^2$ ]:	air/water - 0.0728	air/F1 - 0.055	air/F2 - 0.06	
	water/F1 - 0.044	water/F2 - 0.045	F1/F2 - 0.048	
Gravity [ $m/s^2$ ]:	9.8			

Table 7: Physical parameter values for the air/water/F1/F2 four-phase problem.

two drops are located at

$$\begin{cases} \mathbf{x}_{F1} = (x_{F1}, y_{F1}) = (-0.05L, 1.3L) & \text{(F1 drop)} \\ \mathbf{x}_{F2} = (x_{F2}, y_{F2}) = (0.05L, 0.2L) & \text{(F2 drop)} \end{cases}$$

At  $t = 0$ , the two liquid drops are released, and they fall through the air and rise through the water, and impact the water surface. Our goal is to study this dynamic process.

The values for the physical properties of the four fluid components employed in this problem are listed in

Parameters	Values
$\lambda_{ij}$	computed by equation (17)
$\eta/L$	0.005
$m_0 \varrho_d U_0/L$	$10^{-8}$
$U_0 \Delta t/L$	$1.0 \times 10^{-6}$
$\rho_0$	$\min(\tilde{\rho}_1, \tilde{\rho}_2, \tilde{\rho}_3, \tilde{\rho}_4)$
$\nu_0$	$10 \max\left(\frac{\tilde{\mu}_1}{\tilde{\rho}_1}, \frac{\tilde{\mu}_2}{\tilde{\rho}_2}, \frac{\tilde{\mu}_3}{\tilde{\rho}_3}, \frac{\tilde{\mu}_4}{\tilde{\rho}_4}\right)$
$\mathcal{K}_0$	computed by equation (31)
$S$	$\sqrt{\frac{4\gamma_0}{\mathcal{K}_0 \Delta t}}$
$\alpha$	computed by equation (35)
$J$ (temporal order)	2
Number of elements	1440
Element order	9

Table 8: Simulation parameter values for the air/water/F1/F2 four-phase problem.

Table 7, including the densities, dynamic viscosities, pair-wise surface tensions and the gravity. We assign the air, water, F1 and F2 as the first, the second, the third and the fourth fluid in the simulations, respectively. We choose the air density as the density scale  $\varrho_d$ ,  $L$  as the length scale, and  $U_0 = \sqrt{g_{r0}L}$  as the velocity scale, where  $g_{r0} = 1m/s^2$ . All the variables are then normalized according to Table 1. The source terms in the phase field equations (25) are set to  $d_i = 0$  ( $1 \leq i \leq 3$ ).

We discretize the domain using a spectral element mesh of 1440 quadrilateral elements of equal sizes, with 30 elements along the  $x$  direction and 48 elements along the  $y$  direction. An element order 9 is used in the simulations for all elements. On the top/bottom walls the no slip condition, equation (21) with  $\mathbf{w} = 0$ , is imposed on the velocity, and the boundary conditions (26a) and (26b) with  $d_{ai} = 0$  and  $d_{bi} = 0$  are imposed on the volume fractions  $c_i$  ( $1 \leq i \leq 3$ ). Periodic conditions are employed for all flow variables at  $x = \pm L/2$ . We set the initial velocity to zero, and the initial volume fractions to the following functions:

$$\begin{cases}
 c_1 = \frac{1}{2} \left( 1 + \tanh \frac{y - y_w}{\sqrt{2}\eta} \right) \left[ 1 - \frac{1}{2} \left( 1 - \tanh \frac{|\mathbf{x} - \mathbf{x}_{F1}| - R_0}{\sqrt{2}\eta} \right) \right] \\
 c_2 = \frac{1}{2} \left( 1 - \tanh \frac{y - y_w}{\sqrt{2}\eta} \right) \left[ 1 - \frac{1}{2} \left( 1 - \tanh \frac{|\mathbf{x} - \mathbf{x}_{F2}| - R_0}{\sqrt{2}\eta} \right) \right] \\
 c_3 = \frac{1}{2} \left( 1 - \tanh \frac{|\mathbf{x} - \mathbf{x}_{F1}| - R_0}{\sqrt{2}\eta} \right) \\
 c_4 = 1 - c_1 - c_2 - c_3
 \end{cases} \quad (53)$$

where  $y_w = 0.8L$  is the  $y$  coordinate of the initial water surface, and  $R_0 = 0.15L$  is the initial radius of the F1 and F2 drops. Table 8 lists the values of the simulation parameters for this problem.

Let us look into the dynamics of this four-phase system. Figure 15 shows a temporal sequence of snapshots of the fluid interfaces of the system. The interfaces are visualized by the contour lines of the volume fractions  $c_i = \frac{1}{2}$  ( $i = 1, \dots, 4$ ). From Figures 15(a)–(c), we observe that as the system is released the F1 drop falls rapidly through the air, with little deformation in this process. But as the F1 drop approaches the water surface just before the impact (Figure 15(c)), a depression on the water surface and a deformation of the lower side of the F1 drop can be clearly noticed. At the same time, the F2 drop rises through the water at a much slower speed. The deformation of the F2 drop is substantial, and its shape resembles a circular “cap” (Figures 15(b)–(c)). Subsequently, the falling F1 drop impacts the water, causing a ripple on the water surface (Figure 15(d)). It can be observed that the F1 drop has trapped a thin cushion of air between its underside and the water surface (Figure 15(d)). The impact causes the F1 drop to deform severely, and it forms a pool of the F1 liquid floating on the surface of water (Figure 15(e)–(h)). The air trapped between the F1 drop and the water surface forms a small air bubble at the underside of the pool of F1 fluid (Figure 15(e)–(l)). As the F2 drop rises further and approaches the pool of F1 liquid that now covers a portion of

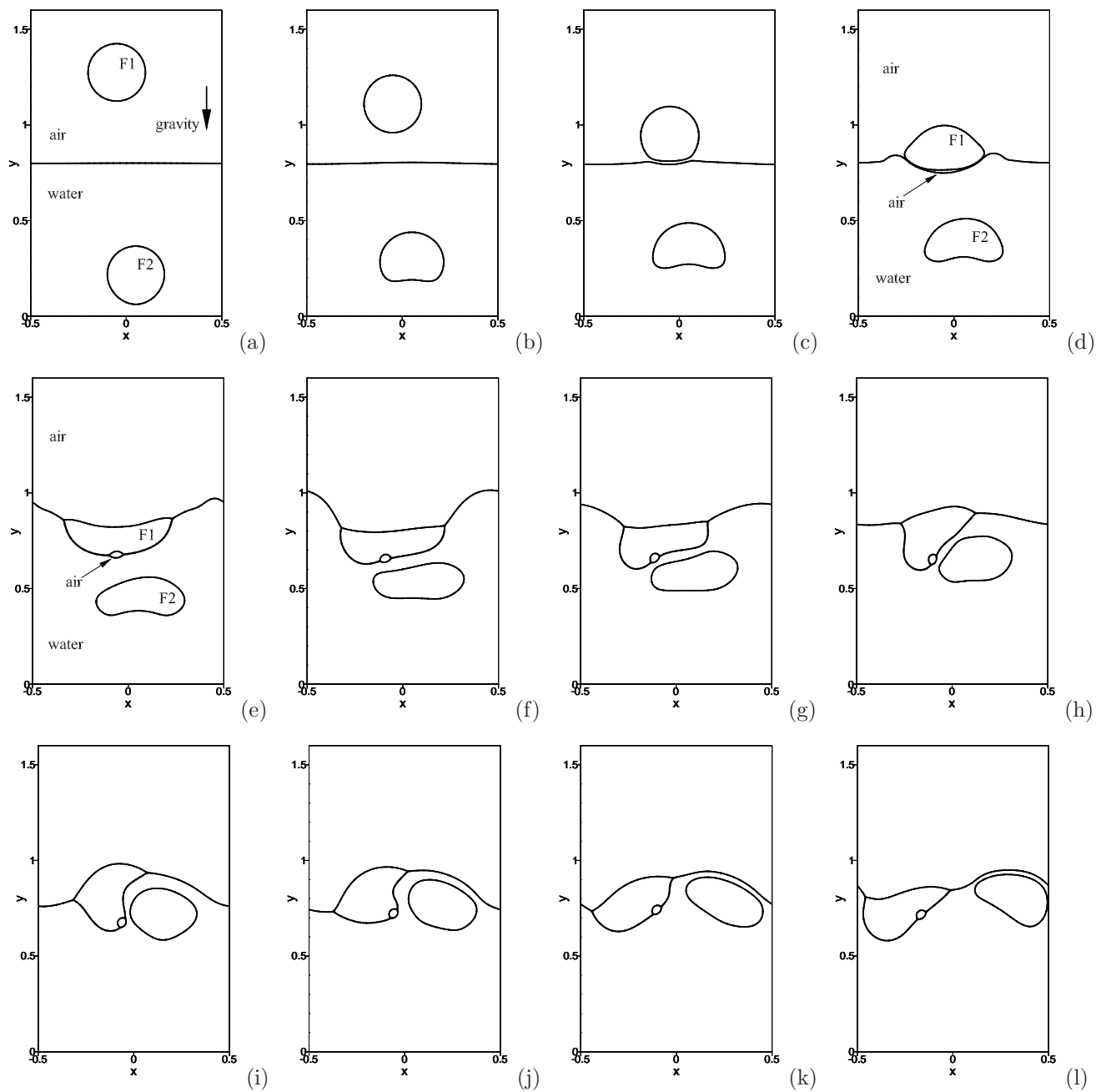


Figure 15: Temporal sequence of snapshots of fluid interfaces, visualized by the volume-fraction contours  $c_i = 1/2$  ( $i = 1, \dots, 4$ ), showing two fluid drops impacting water surface (4 fluid components): (a)  $t = 0.072$ , (b)  $t = 0.198$ , (c)  $t = 0.27$ , (d)  $t = 0.31$ , (e)  $t = 0.41$ , (f)  $t = 0.538$ , (g)  $t = 0.614$ , (h)  $t = 0.702$ , (i)  $t = 0.79$ , (j)  $t = 0.862$ , (k)  $t = 0.934$ , (l)  $t = 1.01$ .

the water surface, it experiences significant deformation and its shape has become highly irregular (Figure 15(d)–(e)). Subsequently, it can be observed from Figures 15(f)–(j) that the interaction between the F1 fluid and the F2 drop appears to cause both fluids to move sideways away from each other while the F2 drop rises further. The F2 drop appears to glide past the pool of F1 fluid (Figures 15(g)–(i)), and rises in an oblique direction toward the open surface of water (Figures 15(j)–(l)). It can be observed that the pool of F1 fluid experiences significant deformations in this process (Figures 15(g)–(l)).

## 5 Concluding Remarks

This paper focuses on the formulation and simulation of multiphase flows consisting of  $N$  ( $N \geq 2$ ) immiscible incompressible fluids with different densities, dynamic viscosities and pair-wise surface tensions. In particular, we have explored how to formulate the N-phase system in a reduction-consistent and thermodynamically consistent manner. Thermodynamic consistency is achieved by adopting a thermodynamically consistent phase field model for the N-phase system derived based on the mass/momentum conservations and the second law of thermodynamics. Reduction consistency is achieved by the construction of the mobility matrix and the free energy density function with appropriate individual reduction properties, which collectively guarantee the full reduction consistency of the N-phase governing equations.

We have made two contributions in this work. The main contribution lies in the method (Theorem 2.1) provided herein, which allows for the systematic construction of reduction-consistent N-phase formulations. This method is quite general, and it suggests many possible forms for reduction-consistent and thermodynamically consistent N-phase formulations. Based on this method, we have developed and presented a specific reduction-consistent and thermodynamically consistent formulation for incompressible N-phase ( $N \geq 2$ ) flows, which is the second contribution of this work. This specific N-phase formulation, together with the boundary conditions presented in Section 3, fully satisfies the reduction consistency conditions (C1), (C2) and (C3).

We can compare the approach to reduction consistency in this work with that of [16], and also perhaps with that of [8] for a Cahn-Hilliard model (without hydrodynamic interactions). The approach of this paper allows us to treat the reduction properties of the mobility matrix and the free energy density function separately and individually. Therefore, it is considerably easier in the construction to satisfy these reduction properties. In contrast, in [16] (and also [8]) the reduction properties for the free energy density function are entangled with that of the mobility matrix. This poses an enormous challenge in the construction of the free energy density function to satisfy these reduction properties for full reduction consistency. Consequently, only a partial reduction consistency (between  $N$  phases and two phases) has been achieved in [16, 8] for an arbitrary set of given pair-wise surface tensions.

For the specific reduction-consistent and thermodynamically consistent N-phase formulation presented herein, we have also presented an efficient numerical algorithm for solving the N-phase governing equations. This is a semi-implicit splitting type scheme, which de-couples the solution of different flow variables. Despite the variable mobility matrix and the variable mixture density/viscosity, our algorithm involves only the solution of linear algebraic systems with *constant and time-independent* coefficient matrices within each time step for all variables. In particular, when solving the system of coupled fourth-order phase field equations, our algorithm only requires the solution of  $2(N - 1)$  individual Helmholtz type equations in a de-coupled fashion.

Extensive numerical experiments have been presented for flow problems involving multiple fluid components, large density ratios and large viscosity ratios to test the performance of the method presented herein, and we have compared simulation results with exact physical solutions or physical theories from the literature. In particular, we have conducted simulations of three- or four-phase systems in which one or two fluid components are absent, and demonstrated that the simulation results indeed match the results obtained on the smaller systems. Comparisons with the Prosperetti’s theory and the Langmuir-de Gennes theory show that our method produces physically accurate results.

Reduction consistency and thermodynamic consistency are important physical consistency requirements, and can have a profound impact on the simulation results. The lack of such consistency properties may lead to un-physical results or result in gross errors. For example, in [16] we have documented the detrimental effect of the lack of reduction consistency in the formulation or boundary condition on the simulation of

wall-bounded N-phase flows and N-phase contact angles. It is observed that, due to the lack of reduction consistency, a “third” fluid can be artificially generated at the base of a liquid drop near the wall, causing a gross deviation of the contact angle from the expected value [16].

## Acknowledgement

This work was partially supported by NSF (DMS-1318820, DMS-1522537).

## Appendix A. Development of Thermodynamically Consistent N-phase Model

In this Appendix we summarize the development of a thermodynamically consistent N-phase model based on the mass conservation, momentum conservation, and the second law of thermodynamics. The development follows a similar procedure to that for the model of [12], but we arrive at an N-phase model that is different from those of [12, 16], due to difference in the representation of mass balances and the specification of constitutive relations to satisfy the second law of thermodynamics. The basic steps in the following development mirror those of [12]. We refer the reader to the appendix of [12] for the derivation of that model therein.

**Definitions and Settings** Consider an iso-thermal mixture of  $N$  ( $N \geq 2$ ) immiscible incompressible fluids in some flow domain in two or three dimensions. Let  $\tilde{\rho}_i$  ( $1 \leq i \leq N$ ) and  $\tilde{\mu}_i$  ( $1 \leq i \leq N$ ) respectively denote the constant densities and constant dynamic viscosities of these  $N$  fluids. Consider an arbitrary control volume  $V$  taken from the mixture. Let  $M_i$  ( $1 \leq i \leq N$ ) denote the mass of fluid  $i$  contained within  $V$ ,  $\rho_i$  ( $1 \leq i \leq N$ ) denote the average density of fluid  $i$  within  $V$ , and  $M$  and  $\rho$  respectively denote the total mass and the average density of the mixture within  $V$ . Then the following relations hold,

$$\rho_i = \frac{M_i}{V}, \quad \rho = \frac{M}{V} = \frac{M_1 + \cdots + M_N}{V} = \rho_1 + \rho_2 + \cdots + \rho_N. \quad (54)$$

We make the following assumption:

(A1): There is no volume addition or volume loss if any of these  $N$  fluids are mixed, in other words, the volume occupied by a given amount of mass of any single fluid  $i$  does not change after mixing.

Let  $V_i$  ( $1 \leq i \leq N$ ) denote the volume occupied by the pure fluid  $i$  (before mixing) of mass  $M_i$ . It follows from the above assumption that

$$V = V_1 + V_2 + \cdots + V_N. \quad (55)$$

Let  $c_i$  ( $1 \leq i \leq N$ ) denote the volume fraction of fluid  $i$  within  $V$ . Then

$$c_i = \frac{V_i}{V} = \frac{M_i/\tilde{\rho}_i}{M_i/\rho_i} = \frac{\rho_i}{\tilde{\rho}_i}, \quad c_1 + c_2 + \cdots + c_N = 1. \quad (56)$$

Let the control volume  $V \rightarrow 0$ , and the average quantities defined above become field variables  $\rho_i(\mathbf{x}, t)$ ,  $c_i(\mathbf{x}, t)$ ,  $\rho(\mathbf{x}, t)$ . These definitions follow those given in [12].

**Mass Balance** Let  $\hat{\mathbf{J}}_i$  ( $1 \leq i \leq N$ ) denote the mass flux vector of fluid  $i$  in the mixture. Then the mass balance of fluid  $i$  leads to

$$\frac{\partial \rho_i}{\partial t} + \nabla \cdot \hat{\mathbf{J}}_i = 0, \quad 1 \leq i \leq N. \quad (57)$$

We define the individual velocity of fluid  $i$ ,  $\mathbf{u}_i$  ( $1 \leq i \leq N$ ), by  $\hat{\mathbf{J}}_i = \rho_i \mathbf{u}_i$ . Following [12], we define the mixture (or bulk) velocity as the volume-averaged velocities of the individual fluids,

$$\mathbf{u} = \sum_{i=1}^N c_i \mathbf{u}_i = \sum_{i=1}^N \frac{\rho_i}{\tilde{\rho}_i} \mathbf{u}_i = \sum_{i=1}^N \frac{\hat{\mathbf{J}}_i}{\tilde{\rho}_i}, \quad (58)$$

where we have used (56). This mixture velocity is divergence free [12],

$$\nabla \cdot \mathbf{u} = \sum_{i=1}^N \frac{1}{\tilde{\rho}_i} \nabla \cdot \hat{\mathbf{J}}_i = -\frac{\partial}{\partial t} \left( \sum_{i=1}^N \frac{\rho_i}{\tilde{\rho}_i} \right) = -\frac{\partial}{\partial t} \left( \sum_{i=1}^N c_i \right) = -\frac{\partial}{\partial t} 1 = 0. \quad (59)$$

Introduce the differential flux,  $\mathbf{J}_i = \hat{\mathbf{J}}_i - \rho_i \mathbf{u}$ , which is the flux of fluid  $i$  relative to the bulk motion characterized by  $\mathbf{u}$ .  $\mathbf{J}_i$  satisfies the relation

$$\sum_{i=1}^N \frac{1}{\tilde{\rho}_i} \mathbf{J}_i = \sum_{i=1}^N \frac{\hat{\mathbf{J}}_i}{\tilde{\rho}_i} - \sum_{i=1}^N \frac{\rho_i}{\tilde{\rho}_i} \mathbf{u} = \mathbf{u} - \left( \sum_{i=1}^N c_i \right) \mathbf{u} = 0. \quad (60)$$

The mass balance equation (57) is then transformed into

$$\frac{\partial \rho_i}{\partial t} + \mathbf{u} \cdot \nabla \rho_i = -\nabla \cdot \mathbf{J}_i, \quad 1 \leq i \leq N \quad (61)$$

where we have used (59). Sum up the  $N$  equations in (61) and we have

$$\frac{\partial \rho}{\partial t} + \mathbf{u} \cdot \nabla \rho = -\nabla \cdot \tilde{\mathbf{J}}, \quad \text{where } \tilde{\mathbf{J}} = \mathbf{J}_1 + \mathbf{J}_2 + \cdots + \mathbf{J}_N. \quad (62)$$

Equation (61) can be written in terms of the volume fractions as

$$\frac{\partial c_i}{\partial t} + \mathbf{u} \cdot \nabla c_i = -\nabla \cdot \left( \frac{\mathbf{J}_i}{\tilde{\rho}_i} \right), \quad 1 \leq i \leq N. \quad (63)$$

The mass balance of the  $N$  individual fluids in the system is represented by the equations (61) or (63). The forms of the differential fluxes  $\mathbf{J}_i$  ( $1 \leq i \leq N$ ) in these equations are to be specified by considering the second law of thermodynamics, and must satisfy the constraint (60).

**Momentum Balance** Following [1, 12], we make the following assumption:

(A2): The inertia and kinetic energy of the relative motion of any fluid with respect to the bulk motion is negligible, and the mixture can be considered as a single fluid, which satisfies the linear-momentum conservation with respect to the volume-averaged velocity  $\mathbf{u}$ .

Consider an arbitrary control volume  $\Omega(t)$ , which moves with the bulk mixture velocity  $\mathbf{u}$ . We assume that there is no external body force. Then the momentum conservation on this control volume is represented by

$$\frac{d}{dt} \int_{\Omega(t)} \rho \mathbf{u} = \int_{\partial\Omega(t)} \mathbf{n} \cdot \mathbf{T} - \int_{\partial\Omega(t)} \sum_{i=1}^N (\mathbf{n} \cdot \mathbf{J}_i) \mathbf{u} \quad (64)$$

where  $\partial\Omega(t)$  denotes the boundary of  $\Omega(t)$ ,  $\mathbf{n}$  is the outward-pointing unit vector normal to the boundary,  $\mathbf{T}$  denotes a stress tensor whose form is to be specified by constitutive relations, and the last term on the right hand side (RHS) denotes the momentum transport due to the relative motion of the fluids with respect to the bulk motion. Since the control volume is arbitrary, by using the Reynolds transport theorem and the divergence theorem we can transform this equation into

$$\frac{\partial}{\partial t} (\rho \mathbf{u}) + \nabla \cdot (\rho \mathbf{u} \mathbf{u}) + \nabla \cdot (\tilde{\mathbf{J}} \mathbf{u}) = \nabla \cdot \mathbf{T} \quad (65)$$

where we have also used the  $\tilde{\mathbf{J}}$  expression in (62). This equation can be further reduced to

$$\rho \left( \frac{\partial \mathbf{u}}{\partial t} + \mathbf{u} \cdot \nabla \mathbf{u} \right) + \tilde{\mathbf{J}} \cdot \nabla \mathbf{u} = \nabla \cdot \mathbf{T} \quad (66)$$

where equation (62) has been used.

We assume that the stress tensor  $\mathbf{T}$  is symmetric, and re-write it as

$$\mathbf{T} = \frac{1}{3}(\text{tr}\mathbf{T})\mathbf{I} + \mathbf{S} = -p\mathbf{I} + \mathbf{S} \quad (67)$$

where  $\mathbf{I}$  is the identity tensor,  $\mathbf{S}$  is a trace-free symmetric tensor, and  $p = \frac{1}{3}\text{tr}\mathbf{T}$  will be referred to as the pressure. The momentum equation (66) is then transformed into

$$\rho \left( \frac{\partial \mathbf{u}}{\partial t} + \mathbf{u} \cdot \nabla \mathbf{u} \right) + \tilde{\mathbf{J}} \cdot \nabla \mathbf{u} = -\nabla p + \nabla \cdot \mathbf{S}. \quad (68)$$

The form for the stress tensor  $\mathbf{S}$  will be specified by considering the second law of thermodynamics.

**Constitutive Relations and Second Law of Thermodynamics** We now consider how to specify the constitutive relations for the tensor  $\mathbf{S}$  and the differential fluxes  $\mathbf{J}_i$  ( $1 \leq i \leq N$ ) based on the second law of thermodynamics.

In the spirit of the phase field approach we introduce a free energy density function  $W(\vec{c}, \nabla \vec{c})$ , where  $\vec{c} = (c_1, c_2, \dots, c_N)$ , to account for the effect of the interfacial energy (surface tensions) among the  $N$  fluids. The total energy density function of the system is  $e(\mathbf{u}, \vec{c}, \nabla \vec{c}) = \frac{1}{2}\rho|\mathbf{u}|^2 + W(\vec{c}, \nabla \vec{c})$ .

Consider an arbitrary control volume  $\Omega(t)$  that moves with the bulk velocity  $\mathbf{u}$ . For an isothermal system, the second law of thermodynamics is represented by the following inequality [23],

$$\frac{d}{dt} \int_{\Omega(t)} e(\mathbf{u}, \vec{c}, \nabla \vec{c}) \leq P_c \quad (69)$$

where  $P_c$  denotes the total conventional power (i.e. excluding heat transfer) expended on  $\Omega(t)$ .

The conventional powers expended on  $\Omega(t)$  consist of several components:

- Work due to the stress tensor,  $\int_{\partial\Omega(t)} \mathbf{n} \cdot \mathbf{T} \cdot \mathbf{u}$ .
- Kinetic energy transport due to the relative motion of the fluids with respect to the bulk motion,

$$- \int_{\partial\Omega(t)} \sum_{i=1}^N (\mathbf{n} \cdot \mathbf{J}_i) \frac{1}{2} |\mathbf{u}|^2 = - \int_{\partial\Omega(t)} (\mathbf{n} \cdot \tilde{\mathbf{J}}) \frac{1}{2} |\mathbf{u}|^2.$$

Note that  $-\mathbf{n} \cdot \mathbf{J}_i$  is the mass of fluid  $i$  transported into  $\Omega(t)$  due to the relative motion with respect to the bulk motion.

- Free energy transport due to the relative motion of the fluids with respect to the bulk motion,

$$- \sum_{i=1}^N \int_{\partial\Omega(t)} (\mathbf{n} \cdot \mathbf{J}_i) \mathcal{C}_i$$

where  $\mathcal{C}_i$  ( $1 \leq i \leq N$ ) is the chemical potential of fluid  $i$  (free energy per unit mass).

- Work due to a surface microforce. Following [22], we assume the existence of a surface microforce  $\xi_i$  ( $1 \leq i \leq N$ ), whose power expended on the system is represented by (see [22])

$$\sum_{i=1}^N \int_{\partial\Omega(t)} \mathbf{n} \cdot \xi_i \left( \frac{\partial c_i}{\partial t} + \mathbf{u} \cdot \nabla c_i \right).$$

By incorporating the above contributions, the inequality (69) becomes

$$\begin{aligned} \frac{d}{dt} \int_{\Omega(t)} e(\mathbf{u}, \vec{c}, \nabla \vec{c}) - \int_{\partial\Omega(t)} \mathbf{n} \cdot \mathbf{T} \cdot \mathbf{u} + \int_{\partial\Omega(t)} (\mathbf{n} \cdot \tilde{\mathbf{J}}) \frac{1}{2} |\mathbf{u}|^2 \\ + \sum_{i=1}^N \int_{\partial\Omega(t)} \mathbf{n} \cdot \mathbf{J}_i \mathcal{C}_i - \sum_{i=1}^N \int_{\partial\Omega(t)} (\mathbf{n} \cdot \xi_i) \frac{Dc_i}{Dt} \leq 0 \end{aligned} \quad (70)$$

where  $\frac{Dc_i}{Dt} = \frac{\partial c_i}{\partial t} + \mathbf{u} \cdot \nabla c_i$  denotes the material derivative. By invoking the Reynolds transport theorem and the divergence theorem, and noting that  $\Omega(t)$  is arbitrary, we transform the above inequality into

$$-D_s \equiv \frac{\partial e}{\partial t} + \nabla \cdot (e\mathbf{u}) - \nabla \cdot (\mathbf{T} \cdot \mathbf{u}) + \nabla \cdot \left( \tilde{\mathbf{J}} \frac{1}{2} |\mathbf{u}|^2 \right) + \sum_{i=1}^N \nabla \cdot (\mathbf{J}_i \mathcal{C}_i) - \sum_{i=1}^N \nabla \cdot \left( \boldsymbol{\xi}_i \frac{Dc_i}{Dt} \right) \leq 0 \quad (71)$$

In light of equations (59), (62) and (66), we can transform (71) into

$$\begin{aligned} -D_s = \frac{\partial W}{\partial t} + \mathbf{u} \cdot \nabla W - \mathbf{T} : \nabla \mathbf{u} + \sum_{i=1}^N (\nabla \cdot \mathbf{J}_i) \mathcal{C}_i + \sum_{i=1}^N \mathbf{J}_i \cdot \nabla \mathcal{C}_i \\ - \sum_{i=1}^N (\nabla \cdot \boldsymbol{\xi}_i) \frac{Dc_i}{Dt} - \sum_{i=1}^N \boldsymbol{\xi}_i \cdot \nabla \frac{Dc_i}{Dt} \leq 0 \end{aligned} \quad (72)$$

where the symmetry assumption about  $\mathbf{T}$  has been used.

In light of equation (63) and the relations

$$\begin{cases} \nabla \frac{Dc_i}{Dt} = \frac{D}{Dt} (\nabla c_i) + (\nabla \mathbf{u}) \cdot \nabla c_i \\ \frac{DW}{Dt} = \sum_{i=1}^N \frac{\partial W}{\partial c_i} \frac{Dc_i}{Dt} + \sum_{i=1}^N \frac{\partial W}{\partial (\nabla c_i)} \cdot \frac{D}{Dt} (\nabla c_i) \end{cases}$$

we can transform equation (72) into

$$\begin{aligned} -D_s = \sum_{i=1}^N \left[ \frac{\partial W}{\partial c_i} - \tilde{\rho}_i \mathcal{C}_i - \nabla \cdot \boldsymbol{\xi}_i \right] \frac{Dc_i}{Dt} + \sum_{i=1}^N \left[ \frac{\partial W}{\partial (\nabla c_i)} - \boldsymbol{\xi}_i \right] \cdot \frac{D(\nabla c_i)}{Dt} \\ - \mathbf{T} : \nabla \mathbf{u} - \sum_{i=1}^N (\nabla c_i \otimes \boldsymbol{\xi}_i) : \nabla \mathbf{u} + \sum_{i=1}^N \mathbf{J}_i \cdot \nabla \mathcal{C}_i \leq 0 \end{aligned} \quad (73)$$

We will make the following choices based on the inequality (73),

$$\boldsymbol{\xi}_i = \frac{\partial W}{\partial (\nabla c_i)}, \quad 1 \leq i \leq N; \quad (74a)$$

$$\mathcal{C}_i = \frac{1}{\tilde{\rho}_i} \left[ \frac{\partial W}{\partial c_i} - \nabla \cdot \frac{\partial W}{\partial (\nabla c_i)} \right], \quad 1 \leq i \leq N. \quad (74b)$$

Note that these are specific choices made in this work to guarantee the inequality (73). They are not the most general possible forms to satisfy (73). Discussion of general constitutive relations is beyond the scope of the current work.

Noting the choices (74a) and (74b) and the relation

$$(\nabla c_i \otimes \boldsymbol{\xi}_i) : \nabla \mathbf{u} = \frac{1}{2} (\nabla c_i \otimes \boldsymbol{\xi}_i + \boldsymbol{\xi}_i \otimes \nabla c_i) : \frac{1}{2} \mathbf{D}(\mathbf{u}) + \frac{1}{2} (\nabla c_i \otimes \boldsymbol{\xi}_i - \boldsymbol{\xi}_i \otimes \nabla c_i) : \frac{1}{2} (\nabla \mathbf{u} - \nabla \mathbf{u}^T),$$

where  $\mathbf{D}(\mathbf{u}) = \nabla \mathbf{u} + \nabla \mathbf{u}^T$ , we can transform (73) into

$$\begin{aligned} -D_s = - \left[ \mathbf{S} + \sum_{i=1}^N \frac{1}{2} \left( \nabla c_i \otimes \frac{\partial W}{\partial \nabla c_i} + \frac{\partial W}{\partial \nabla c_i} \otimes \nabla c_i \right) \right] : \frac{1}{2} \mathbf{D}(\mathbf{u}) \\ - \sum_{i=1}^N \frac{1}{2} \left( \nabla c_i \otimes \frac{\partial W}{\partial \nabla c_i} - \frac{\partial W}{\partial \nabla c_i} \otimes \nabla c_i \right) : \frac{1}{2} (\nabla \mathbf{u} - \nabla \mathbf{u}^T) + \sum_{i=1}^N \mathbf{J}_i \cdot \nabla \mathcal{C}_i \\ \leq 0 \end{aligned} \quad (75)$$

where we have used (67), (59), and the symmetry of  $\mathbf{S}$ . Since  $\frac{1}{2}(\nabla\mathbf{u} - \nabla\mathbf{u}^T)$  is independent of  $c_i$  ( $1 \leq i \leq N$ ) and  $W(\vec{c}, \nabla\vec{c})$ , and can attain arbitrary values, we conclude that

$$\sum_{i=1}^N \nabla c_i \otimes \frac{\partial W}{\partial(\nabla c_i)} = \sum_{i=1}^N \frac{\partial W}{\partial(\nabla c_i)} \otimes \nabla c_i, \quad (76)$$

which is a condition the free energy density function  $W(\vec{c}, \nabla\vec{c})$  must satisfy.

The inequality (75) is then reduced to

$$-D_s = - \left[ \mathbf{S} + \sum_{i=1}^N \nabla c_i \otimes \frac{\partial W}{\partial(\nabla c_i)} \right] : \frac{1}{2} \mathbf{D}(\mathbf{u}) + \sum_{i=1}^N \left( \frac{1}{\tilde{\rho}_i} \mathbf{J}_i \right) \cdot \nabla(\tilde{\rho}_i \mathcal{C}_i) \leq 0. \quad (77)$$

To ensure the above inequality we assume the following constitutive relations

$$\mathbf{S} + \sum_{i=1}^N \nabla c_i \otimes \frac{\partial W}{\partial(\nabla c_i)} = \mu(\vec{c}) \mathbf{D}(\mathbf{u}), \quad (78a)$$

$$\frac{1}{\tilde{\rho}_i} \mathbf{J}_i = - \sum_{j=1}^N m_{ij}(\vec{c}) \nabla(\tilde{\rho}_j \mathcal{C}_j) = - \sum_{j=1}^N m_{ij}(\vec{c}) \nabla \left[ \frac{\partial W}{\partial c_j} - \nabla \cdot \frac{\partial W}{\partial(\nabla c_j)} \right] \quad 1 \leq i \leq N, \quad (78b)$$

where  $\mu(\vec{c}) \geq 0$  plays the role of dynamic viscosity, and the matrix formed by the coefficients  $m_{ij}(\vec{c})$  ( $1 \leq i, j \leq N$ )

$$\mathbf{m} = [m_{ij}]_{N \times N} \quad (79)$$

is referred to as the mobility matrix.  $\mathbf{m}$  is required to be symmetric based on the Onsager's reciprocal relation and to be positive semi-definite in order to ensure non-positivity of the second term in the inequality (77). To ensure the relation (60) for arbitrary  $W(\vec{c}, \nabla\vec{c})$ , we further require that

$$\sum_{j=1}^N m_{ij}(\vec{c}) = \sum_{j=1}^N m_{ji}(\vec{c}) = 0, \quad 1 \leq i \leq N. \quad (80)$$

In light of the condition (80), the constitutive relation (78b) can be re-written as

$$\begin{aligned} \frac{1}{\tilde{\rho}_i} \mathbf{J}_i &= -m_{ii} \nabla(\tilde{\rho}_i \mathcal{C}_i) - \sum_{\substack{j=1 \\ j \neq i}}^N m_{ij} \nabla(\tilde{\rho}_j \mathcal{C}_j) = \sum_{\substack{j=1 \\ j \neq i}}^N m_{ij} \nabla(\tilde{\rho}_i \mathcal{C}_i) - \sum_{\substack{j=1 \\ j \neq i}}^N m_{ij} \nabla(\tilde{\rho}_j \mathcal{C}_j) \\ &= \sum_{\substack{j=1 \\ j \neq i}}^N m_{ij} [\nabla(\tilde{\rho}_i \mathcal{C}_i) - \nabla(\tilde{\rho}_j \mathcal{C}_j)] = \sum_{j=1}^N m_{ij} [\nabla(\tilde{\rho}_i \mathcal{C}_i) - \nabla(\tilde{\rho}_j \mathcal{C}_j)]. \end{aligned} \quad (81)$$

Consequently, the second term in the inequality (77) can be transformed into

$$\begin{aligned} \sum_{i=1}^N \frac{1}{\tilde{\rho}_i} \mathbf{J}_i \cdot \nabla(\tilde{\rho}_i \mathcal{C}_i) &= \sum_{i,j=1}^N m_{ij} [\nabla(\tilde{\rho}_i \mathcal{C}_i) - \nabla(\tilde{\rho}_j \mathcal{C}_j)] \cdot \nabla(\tilde{\rho}_i \mathcal{C}_i) \\ &= \sum_{i,j=1}^N \frac{1}{2} m_{ij} [\nabla(\tilde{\rho}_i \mathcal{C}_i) - \nabla(\tilde{\rho}_j \mathcal{C}_j)] \cdot [\nabla(\tilde{\rho}_i \mathcal{C}_i) - \nabla(\tilde{\rho}_j \mathcal{C}_j)] \\ &= \sum_{\substack{i,j=1 \\ j \neq i}}^N \frac{1}{2} m_{ij} |\nabla(\tilde{\rho}_i \mathcal{C}_i) - \nabla(\tilde{\rho}_j \mathcal{C}_j)|^2, \end{aligned}$$

where we have used the symmetry of  $m_{ij}$ . Therefore, a sufficient condition to ensure the non-positivity of above term, and the positive semi-definiteness of the mobility matrix  $\mathbf{m}$ , is

$$m_{ij}(\vec{c}) \leq 0, \quad 1 \leq i \neq j \leq N. \quad (82)$$

**A Thermodynamically Consistent N-Phase Model** Substituting the constitutive relations (78a) and (78b) into equations (68) and (63), we obtain the following N-phase formulation

$$\rho(\vec{c}) \left( \frac{\partial \mathbf{u}}{\partial t} + \mathbf{u} \cdot \nabla \mathbf{u} \right) + \tilde{\mathbf{J}} \cdot \nabla \mathbf{u} = -\nabla p + \nabla \cdot [\mu(\vec{c}) \mathbf{D}(\mathbf{u})] - \sum_{i=1}^N \nabla \cdot \left[ \nabla c_i \otimes \frac{\partial W}{\partial (\nabla c_i)} \right], \quad (83a)$$

$$\nabla \cdot \mathbf{u} = 0, \quad (83b)$$

$$\frac{\partial c_i}{\partial t} + \mathbf{u} \cdot \nabla c_i = \sum_{j=1}^N \nabla \cdot \left[ m_{ij}(\vec{c}) \nabla \left( \frac{\partial W}{\partial c_j} - \nabla \cdot \frac{\partial W}{\partial \nabla c_j} \right) \right], \quad 1 \leq i \leq N, \quad (83c)$$

where  $W(\vec{c}, \nabla \vec{c})$  is the free energy density function whose form satisfies the condition (76), and the coefficients  $m_{ij}(\vec{c})$  ( $1 \leq i, j \leq N$ ) form a symmetric positive semi-definite matrix and satisfy the condition (80). Note that only  $(N-1)$  equations among the  $N$  equations in (83c) are independent due to the conditions (56) and (80). The mixture density is given by, in light of (54) and (56),

$$\rho(\vec{c}) = \sum_{i=1}^N \rho_i(\vec{c}) = \sum_{i=1}^N \tilde{\rho}_i c_i. \quad (84)$$

$\tilde{\mathbf{J}}$  is given by, in light of (62) and (78b),

$$\tilde{\mathbf{J}}(\vec{c}, \nabla \vec{c}) = - \sum_{i,j=1}^N \tilde{\rho}_i m_{ij}(\vec{c}) \nabla \left( \frac{\partial W}{\partial c_j} - \nabla \cdot \frac{\partial W}{\partial \nabla c_j} \right). \quad (85)$$

In the current work we assume that the mixture dynamic viscosity  $\mu(\vec{c})$  depends on  $\vec{c}$  in a way analogous to the mixture density  $\rho(\vec{c})$ ,

$$\mu(\vec{c}) = \sum_{i=1}^N \tilde{\mu}_i c_i, \quad (86)$$

where  $\tilde{\mu}_i$  ( $1 \leq i \leq N$ ) denote the constant dynamic viscosities of these  $N$  individual fluids. This model satisfies the mass conservation, momentum conservation, and the second law of thermodynamics, and it is also Galilean invariant. This is a thermodynamically consistent N-phase model.

## Appendix B. Proof of Properties About Reduction-Consistent Functions

In this appendix we prove several properties of the reduction-consistent and reduction-compatible functions listed in Section 2.

(J7): If  $v_{ij}(\vec{c})$  ( $1 \leq i, j \leq N$ ) are a reduction-consistent set of functions, and  $w_i(\vec{c})$  ( $1 \leq i \leq N$ ) are a reduction-compatible set of functions, then  $\sum_{j=1}^N v_{ij} w_j$  ( $1 \leq i \leq N$ ) and  $\sum_{i=1}^N v_{ij} w_i$  ( $1 \leq j \leq N$ ) form two reduction-consistent sets of functions.

Proof: Consider  $N \geq 2$ . Let  $z_i = \sum_{j=1}^N v_{ij} w_j$  ( $1 \leq i \leq N$ ). Suppose fluid  $k$  ( $1 \leq k \leq N$ ) is absent from the N-phase system. Then  $v_{ij}^{(N)}$  satisfy the reduction relations in (7) and (8).  $w_i^{(N)}$  satisfy the reduction relations

$$w_i^{(N)} = \begin{cases} w_i^{(N-1)}, & 1 \leq i \leq k-1, \\ w_{i-1}^{(N-1)}, & k+1 \leq i \leq N. \end{cases} \quad (87)$$

Consequently, we have

$$z_k^{(N)} = \sum_{j=1}^N v_{kj}^{(N)} w_j^{(N)} = 0.$$

For  $1 \leq i \leq k-1$ ,

$$\begin{aligned}
z_i^{(N)} &= \sum_{j=1}^N v_{ij}^{(N)} w_j^{(N)} = \sum_{j=1}^{k-1} v_{ij}^{(N)} w_j^{(N)} + \sum_{j=k+1}^N v_{ij}^{(N)} w_j^{(N)} + v_{ik}^{(N)} w_k^{(N)} \\
&= \sum_{j=1}^{k-1} v_{ij}^{(N-1)} w_j^{(N-1)} + \sum_{j=k+1}^N v_{ij-1}^{(N-1)} w_{j-1}^{(N-1)} = \sum_{j=1}^{k-1} v_{ij}^{(N-1)} w_j^{(N-1)} + \sum_{j=k}^{N-1} v_{ij}^{(N-1)} w_j^{(N-1)} \\
&= \sum_{j=1}^{N-1} v_{ij}^{(N-1)} w_j^{(N-1)} = z_i^{(N-1)}.
\end{aligned}$$

For  $k+1 \leq i \leq N$ ,

$$\begin{aligned}
z_i^{(N)} &= \sum_{j=1}^N v_{ij}^{(N)} w_j^{(N)} = \sum_{j=1}^{k-1} v_{ij}^{(N)} w_j^{(N)} + \sum_{j=k+1}^N v_{ij}^{(N)} w_j^{(N)} + v_{ik}^{(N)} w_k^{(N)} \\
&= \sum_{j=1}^{k-1} v_{i-1j}^{(N-1)} w_j^{(N-1)} + \sum_{j=k+1}^N v_{i-1j-1}^{(N-1)} w_{j-1}^{(N-1)} = \sum_{j=1}^{k-1} v_{i-1j}^{(N-1)} w_j^{(N-1)} + \sum_{j=k}^{N-1} v_{i-1j}^{(N-1)} w_j^{(N-1)} \\
&= \sum_{j=1}^{N-1} v_{i-1j}^{(N-1)} w_j^{(N-1)} = z_{i-1}^{(N-1)}.
\end{aligned}$$

We therefore conclude that  $z_i = \sum_{j=1}^N v_{ij} w_j$  ( $1 \leq i \leq N$ ) forms a reduction consistent set of functions.

One can show that  $\sum_{i=1}^N v_{ij} w_i$  ( $1 \leq j \leq N$ ) are a reduction-consistent set in a similar way.

(T8): If  $v_{ij}(\vec{c})$  ( $1 \leq i, j \leq N$ ) are a reduction-compatible set of functions, and  $w_i(\vec{c})$  ( $1 \leq i \leq N$ ) are a reduction-consistent set of functions, then  $\sum_{j=1}^N v_{ij} w_j$  ( $1 \leq i \leq N$ ) and  $\sum_{i=1}^N v_{ij} w_i$  ( $1 \leq j \leq N$ ) form two reduction-compatible sets of functions.

**Proof:** Consider  $N \geq 2$ . Let  $z_i = \sum_{j=1}^N v_{ij} w_j$  ( $1 \leq i \leq N$ ). Suppose fluid  $k$  ( $1 \leq k \leq N$ ) is absent from the system. Then  $v_{ij}^{(N)}$  satisfy the reduction relations in (7) and  $w_i^{(N)}$  satisfy the reduction relations

$$w_i^{(N)} = \begin{cases} w_i^{(N-1)}, & 1 \leq i \leq k-1, \\ 0, & i = k \\ w_{i-1}^{(N-1)}, & k+1 \leq i \leq N. \end{cases} \quad (88)$$

Consequently, we have for  $1 \leq i \leq k-1$ ,

$$\begin{aligned}
z_i^{(N)} &= \sum_{j=1}^N v_{ij}^{(N)} w_j^{(N)} = \sum_{j=1}^{k-1} v_{ij}^{(N)} w_j^{(N)} + \sum_{j=k+1}^N v_{ij}^{(N)} w_j^{(N)} = \sum_{j=1}^{k-1} v_{ij}^{(N-1)} w_j^{(N-1)} + \sum_{j=k+1}^N v_{ij-1}^{(N-1)} w_{j-1}^{(N-1)} \\
&= \sum_{j=1}^{k-1} v_{ij}^{(N-1)} w_j^{(N-1)} + \sum_{j=k}^{N-1} v_{ij}^{(N-1)} w_j^{(N-1)} = \sum_{j=1}^{N-1} v_{ij}^{(N-1)} w_j^{(N-1)} \\
&= z_i^{(N-1)}.
\end{aligned}$$

For  $k+1 \leq i \leq N$ ,

$$\begin{aligned}
z_i^{(N)} &= \sum_{j=1}^N v_{ij}^{(N)} w_j^{(N)} = \sum_{j=1}^{k-1} v_{ij}^{(N)} w_j^{(N)} + \sum_{j=k+1}^N v_{ij}^{(N)} w_j^{(N)} = \sum_{j=1}^{k-1} v_{i-1j}^{(N-1)} w_j^{(N-1)} + \sum_{j=k+1}^N v_{i-1j-1}^{(N-1)} w_{j-1}^{(N-1)} \\
&= \sum_{j=1}^{k-1} v_{i-1j}^{(N-1)} w_j^{(N-1)} + \sum_{j=k}^{N-1} v_{i-1j}^{(N-1)} w_j^{(N-1)} = \sum_{j=1}^{N-1} v_{i-1j}^{(N-1)} w_j^{(N-1)} \\
&= z_{i-1}^{(N-1)}.
\end{aligned}$$

We therefore conclude that  $\sum_{j=1}^N v_{ij}w_j$  ( $1 \leq i \leq N$ ) are a reduction-compatible set of variables.  $\sum_{i=1}^N v_{ij}w_i$  ( $1 \leq j \leq N$ ) can be shown to be a reduction-compatible set in a similar way.

(J9): If  $v_i(\vec{c})$  ( $1 \leq i \leq N$ ) are a reduction-consistent set of functions, then  $\sum_{i=1}^N v_i(\vec{c})$  is a reduction-consistent function.

**Proof:** Consider  $N \geq 2$ . Let  $z(\vec{c}) = \sum_{i=1}^N v_i(\vec{c})$ . Suppose fluid  $k$  ( $1 \leq k \leq N$ ) is absent from the system. Then  $v_i^{(N)}$  satisfies the reduction relations given by (5) and (6). Then

$$\begin{aligned} z^{(N)}(\vec{c}^{(N)}) &= \sum_{i=1}^N v_i^{(N)} = \sum_{i=1}^{k-1} v_i^{(N)} + \sum_{i=k+1}^N v_i^{(N)} = \sum_{i=1}^{k-1} v_i^{(N-1)} + \sum_{i=k+1}^N v_i^{(N-1)} \\ &= \sum_{i=1}^{k-1} v_i^{(N-1)} + \sum_{i=k}^{N-1} v_i^{(N-1)} = \sum_{i=1}^{N-1} v_i^{(N-1)} \\ &= z^{(N-1)}(\vec{c}^{(N-1)}). \end{aligned}$$

Therefore  $\sum_{i=1}^N v_i$  is a reduction-consistent function.

(J10): If  $v_{ij}(\vec{c})$  ( $1 \leq i, j \leq N$ ) is a reduction-consistent set of functions, then  $\sum_{j=1}^N v_{ij}(\vec{c})$  ( $1 \leq i \leq N$ ) and  $\sum_{i=1}^N v_{ij}(\vec{c})$  ( $1 \leq j \leq N$ ) are two reduction-consistent sets of functions, and  $\sum_{i,j=1}^N v_{ij}(\vec{c})$  is a reduction-consistent function.

**Proof:** Consider  $N \geq 2$ . Let  $z_i(\vec{c}) = \sum_{j=1}^N v_{ij}(\vec{c})$  ( $1 \leq i \leq N$ ) and  $z(\vec{c}) = \sum_{i,j=1}^N v_{ij}(\vec{c})$ . Suppose fluid  $k$  ( $1 \leq k \leq N$ ) is absent from the system. Then  $v_{ij}$  satisfy the reduction relations given by (7) and (8). We have

$$z_k^{(N)} = \sum_{j=1}^N v_{kj}^{(N)} = 0.$$

For  $1 \leq i \leq k-1$ ,

$$\begin{aligned} z_i^{(N)} &= \sum_{j=1}^N v_{ij}^{(N)} = \sum_{j=1}^{k-1} v_{ij}^{(N)} + \sum_{j=k+1}^N v_{ij}^{(N)} = \sum_{j=1}^{k-1} v_{ij}^{(N-1)} + \sum_{j=k+1}^N v_{ij}^{(N-1)} = \sum_{j=1}^{k-1} v_{ij}^{(N-1)} + \sum_{j=k}^{N-1} v_{ij}^{(N-1)} \\ &= \sum_{j=1}^{N-1} v_{ij}^{(N-1)} = z_i^{(N-1)}. \end{aligned}$$

For  $k+1 \leq i \leq N$ ,

$$\begin{aligned} z_i^{(N)} &= \sum_{j=1}^N v_{ij}^{(N)} = \sum_{j=1}^{k-1} v_{ij}^{(N)} + \sum_{j=k+1}^N v_{ij}^{(N)} = \sum_{j=1}^{k-1} v_{i-1j}^{(N-1)} + \sum_{j=k+1}^N v_{i-1j-1}^{(N-1)} = \sum_{j=1}^{k-1} v_{i-1j}^{(N-1)} + \sum_{j=k}^{N-1} v_{i-1j}^{(N-1)} \\ &= \sum_{j=1}^{N-1} v_{i-1j}^{(N-1)} = z_{i-1}^{(N-1)}. \end{aligned}$$

We conclude that  $\sum_{j=1}^N v_{ij}$  ( $1 \leq i \leq N$ ) is a reduction-consistent set of functions. One can show that  $\sum_{i=1}^N v_{ij}$  ( $1 \leq j \leq N$ ) is another reduction-consistent set of functions in a similar way.

Since  $z_i(\vec{c})$  ( $1 \leq i \leq N$ ) form a reduction-consistent set of functions and  $z(\vec{c}) = \sum_{i=1}^N z_i(\vec{c})$ , we conclude that  $\sum_{i,j=1}^N v_{ij}$  is a reduction-consistent function in light of the property (J9).

(J11): If  $v_{ij}(\vec{c})$  ( $1 \leq i, j \leq N$ ) are a reduction-compatible set of functions and  $w_i(\vec{c})$  ( $1 \leq i \leq N$ ) are a reduction-consistent set of functions, then  $\sum_{i,j=1}^N v_{ij}w_iw_j$  is a reduction-consistent function.

**Proof:**  $\sum_{j=1}^N v_{ij}w_j$  ( $1 \leq i \leq N$ ) are a reduction-compatible set of functions according to property (J8). So  $w_i \sum_{j=1}^N v_{ij}w_j$  ( $1 \leq i \leq N$ ) form a reduction-consistent set of functions according to property (J4). We then conclude that  $\sum_{i,j=1}^N v_{ij}w_iw_j$  is a reduction-consistent function based on property (J9).

(J12): If  $v_{ij}(\vec{c})$  ( $1 \leq i, j \leq N$ ) are a reduction-consistent set of functions and  $w_i(\vec{c})$  ( $1 \leq i \leq N$ ) are a reduction-compatible set of functions, then  $\sum_{i,j=1}^N v_{ij}w_iw_j$  is a reduction-consistent function.

**Proof:**  $\sum_{j=1}^N v_{ij}w_j$  ( $1 \leq i \leq N$ ) are a reduction-consistent set of functions according to property (J7). So  $w_i \sum_{j=1}^N v_{ij}w_j$  ( $1 \leq i \leq N$ ) form a reduction-consistent set of functions according to property (J4). We then conclude that  $\sum_{i,j=1}^N v_{ij}w_iw_j$  is a reduction-consistent function based on property (J9).

## Appendix C. Proof of Theorem 2.1

It suffices to show that the  $\mathcal{M}(\vec{c})$  defined in (11a) and  $\mathcal{N}(\vec{c})$  defined in (11b) are each a reduction-consistent function, and that the  $\mathcal{F}_i(\vec{c})$  ( $1 \leq i \leq N$ ) defined in (11c) form a reduction-consistent set of functions.

Because  $\mathcal{N}(\vec{c}) = \nabla \cdot \mathbf{u}$  is independent of  $\vec{c}$ , it is reduction-consistent based on the property (J14) of Section 2.1.

Let us consider the reduction consistency of  $\mathcal{F}_i(\vec{c})$ . Because both  $\frac{\partial c_i}{\partial t}$  ( $1 \leq i \leq N$ ) and  $\mathbf{u} \cdot \nabla c_i$  ( $1 \leq i \leq N$ ) are reduction-consistent sets of functions, it suffices to show that  $\sum_{j=1}^N m_{ij} \nabla \left( \frac{\partial W}{\partial c_j} - \nabla \cdot \frac{\partial W}{\partial \nabla c_j} \right) = \sum_{j=1}^N m_{ij} \nabla (\mathcal{H}_i - \mathcal{J}_i)$  for  $1 \leq i \leq N$  are a reduction-consistent set of functions. That  $\mathcal{G}_i(\vec{c})$  ( $1 \leq i \leq N$ ) are a reduction-compatible set of functions implies that  $\mathcal{J}_i(\vec{c})$  ( $1 \leq i \leq N$ ) are a reduction-compatible set according to property (J13). Because  $\mathcal{H}_i$  and  $\mathcal{J}_i$  are both reduction-compatible sets of functions,  $\nabla(\mathcal{H}_i - \mathcal{J}_i)$  is a reduction-compatible set of functions according to properties (J3) and (J13) of Section 2.1. Since  $m_{ij}$  ( $1 \leq i, j \leq N$ ) are a reduction-consistent set,  $\sum_{j=1}^N m_{ij} \nabla (\mathcal{H}_i - \mathcal{J}_i)$  ( $1 \leq i \leq N$ ) are then a reduction-consistent set of functions according to the property (J7). Therefore, all the three terms in (11c) are individually reduction-consistent sets of functions. We can then conclude that  $\mathcal{F}_i(\vec{c})$  ( $1 \leq i \leq N$ ) are a reduction-consistent set of functions based on the property (J2).

Consider next the reduction consistency of  $\mathcal{M}(\vec{c})$ . Note that both  $\rho(\vec{c})$  and  $\mu(\vec{c})$  are reduction-consistent functions according to the property (J15), and that those terms independent of  $\vec{c}$  are reduction-consistent according to the property (J14). It suffices to show that the  $\tilde{\mathbf{J}}$  term given by (85) and the term  $\sum_{i=1}^N \nabla c_i \otimes \frac{\partial W}{\partial \nabla c_i} = \sum_{i=1}^N \nabla c_i \otimes \mathcal{G}_i$  are both reduction-consistent functions. According to (85),  $\tilde{\mathbf{J}} = -\sum_{i=1}^N \tilde{\rho}_i \left[ \sum_{j=1}^N m_{ij} \nabla (\mathcal{H}_j - \mathcal{J}_j) \right]$ . Since  $\sum_{j=1}^N m_{ij} \nabla (\mathcal{H}_j - \mathcal{J}_j)$  ( $1 \leq i \leq N$ ) are a reduction-consistent set of functions and  $\tilde{\rho}_i$  ( $1 \leq i \leq N$ ) are a reduction-compatible set of variables, we conclude based on the properties (J4) and (J9) that  $\tilde{\mathbf{J}}$  is a reduction-consistent function. Since  $\nabla c_i$  ( $1 \leq i \leq N$ ) are a reduction-consistent set and  $\mathcal{G}_i$  ( $1 \leq i \leq N$ ) are a reduction-compatible set,  $\nabla c_i \otimes \mathcal{G}_i$  ( $1 \leq i \leq N$ ) form a reduction-consistent set of functions based on property (J4). Therefore,  $\sum_{i=1}^N \nabla c_i \otimes \mathcal{G}_i$  is a reduction-consistent function based on the property (J9). We can then conclude that  $\mathcal{M}(\vec{c})$  is a reduction-consistent function.

## Appendix D. Proof of Theorem 2.2

**Reduction Consistency of  $m_{ij}(\vec{c})$**  We first show that the  $m_{ij}(\vec{c})$  defined by (15) form a reduction-consistent set of functions. Consider an N-phase system ( $N \geq 2$ ). Suppose that fluid  $k$  ( $1 \leq k \leq N$ ) is absent from the system, i.e. the system is characterized by (2), and the correspondence relations in (3) hold. Then we have the following relations

$$\tilde{m}_{ij}^{(N)} = \begin{cases} \tilde{m}_{ij}^{(N-1)}, & 1 \leq i \leq k-1, 1 \leq j \leq k-1, \\ \tilde{m}_{ij}^{(N-1)}, & 1 \leq i \leq k-1, k+1 \leq j \leq N, \\ \tilde{m}_{i-1j}^{(N-1)}, & k+1 \leq i \leq N, 1 \leq j \leq k-1, \\ \tilde{m}_{i-1j-1}^{(N-1)}, & k+1 \leq i \leq N, k+1 \leq j \leq N, \end{cases} \quad f(c_i^{(N)}) = \begin{cases} f(c_i^{(N-1)}), & 1 \leq i \leq k-1, \\ 0, & i = k \\ f(c_{i-1}^{(N-1)}), & k+1 \leq i \leq N, \end{cases} \quad (89)$$

because of the properties of  $f(c)$  given in (12) and the fact that  $\tilde{m}_{ij}$  form a reduction-compatible set.

Let us look into the reduction for  $m_{ij}(\vec{c})$ . We divide the problem into two cases: (i)  $i = k$  or  $j = k$ ; (ii)  $i \neq k$  and  $j \neq k$ . Consider the first case:  $i = k$  or  $j = k$ . For  $i = k$ , if  $j \neq k$ , then

$$m_{kj}^{(N)} = -\tilde{m}_{kj}^{(N)} f(c_k^{(N)}) f(c_j^{(N)}) = 0, \quad 1 \leq j \leq N, j \neq k.$$

For  $i = j = k$ ,

$$m_{kk}^{(N)} = - \sum_{\substack{j=1 \\ j \neq k}}^N m_{kj}^{(N)} = 0.$$

For  $j = k$  and  $i \neq k$ ,

$$m_{ik}^{(N)} = -\tilde{m}_{ik}^{(N)} f(c_i^{(N)}) f(c_k^{(N)}) = 0, \quad 1 \leq i \leq N, \quad i \neq k.$$

Consider the second case:  $i \neq k$  and  $j \neq k$ . First consider the subcase  $j \neq i$ . For  $1 \leq i \leq k-1$  and  $1 \leq j \leq k-1$  and  $j \neq i$ ,

$$m_{ij}^{(N)} = -\tilde{m}_{ij}^{(N)} f(c_i^{(N)}) f(c_j^{(N)}) = -\tilde{m}_{ij}^{(N-1)} f(c_i^{(N-1)}) f(c_j^{(N-1)}) = m_{ij}^{(N-1)}.$$

For  $1 \leq i \leq k-1$  and  $k+1 \leq j \leq N$ ,

$$m_{ij}^{(N)} = -\tilde{m}_{ij}^{(N)} f(c_i^{(N)}) f(c_j^{(N)}) = -\tilde{m}_{ij-1}^{(N-1)} f(c_i^{(N-1)}) f(c_{j-1}^{(N-1)}) = m_{ij-1}^{(N-1)}.$$

For  $k+1 \leq i \leq N$  and  $1 \leq j \leq k-1$ ,

$$m_{ij}^{(N)} = -\tilde{m}_{ij}^{(N)} f(c_i^{(N)}) f(c_j^{(N)}) = -\tilde{m}_{i-1j}^{(N-1)} f(c_{i-1}^{(N-1)}) f(c_j^{(N-1)}) = m_{i-1j}^{(N-1)}.$$

For  $k+1 \leq i \leq N$  and  $k+1 \leq j \leq N$  and  $j \neq i$ ,

$$m_{ij}^{(N)} = -\tilde{m}_{ij}^{(N)} f(c_i^{(N)}) f(c_j^{(N)}) = -\tilde{m}_{i-1j-1}^{(N-1)} f(c_{i-1}^{(N-1)}) f(c_{j-1}^{(N-1)}) = m_{i-1j-1}^{(N-1)}.$$

Now we consider the subcase  $i = j \neq k$ . For  $1 \leq i \leq k-1$ ,

$$\begin{aligned} m_{ii}^{(N)} &= - \sum_{\substack{j=1 \\ j \neq i}}^N m_{ij}^{(N)} = - \sum_{\substack{j=1 \\ j \neq i}}^{k-1} m_{ij}^{(N)} - m_{ik}^{(N)} - \sum_{\substack{j=k+1 \\ j \neq i}}^N m_{ij}^{(N)} = - \sum_{\substack{j=1 \\ j \neq i}}^{k-1} m_{ij}^{(N-1)} - \sum_{j=k+1}^N m_{ij}^{(N-1)} \\ &= - \sum_{\substack{j=1 \\ j \neq i}}^{k-1} m_{ij}^{(N-1)} - \sum_{j=k}^{N-1} m_{ij}^{(N-1)} = - \sum_{\substack{j=1 \\ j \neq i}}^{N-1} m_{ij}^{(N-1)} = m_{ii}^{(N-1)}. \end{aligned}$$

For  $k+1 \leq i \leq N$ ,

$$\begin{aligned} m_{ii}^{(N)} &= - \sum_{\substack{j=1 \\ j \neq i}}^N m_{ij}^{(N)} = - \sum_{j=1}^{k-1} m_{ij}^{(N)} - m_{ik}^{(N)} - \sum_{\substack{j=k+1 \\ j \neq i}}^N m_{ij}^{(N)} = - \sum_{j=1}^{k-1} m_{i-1j}^{(N-1)} - \sum_{\substack{j=k+1 \\ j \neq i}}^N m_{i-1j}^{(N-1)} \\ &= - \sum_{j=1}^{k-1} m_{i-1j}^{(N-1)} - \sum_{\substack{j=k \\ j \neq i-1}}^{N-1} m_{i-1j}^{(N-1)} = - \sum_{\substack{j=1 \\ j \neq i-1}}^{N-1} m_{i-1j}^{(N-1)} = m_{i-1i-1}^{(N-1)}. \end{aligned}$$

Combining the above, we have the following reduction relations

$$m_{ij}^{(N)} = \begin{cases} m_{ij}^{(N-1)}, & 1 \leq i \leq k-1, \quad 1 \leq j \leq k-1 \\ m_{ij-1}^{(N-1)}, & 1 \leq i \leq k-1, \quad k+1 \leq j \leq N \\ m_{i-1j}^{(N-1)}, & k+1 \leq i \leq N, \quad 1 \leq j \leq k-1 \\ m_{i-1j-1}^{(N-1)}, & k+1 \leq i \leq N, \quad k+1 \leq j \leq N \\ 0, & i = k, \quad 1 \leq j \leq N \\ 0, & 1 \leq i \leq N, \quad j = k. \end{cases} \quad (90)$$

Therefore, we conclude that  $m_{ij}(\vec{c})$  ( $1 \leq i, j \leq N$ ) defined by (15) are a reduction-consistent set of functions.

**Reduction Consistency of  $W(\vec{c}, \nabla \vec{c})$**  We will show that the two terms in the free energy density function (16) are each a reduction-consistent function. Consequently,  $W(\vec{c}, \nabla \vec{c})$  given by (16) is a reduction-consistent function.

The first term  $\sum_{i,j=1}^N \frac{\lambda_{ij}}{2} \nabla c_i \cdot \nabla c_j$  is reduction-consistent. Since  $\sigma_{ij}$  are a reduction-compatible set (property (J16)),  $\lambda_{ij}$  ( $1 \leq i, j \leq N$ ) given in (17) are a reduction-compatible set according to property (J3). Noting that  $\nabla c_i$  ( $1 \leq i \leq N$ ) are a reduction-consistent set, we can conclude that  $\sum_{i,j=1}^N \frac{\lambda_{ij}}{2} \nabla c_i \cdot \nabla c_j$  is a reduction-consistent function based on property (J11).

Let us now show that the second term  $H(\vec{c}) = \beta \sum_{i,j=1}^N \frac{\sigma_{ij}}{2} [g(c_i) + g(c_j) - g(c_i + c_j)]$  is reduction-consistent. Suppose fluid  $k$  ( $1 \leq k \leq N$ ) is absent from the system, i.e. the system is characterized by (2) and the relations (3) hold. Then we have the relations

$$\sigma_{ij}^{(N)} = \begin{cases} \sigma_{ij}^{(N-1)}, & 1 \leq i \leq k-1, 1 \leq j \leq k-1, \\ \sigma_{ij-1}^{(N-1)}, & 1 \leq i \leq k-1, k+1 \leq j \leq N, \\ \sigma_{i-1j}^{(N-1)}, & k+1 \leq i \leq N, 1 \leq j \leq k-1, \\ \sigma_{i-1j-1}^{(N-1)}, & k+1 \leq i \leq N, k+1 \leq j \leq N, \end{cases} \quad g(c_i^{(N)}) = \begin{cases} g(c_i^{(N-1)}), & 1 \leq i \leq k-1, \\ 0, & i = k, \\ g(c_{i-1}^{(N-1)}), & k+1 \leq i \leq N. \end{cases} \quad (91)$$

Then we have

$$\begin{aligned} \frac{1}{\beta} H^{(N)} &= \sum_{i,j=1}^N \frac{\sigma_{ij}^{(N)}}{2} [g(c_i^{(N)}) + g(c_j^{(N)}) - g(c_i^{(N)} + c_j^{(N)})] = \sum_{\substack{i,j=1 \\ i,j \neq k}}^N \frac{\sigma_{ij}^{(N)}}{2} [g(c_i^{(N)}) + g(c_j^{(N)}) - g(c_i^{(N)} + c_j^{(N)})] \\ &= \left( \sum_{i,j=1}^{k-1} + \sum_{i=1}^{k-1} \sum_{j=k+1}^N + \sum_{i=k+1}^N \sum_{j=1}^{k-1} + \sum_{i,j=k+1}^N \right) \frac{\sigma_{ij}^{(N)}}{2} [g(c_i^{(N)}) + g(c_j^{(N)}) - g(c_i^{(N)} + c_j^{(N)})] \\ &= \sum_{i,j=1}^{k-1} \frac{\sigma_{ij}^{(N-1)}}{2} [g(c_i^{(N-1)}) + g(c_j^{(N-1)}) - g(c_i^{(N-1)} + c_j^{(N-1)})] \\ &\quad + \sum_{i=1}^{k-1} \sum_{j=k+1}^N \frac{\sigma_{ij-1}^{(N-1)}}{2} [g(c_i^{(N-1)}) + g(c_{j-1}^{(N-1)}) - g(c_i^{(N-1)} + c_{j-1}^{(N-1)})] \\ &\quad + \sum_{i=k+1}^N \sum_{j=1}^{k-1} \frac{\sigma_{i-1j}^{(N-1)}}{2} [g(c_{i-1}^{(N-1)}) + g(c_j^{(N-1)}) - g(c_{i-1}^{(N-1)} + c_j^{(N-1)})] \\ &\quad + \sum_{i,j=k+1}^N \frac{\sigma_{i-1j-1}^{(N-1)}}{2} [g(c_{i-1}^{(N-1)}) + g(c_{j-1}^{(N-1)}) - g(c_{i-1}^{(N-1)} + c_{j-1}^{(N-1)})] \\ &= \sum_{i,j=1}^{k-1} \frac{\sigma_{ij}^{(N-1)}}{2} [g(c_i^{(N-1)}) + g(c_j^{(N-1)}) - g(c_i^{(N-1)} + c_j^{(N-1)})] \\ &\quad + \sum_{i=1}^{k-1} \sum_{j=k}^{N-1} \frac{\sigma_{ij}^{(N-1)}}{2} [g(c_i^{(N-1)}) + g(c_j^{(N-1)}) - g(c_i^{(N-1)} + c_j^{(N-1)})] \\ &\quad + \sum_{i=k}^{N-1} \sum_{j=1}^{k-1} \frac{\sigma_{ij}^{(N-1)}}{2} [g(c_i^{(N-1)}) + g(c_j^{(N-1)}) - g(c_i^{(N-1)} + c_j^{(N-1)})] \\ &\quad + \sum_{i,j=k}^{N-1} \frac{\sigma_{ij}^{(N-1)}}{2} [g(c_i^{(N-1)}) + g(c_j^{(N-1)}) - g(c_i^{(N-1)} + c_j^{(N-1)})] \\ &= \sum_{i,j=1}^{N-1} \frac{\sigma_{ij}^{(N-1)}}{2} [g(c_i^{(N-1)}) + g(c_j^{(N-1)}) - g(c_i^{(N-1)} + c_j^{(N-1)})] \\ &= \frac{1}{\beta} H^{(N-1)}. \end{aligned}$$

So we conclude that  $H(\vec{c})$  is a reduction-consistent function.

**Reduction Compatibility of  $\mathcal{H}_i(\vec{c})$  and  $\mathcal{G}_i(\vec{c})$**  With  $W(\vec{c}, \nabla \vec{c})$  given by (16),

$$\mathcal{H}_i(\vec{c}) = \frac{\partial W}{\partial c_i} = \beta \sum_{j=1}^N \sigma_{ij} [g'(c_i) - g'(c_i + c_j)], \quad 1 \leq i \leq N; \quad (92)$$

$$\mathcal{G}_i(\vec{c}) = \frac{\partial W}{\partial \nabla c_i} = \sum_{j=1}^N \lambda_{ij} \nabla c_j, \quad 1 \leq i \leq N, \quad (93)$$

where  $g'(c)$  is the derivative of  $g(c)$  defined in (17).

$\mathcal{G}_i(\vec{c})$  ( $1 \leq i \leq N$ ) are evidently a reduction-compatible set of functions. This is because  $\lambda_{ij}$  ( $1 \leq i, j \leq N$ ) are a reduction-compatible set and  $\nabla c_i$  ( $1 \leq i \leq N$ ) are a reduction-consistent set. Based on the property (T8) in Section 2, we conclude that  $\mathcal{G}_i$  ( $1 \leq i \leq N$ ) are a reduction-compatible set of functions.

We next show that  $\mathcal{H}_i(\vec{c})$  ( $1 \leq i \leq N$ ) given by (92) are a reduction-compatible set of functions. Suppose fluid  $k$  ( $1 \leq k \leq N$ ) is absent from the system, i.e. the system is characterized by (2) and the reduction relations (3) hold. Then  $\sigma_{ij}$  satisfy the reduction relations given in (91), and  $g'(c_i)$  (with  $g(c)$  defined in (17)) satisfies the following relations

$$g'(c_i^{(N)}) = \begin{cases} g'(c_i^{(N-1)}), & 1 \leq i \leq k-1, \\ 0, & i = k, \\ g'(c_{i-1}^{(N-1)}), & k+1 \leq i \leq N. \end{cases} \quad (94)$$

For  $1 \leq i \leq k-1$ ,

$$\begin{aligned} \frac{1}{\beta} \mathcal{H}_i^{(N)} &= \sum_{j=1}^{k-1} \sigma_{ij}^{(N)} [g'(c_i^{(N)}) - g'(c_i^{(N)} + c_j^{(N)})] + \sum_{j=k+1}^N \sigma_{ij}^{(N)} [g'(c_i^{(N)}) - g'(c_i^{(N)} + c_j^{(N)})] \\ &= \sum_{j=1}^{k-1} \sigma_{ij}^{(N-1)} [g'(c_i^{(N-1)}) - g'(c_i^{(N-1)} + c_j^{(N-1)})] \\ &\quad + \sum_{j=k+1}^N \sigma_{ij-1}^{(N-1)} [g'(c_i^{(N-1)}) - g'(c_i^{(N-1)} + c_{j-1}^{(N-1)})] \\ &= \sum_{j=1}^{k-1} \sigma_{ij}^{(N-1)} [g'(c_i^{(N-1)}) - g'(c_i^{(N-1)} + c_j^{(N-1)})] \\ &\quad + \sum_{j=k}^{N-1} \sigma_{ij}^{(N-1)} [g'(c_i^{(N-1)}) - g'(c_i^{(N-1)} + c_j^{(N-1)})] \\ &= \sum_{j=1}^{N-1} \sigma_{ij}^{(N-1)} [g'(c_i^{(N-1)}) - g'(c_i^{(N-1)} + c_j^{(N-1)})] \\ &= \frac{1}{\beta} \mathcal{H}_i^{(N-1)}. \end{aligned}$$

For  $k + 1 \leq i \leq N$ ,

$$\begin{aligned}
\frac{1}{\beta} \mathcal{H}_i^{(N)} &= \sum_{j=1}^{k-1} \sigma_{ij}^{(N)} \left[ g'(c_i^{(N)}) - g'(c_i^{(N)} + c_j^{(N)}) \right] + \sum_{j=k+1}^N \sigma_{ij}^{(N)} \left[ g'(c_i^{(N)}) - g'(c_i^{(N)} + c_j^{(N)}) \right] \\
&= \sum_{j=1}^{k-1} \sigma_{i-1j}^{(N-1)} \left[ g'(c_{i-1}^{(N-1)}) - g'(c_{i-1}^{(N-1)} + c_j^{(N-1)}) \right] \\
&\quad + \sum_{j=k+1}^N \sigma_{i-1j-1}^{(N-1)} \left[ g'(c_{i-1}^{(N-1)}) - g'(c_{i-1}^{(N-1)} + c_{j-1}^{(N-1)}) \right] \\
&= \sum_{j=1}^{k-1} \sigma_{i-1j}^{(N-1)} \left[ g'(c_{i-1}^{(N-1)}) - g'(c_{i-1}^{(N-1)} + c_j^{(N-1)}) \right] \\
&\quad + \sum_{j=k}^{N-1} \sigma_{i-1j}^{(N-1)} \left[ g'(c_{i-1}^{(N-1)}) - g'(c_{i-1}^{(N-1)} + c_j^{(N-1)}) \right] \\
&= \sum_{j=1}^{N-1} \sigma_{i-1j}^{(N-1)} \left[ g'(c_{i-1}^{(N-1)}) - g'(c_{i-1}^{(N-1)} + c_j^{(N-1)}) \right] \\
&= \frac{1}{\beta} \mathcal{H}_{i-1}^{(N-1)}.
\end{aligned}$$

Combining the above results, we conclude that  $\mathcal{H}_i(\vec{c})$  ( $1 \leq i \leq N$ ) given by (92) form a reduction-compatible set of functions.

## Appendix E. Algorithm for N-Phase Momentum Equations

We summarize the algorithm developed in [15] for the N-phase momentum equations, which is employed in the current work. The algorithm is for the equations (24) and (83b), together with the boundary condition (21). It is assumed that the volume fractions  $c_i^{n+1}$  ( $1 \leq i \leq N$ ) and the auxiliary variables  $\psi_i^{n+1}$  ( $1 \leq i \leq N$ ) have already been computed using the algorithm presented in Section 3. The goal here is to compute the velocity  $\mathbf{u}^{n+1}$  and the pressure  $P^{n+1}$  with given  $\mathbf{u}^n$ ,  $P^n$ ,  $c_i^{n+1}$  and  $\psi_i^{n+1}$ .

The algorithm consists of two steps. The pressure and the velocity are computed successively in a decoupled fashion in the first and the second steps, respectively.

For  $P^{n+1}$ :

$$\begin{aligned}
\frac{\gamma_0 \tilde{\mathbf{u}}^{n+1} - \hat{\mathbf{u}}}{\Delta t} + \mathbf{u}^{*,n+1} \cdot \nabla \mathbf{u}^{*,n+1} + \frac{1}{\rho^{n+1}} \tilde{\mathbf{J}}^{n+1} \cdot \nabla \mathbf{u}^{*,n+1} + \frac{1}{\rho_0} \nabla P^{n+1} &= \left( \frac{1}{\rho_0} - \frac{1}{\rho^{n+1}} \right) \nabla P^{*,n+1} \\
&\quad - \frac{\mu^{n+1}}{\rho^{n+1}} \nabla \times \nabla \times \mathbf{u}^{*,n+1} + \frac{1}{\rho^{n+1}} \nabla \mu^{n+1} \cdot \mathbf{D}(\mathbf{u}^{*,n+1}) \\
&\quad - \frac{1}{\rho^{n+1}} \sum_{i,j=1}^N \lambda_{ij} (\psi_j^{n+1} - \alpha c_j^{n+1}) \nabla c_i^{n+1} + \frac{1}{\rho^{n+1}} \mathbf{f}^{n+1},
\end{aligned} \tag{95a}$$

$$\nabla \cdot \tilde{\mathbf{u}}^{n+1} = 0, \tag{95b}$$

$$\mathbf{n} \cdot \tilde{\mathbf{u}}^{n+1} \Big|_{\partial\Omega} = \mathbf{n} \cdot \mathbf{w}^{n+1}. \tag{95c}$$

For  $\mathbf{u}^{n+1}$ :

$$\frac{\gamma_0 \mathbf{u}^{n+1} - \gamma_0 \tilde{\mathbf{u}}^{n+1}}{\Delta t} - \nu_0 \nabla^2 \mathbf{u}^{n+1} = \nu_0 \nabla \times \nabla \times \mathbf{u}^{*,n+1}, \tag{96a}$$

$$\mathbf{u}^{n+1}|_{\partial\Omega} = \mathbf{w}^{n+1}. \quad (96b)$$

In the above equations all the symbols follow the same notation as outlined in Section 3.  $\mathbf{u}^{*,n+1}$  and  $P^{*,n+1}$  are defined by (30).  $\hat{\mathbf{u}}$  and  $\gamma_0$  are defined by (29).  $\tilde{\mathbf{J}}^{n+1}$  is given by (see equation (20))

$$\tilde{\mathbf{J}}^{n+1} = - \sum_{i,j=1}^N \tilde{\rho}_i m_{ij}(\bar{c}^{n+1}) \nabla \left[ - \sum_{k=1}^N \lambda_{jk} (\psi_k^{n+1} - \alpha c_k^{n+1}) + \mathcal{H}_j(\bar{c}^{n+1}) \right]. \quad (97)$$

Note that in both the above equation and in equation (95a) we have replaced  $\nabla^2 c_i^{n+1}$  by  $(\psi_i^{n+1} - \alpha c_i^{n+1})$  according to equations (36b) and (45).  $\mathbf{n}$  is the outward-pointing unit vector normal to  $\partial\Omega$ .  $\tilde{\mathbf{u}}^{n+1}$  is an auxiliary velocity that approximates  $\mathbf{u}^{n+1}$ .  $\rho^{n+1}$  and  $\mu^{n+1}$  are given by (84) and (86), and in case of large density ratios we follow [15] and further clamp the values of  $\rho^{n+1}$  and  $\mu^{n+1}$  as follows (see [15] for details)

$$\rho^{n+1} = \begin{cases} \rho^{n+1}, & \text{if } \rho^{n+1} \in [\tilde{\rho}_{\min}, \tilde{\rho}_{\max}] \\ \tilde{\rho}_{\max}, & \text{if } \rho^{n+1} > \tilde{\rho}_{\max} \\ \tilde{\rho}_{\min}, & \text{if } \rho^{n+1} < \tilde{\rho}_{\min}, \end{cases} \quad \mu^{n+1} = \begin{cases} \mu^{n+1}, & \text{if } \mu^{n+1} \in [\tilde{\mu}_{\min}, \tilde{\mu}_{\max}] \\ \tilde{\mu}_{\max}, & \text{if } \mu^{n+1} > \tilde{\mu}_{\max} \\ \tilde{\mu}_{\min}, & \text{if } \mu^{n+1} < \tilde{\mu}_{\min}, \end{cases} \quad (98)$$

where  $\tilde{\rho}_{\max} = \max_{1 \leq i \leq N} \{\tilde{\rho}_i\}$ ,  $\tilde{\rho}_{\min} = \min_{1 \leq i \leq N} \{\tilde{\rho}_i\}$ ,  $\tilde{\mu}_{\max} = \max_{1 \leq i \leq N} \{\tilde{\mu}_i\}$ , and  $\tilde{\mu}_{\min} = \min_{1 \leq i \leq N} \{\tilde{\mu}_i\}$ . The constant  $\rho_0$  is given by  $\rho_0 = \tilde{\rho}_{\min} = \min_{1 \leq i \leq N} \{\tilde{\rho}_i\}$ .  $\nu_0$  in (96a) is a chosen positive constant that is sufficiently large. We employ an  $\nu_0$  value with the following property,  $\nu_0 \geq \max\left(\frac{\tilde{\mu}_1}{\tilde{\rho}_1}, \frac{\tilde{\mu}_2}{\tilde{\rho}_2}, \dots, \frac{\tilde{\mu}_N}{\tilde{\rho}_N}\right)$ .

The above algorithm employs a velocity correction-type idea [18, 17, 14] to de-couple the computations for the pressure and the velocity. With this algorithm the linear algebraic systems resulting from the discretization involve only *constant* and *time-independent* coefficient matrices, like in two-phase flows [19, 11, 13].

It is straightforward to derive the weak forms for the pressure and the velocity for the implementation of the algorithm using  $C^0$  spectral elements; see [15] for details. We only provide the final weak forms here. Let  $q \in H^1(\Omega)$  denote the test function, and

$$\begin{aligned} \mathbf{G}^{n+1} &= \frac{1}{\rho^{n+1}} \mathbf{f}^{n+1} - \left( \mathbf{u}^{*,n+1} + \frac{1}{\rho^{n+1}} \tilde{\mathbf{J}}^{n+1} \right) \cdot \nabla \mathbf{u}^{*,n+1} + \frac{\hat{\mathbf{u}}}{\Delta t} + \left( \frac{1}{\rho_0} - \frac{1}{\rho^{n+1}} \right) \nabla P^{*,n+1} \\ &+ \frac{1}{\rho^{n+1}} \nabla \mu^{n+1} \cdot \mathbf{D}(\mathbf{u}^{*,n+1}) - \frac{1}{\rho^{n+1}} \sum_{i,j=1}^N \lambda_{ij} (\psi_j^{n+1} - \alpha c_j^{n+1}) \nabla c_i^{n+1} + \nabla \left( \frac{\mu^{n+1}}{\rho^{n+1}} \right) \times \boldsymbol{\omega}^{*,n+1}, \end{aligned} \quad (99)$$

where  $\boldsymbol{\omega} = \nabla \times \mathbf{u}$  is the vorticity. The weak form for the pressure  $P^{n+1}$  is

$$\int_{\Omega} \nabla P^{n+1} \cdot \nabla q = \rho_0 \int_{\Omega} \mathbf{G}^{n+1} \cdot \nabla q - \rho_0 \int_{\partial\Omega} \frac{\mu^{n+1}}{\rho^{n+1}} \mathbf{n} \times \boldsymbol{\omega}^{*,n+1} \cdot \nabla q - \frac{\gamma_0 \rho_0}{\Delta t} \int_{\partial\Omega} \mathbf{n} \cdot \mathbf{w}^{n+1} q, \quad \forall q \in H^1(\Omega). \quad (100)$$

Let  $H_0^1(\Omega) = \{v \in H^1(\Omega) : v|_{\partial\Omega} = 0\}$ , and  $\varphi \in H_0^1(\Omega)$  denote the test function. The weak form about the velocity  $\mathbf{u}^{n+1}$  is

$$\begin{aligned} \int_{\Omega} \nabla \varphi \cdot \nabla \mathbf{u}^{n+1} + \frac{\gamma_0}{\nu_0 \Delta t} \int_{\Omega} \varphi \mathbf{u}^{n+1} &= \frac{1}{\nu_0} \int_{\Omega} \left( \mathbf{G}^{n+1} - \frac{1}{\rho_0} \nabla P^{n+1} \right) \varphi \\ &- \frac{1}{\nu_0} \int_{\Omega} \left( \frac{\mu^{n+1}}{\rho^{n+1}} - \nu_0 \right) \boldsymbol{\omega}^{*,n+1} \times \nabla \varphi, \quad \forall \varphi \in H_0^1(\Omega). \end{aligned} \quad (101)$$

These weak forms, (100) and (101), can be discretized in space using  $C^0$  spectral elements in a straightforward fashion [15].

Solving the N-phase momentum equations (24) and (83b) amounts to the following two successive operations. First, solve equation (100) for pressure  $P^{n+1}$ . Then, solve equation (101), together with the Dirichlet condition (96b) on  $\partial\Omega$ , for  $\mathbf{u}^{n+1}$ .

## References

- [1] H. Abels, H. Garcke, and G. Grün. Thermodynamically consistent, frame indifferent diffuse interface models for incompressible two-phase flows with different densities. *Mathematical Models and Methods in Applied Sciences*, 22:1150013, 2012.
- [2] D.M. Anderson, G.B. McFadden, and A.A. Wheeler. Diffuse-interface methods in fluid mechanics. *Annu. Rev. Fluid Mech.*, 30:139–165, 1998.
- [3] L. Banas and R. Nurnberg. Numerical approximation of a non-smooth phase-field model for multicomponent incompressible flow. *ESAIM: Mathematical Modelling and Numerical Analysis*, 51:1089–1117, 2017.
- [4] P.C. Bollada, P.K. Jimack, and A.M. Mullis. A new approach to multi-phase formulation for the solidification of alloys. *Physica D*, 241:816–829, 2012.
- [5] P. Boyanova and M. Neytcheva. Efficient numerical solution of discrete multi-component cahn-hilliard systems. *Computers and Mathematics with Applications*, 67:106–121, 2014.
- [6] F. Boyer and C. Lapuerta. Study of a three component cahn-hilliard flow model. *ESAIM: M2AN*, 40:653–687, 2006.
- [7] F. Boyer, C. Lapuerta, S. Minjeaud, B. Piar, and M. Quintard. Cahn-hilliard/navier-stokes model for the simulation of three-phase flows. *Transp. Porous Med.*, 82:463–483, 2010.
- [8] F. Boyer and S. Minjeaud. Hierarchy of consistent n-component Cahn-Hilliard systems. *Mathematical Models and Methods in Applied Sciences*, 24:2885–2928, 2014.
- [9] J. Brannick, C. Liu, T. Qian, and H. Sun. Diffuse interface methods for multiple phase materials: an energetic variational approach. *Numer. Math. Theory Methods Appl.*, 8:220–236, 2015.
- [10] P.G. de Gennes, F. Brochard-Wyart, and D. Quere. *Capillarity and Wetting Phenomena*. Springer, 2003.
- [11] S. Dong. On imposing dynamic contact-angle boundary conditions for wall-bounded liquid-gas flows. *Computer Methods in Applied Mechanics and Engineering*, 247–248:179–200, 2012.
- [12] S. Dong. An efficient algorithm for incompressible N-phase flows. *Journal of Computational Physics*, 276:691–728, 2014.
- [13] S. Dong. An outflow boundary condition and algorithm for incompressible two-phase flows with phase field approach. *Journal of Computational Physics*, 266:47–73, 2014.
- [14] S. Dong. A convective-like energy-stable open boundary condition for simulations of incompressible flows. *Journal of Computational Physics*, 302:300–328, 2015.
- [15] S. Dong. Physical formulation and numerical algorithm for simulating N immiscible incompressible fluids involving general order parameters. *Journal of Computational Physics*, 283:98–128, 2015.
- [16] S. Dong. Wall-bounded multiphase flows of N immiscible incompressible fluids: consistency and contact-angle boundary condition. *Journal of Computational Physics*, 338:21–67, 2017.
- [17] S. Dong, G.E. Karniadakis, and C. Chrysosostomidis. A robust and accurate outflow boundary condition for incompressible flow simulations on severely-truncated unbounded domains. *Journal of Computational Physics*, 261:83–105, 2014.
- [18] S. Dong and J. Shen. An unconditionally stable rotational velocity-correction scheme for incompressible flows. *Journal of Computational Physics*, 229:7013–7029, 2010.

- [19] S. Dong and J. Shen. A time-stepping scheme involving constant coefficient matrices for phase field simulations of two-phase incompressible flows with large density ratios. *Journal of Computational Physics*, 231:5788–5804, 2012.
- [20] S. Dong and X. Wang. A rotational pressure-correction scheme for incompressible two-phase flows with open boundaries. *PLOS One*, 11(5):e0154565, 2016.
- [21] R. Folch and M. Plapp. Quantitative phase-field modeling of two-phase growth. *Physical Review E*, 72:011602, 2005.
- [22] M.E. Gurtin. Generalized Ginzburg-Landau and Cahn-Hilliard equations based on a microforce balance. *Physica D*, 92:178–192, 1996.
- [23] M.E. Gurtin, E. Fried, and L. Anand. *The Mechanics and Thermodynamics of Continua*. Cambridge University Press, 2010.
- [24] M. Heida, J. Malek, and K.R. Rajagopal. On the development and generalization of cahn-hilliard equations within a thermodynamic framework. *Z. Angew. Math. Phys.*, 63:145–169, 2012.
- [25] G.E. Karniadakis and S.J. Sherwin. *Spectral/hp element methods for computational fluid dynamics, 2nd edn*. Oxford University Press, 2005.
- [26] J. Kim. A generalized continuous surface tension force formulation for phase-field models for multi-component immiscible fluid flows. *Comput. Methods Appl. Mech. Engrg.*, 198:3105–3112, 2009.
- [27] J. Kim. Phase-field models for multi-component fluid flows. *Commun. Comput. Phys.*, 12:613–661, 2012.
- [28] J. Kim and J. Lowengrub. Phase field modeling and simulation of three-phase flows. *Interfaces and Free Boundaries*, 7:435–466, 2005.
- [29] I. Langmuir. Oil lenses on water and the nature of monomolecular expanded films. *Journal of Chemical Physics*, 1:756–776, 1933.
- [30] A. Prosperetti. Motion of two superposed viscous fluids. *Phys. Fluids*, 24:1217–1223, 1981.
- [31] R. Scardovelli and S. Zaleski. Direct numerical simulation of free-surface and interfacial flow. *Annu. Rev. Fluid Mech.*, 31:567–603, 1999.
- [32] J.A. Sethian and P. Semerka. Level set methods for fluid interfaces. *Annu. Rev. Fluid Mech.*, 35:341–372, 2003.
- [33] S.J. Sherwin and G.E. Karniadakis. A triangular spectral element method: applications to the incompressible navier-stokes equations. *Comput. Meth. Appl. Mech. Engrg.*, 123:189–229, 1995.
- [34] I. Steinbach, I. Pezzolla, and B. Nestler et al. A phase field concept for multiphase systems. *Physica D*, 94:135–147, 1996.
- [35] G.I. Toth, T. Pusztai, and L. Granasy. Consistent multiphase-field theory for interface driven multidomain dynamics. *Physical Review B*, page 184105, 2015.
- [36] G. Tryggvason, B. Bunner, and A. Esmaeeli et al. A front-tracking method for computations of multiphase flow. *J. Comput. Phys.*, 169:708–759, 2001.
- [37] S. Wu and J. Xu. Multiphase allen-cahn and cahn-hilliard models and their discretizations with the effect of pairwise surface tensions. *Journal of Computational Physics*, 343:10–32, 2017.
- [38] P. Yue, J.J. Feng, C. Liu, and J. Shen. A diffuse-interface method for simulating two-phase flows of complex fluids. *J. Fluid Mech.*, 515:293–317, 2004.
- [39] Q. Zhang and X.P. Wang. Phase field modeling and simulation of three-phase flow on solid surfaces. *Journal of Computational Physics*, 319:79–107, 2016.

- [40] X. Zheng and S. Dong. An eigen-based high-order expansion basis for structured spectral elements. *Journal of Computational Physics*, 230:8573–8602, 2011.